UNIVERSITÀ DEGLI STUDI DI PADOVA

DIPARTIMENTO DI INGEGNERIA DELL'INFORMAZIONE

Department of Information Engineering

Master Degree in ICT for Internet and Multimedia:

curriculum Photonics

Enhancing the efficiency of photodynamic therapy by engineering plasmonic nanostructures

Supervisor

Luca Palmieri

External supervisor

Domenico de Ceglia

Student

Aura Cencini

Accademic Year 2021/2022

To the ones who taught me what I know,
and to the ones who made me feel less alone in my darkness.

Abstract

Photodynamic therapy, an innovative technique for the treatment of tumors and other types of lesions, acquired a lot of interest in the research field for its advantages with respect to more traditional therapies as radiotherapy and chemotherapy. However, since this technique is quite recent, it is still premature to be applied to a clinical use on a large scale. Indeed, even if this therapy is really promising, its full potential is still to be developed. Hence, lots of efforts have been made by researchers to increase its efficacy. In particular, the use of metallic nanoparticle has been proposed for their plasmonic properties, since they result to be very efficient in the enhancement of the absorption of a fundamental component of photodynamic therapy, the photosensitizer. This latter is a molecule or a compound that is able to absorb incident light and start a series of reactions that lead to the formation of singlet oxygen, a product that is obtained from the oxygen present in the cells and that is highly cytotoxic. Photodynamic therapy is mainly based on the production of singlet oxygen to obtain the death of tumoral cells, and it has been experimentally demonstrated that the use of metallic nanoparticles, by increasing the photosensitizer absorption, leads to an enhancement of the generation of this product. The increase of absorption by the photosensitizer is maximum when the spectral position of its peak of absorption and of the peak of plasmonic resonance of the plasmonic nanoparticle coincide. The aim of this thesis is to engineer metallic nanoparticles of different shapes and sizes to obtain this superposition, and in particular to understand how the spectral position of the plasmonic resonance peak of a nanoparticle varies depending on its shape and size. Several photosensitizers will be studied and for each of them different nanoparticles will be simulated, showing for which of them we have a superposition of the resonance and absorption peaks. Moreover, the effective

enhancement of the photosensitizer absorption in presence of the metallic nanoparticle is going to be evaluated, in order to understand which structures shapes and sizes are more effective.

Abstract

La terapia fotodinamica, un'innovativa tecnica per il trattamento di tumori o altro tipo di lesioni, ha acquisito notevole interesse nell'ambito della ricerca per i suoi innumerevoli vantaggi rispetto alle più classiche radioterapie e chemioterapie. Tuttavia, essendo una tecnica relativamente recente, è ancora a uno stadio prematuro per essere portata a un utilizzo clinico su larga scala. Infatti, per quanto questa terapia risulti estremamente promettente, non ne è stato ancora sviluppato l'intero potenziale, dunque sono stati fatti notevoli sforzi da parte dei ricercatori per il miglioramento della sua efficienza. In particolare, è stato proposto l'utilizzo di nanoparticelle metalliche per le loro proprietà plasmoniche, che risultano efficaci nell'aumentare l'assorbimento da parte di un fondamentale componente della terapia fotodinamica, il fotosensibilizzatore. Quest'ultimo è una molecola o un composto in grado di assorbire la luce incidente e dare inizio a una serie di reazioni che portano alla formazione dell'ossigeno singoletto, un prodotto ottenuto dall'ossigeno presente nelle cellule che è altamente citotossico. La terapia fotodinamica si basa proprio sulla produzione di ossigeno singoletto per ottenere la morte delle cellule tumorali, ed è stato dimostrato sperimentalmente che l'utilizzo di nanoparticelle metalliche, aumentando notevolmente l'assorbimento da parte del fotosensibilizzatore, porta a un incremento della creazione di questo prodotto. L'aumento dell'assorbimento da parte del fotosensibilizzatore è massimo quando la posizione spettrale del suo picco di assorbimento e quella del picco di risonanza plasmonica della nanoparticella coincidono. Lo scopo di questa tesi è di ingegnerizzare nanoparticelle metalliche di varie forme e dimensioni per ottenere questa sovrapposizione, e in particolare di capire come la posizione spettrale del picco di risonanza plasmonica di una nanoparticella varia a seconda della sua forma e della sua dimensione. Diversi fotosensibilizzatori saranno studiati e per ognuno di essi diverse nanoparticelle saranno simulate,

mostrando per quali si ha una sovrapposizione dei picchi di risonanza e di assorbimento. Inoltre sarà valutato l'incremento effettivo dell'assorbimento in presenza della nanoparticella metallica, per valutare quali strutture e quali dimensioni sono maggiormente efficaci.

Contents

Introduction

Photodynamic therapy (PDT) is an innovative therapeutic technique based on the use of light and a photosensitizer agent, which is able to generate a photodynamic reaction that leads to lesion ablation upon illumination. PDT has been proposed and studied to treat mainly cancer, but it has been proved to be efficient also in the treatment of other diseases. It is minimally invasive and has very few side effects, which makes it very interesting for the final user of the treatment: the patient. However, it is relatively recent and its full potential is still to be discovered, limiting its application on a large clinical scale. In particular, the lack of systematicity in the study of PDT is evident. In fact, despite researchers were able to obtain very promising results, the majority of studies on PDT have been made in laboratories by experiments ex vivo and in vivo, while very few studies have been conducted regarding the theory behind PDT. In this thesis work we will focus in particular on the study and the engineering of plasmonic nanostructures, which have been investigated to enhance PDT efficiency.

The roots of PDT date back to 3000 years ago, when the Greeks promoted the body exposure to the sun (heliotherapy) for health improvement. Light was used as a therapeutic agent also by other ancient cultures, like Egyptians, Chinese and Indians to treat lots of diseases, as for example psoriasis and skin cancer[1]. The study of light as a clinical tool was brought again to the interest of researchers and physicians at the end of the 18th century, who re established the benefit of sun exposure to treat diseases as scrofula, rickets and scurvy, also acknowledging that ultraviolet light has a inhibiting effect on bacteria[2]. But it was Niels Finsen, a danish physician, who developed phototherapy into a science, receiving the Nobel Prize in Medicine in 1903 for its research on phototherapy to treat lupus vulgaris[3].

Also the therapeutic use of photosensitizers (PSs), molecules or compounds able to

absorb photons and generate a photochemical or photophysical, has a long history. Their therapeutic use was reported in India as early as 1400 BC, and also in Egypt in the 12th century AD[2]. However, it was only at the beginning of the 20th century that the in vitro experiments made by Oscar Raab and Professor Herman von Tappeiner confirmed that the simultaneous use of a photosensitizer and light led to the generation of a toxic environment in the analyzed cells[4, 5]. In 1904 von Tappeiner found that the presence of oxygen was a necessity for the photosensitization process[6], and he later coined the term 'photodynamic therapy' to describe this oxygen dependence. He was also the first to try and apply this therapeutic modality to tumors[2].

After the works by von Tappeiner, in the last century many other scientists and researchers extended the knowledge regarding the mechanisms of PDT and were able to successfully treat many patients, leading to the approval of several photodynamic agents by the US Food and Drug Administration for the treatment of cancer.

However, the full potential of PDT is still to be achieved. In fact, despite this treatment modality has proven to be very useful, there are many limitations, as example the ones related to the photosensitizers ability to accumulate in the tumoral region and the unclear dosimetry for the treatment to be effective. Many studies and experiments have been conducted to enhance the efficacy of PDT, in particular regarding the use of plasmonic nanoparticles. These have proven to be useful as carriers of the PS, providing a better accumulation in the site to be treated, as photothermal agents and also as enhancer of the PS absorption, leading to an increase in the generation of singlet oxygen and therefore in the consequent citotoxicity. The absorption enhancement is maximum when the surface localized plasmon resonance (LSPR) of the nanostructure occurs at the same frequency as the peak of the PS absorption.

In this thesis work we will focus in particular on this latter use of plasmonic nanoparticles. Indeed, there is a lack of sistematicity in the study of plasmonic nanoparticles applied to PDT. Lots of experiments have been conducted to prove that their use in PDT actually enhances the treatment efficacy, but without a proper understanding of which geometries or sizes would be the best ones for specific PSs.

Hence, the objective of this thesis work is to provide a guide for the use of plasmonic nanoparticles for PDT, giving a panoramic of the theory behind their physical aspects and

a way to simulate them to study how they physically behave depending on their geometry and their size. The aim was also to explain and provide evidence, through simulations, of the enhanced absorption of some frequently used PSs in PDT by the presence of a plasmonic nanostructure. This was done by simulating a shell made of PS around the nanostructures and computing the ratio between the absorption of the PS in the presence of the plasmonic nanostructure and the one in absence of it.

The hope is that this thesis work will provide a base for a better understanding of how plasmonic nanoparticles work to enhance PDT efficacy, but also some simulation tools for a more sistematic study in the PDT field. Simulations are very useful as they are more cost effective with respect to laboratory experiments, and they are a very useful tool to achieve a study sistematicity, which is fundamental for every research field.

It is to mentioned, however, the limitation of this work. In fact, being simulations an approximation of the problem, the obtained results will be different from the ones that would be obtained from ex vivo or in vivo experiments. Moreover, we considered just some PSs and some nanostructures geometries, hence the work could easily be extended. Also, plasmonic nanostructures could be used also in different ways in PDT, as mentioned above, hence it would be interesting to better study their effects in the treatment efficacy and to better understand the working principles behind them.

To give an outline of the work, in the first chapter we will give some fundamentals about PDT, describing the components needed to perform the treatment and how it works, and about plasmonics, explaining the theory behind localized surface plasmon resonance and the resonance spectral position can change with the size and the shape of the nanostructures. The second chapter will be a step-by-step guide to the simulation software that was used to engineer the plasmonic nanostructure, COMSOL Multiphysics® , where we will show also how to compute some quantities of interest and some of the results obtained. We will also show how to model PSs in the simulation software from their absorbance or molar extinction spectrum, which can be generalized for every other molecule. In the third chapter the obtained results will be shown and commented. In particular, for every PS we will show the respective absorption spectrum and the maximum surface field spectra whose peaks spectrally overlap with the PS absorption peak. Also the ratios between the PS absorption in the presence of the overlapping

plasmonic nanostructure and the absorption in absence of it will be shown.

Chapter 1

Fundamentals of photodynamic therapy and plasmonics

1.1 Photodynamic therapy

Photodynamic therapy is an emerging therapeutic treatment for tumors, which has already been clinically approved by the US Food and Drug Administration. It has been proved to be very successful in terms of treating neoplastic and nonmalignant diseases, however it is still underutilized as tumor therapy. The main strength of this technique is that it has very few side effects with respect to chemotherapy and radiotherapy, making it very interesting for clinical applications and for further studies.

The main components of photodynamic therapy (PDT) are three: light, a photosensitizer and singlet oxygen. A photosensitizer (PS) is a photosensitive compound that is able to absorb light and initiate a photochemical or photophysical reaction and produce singlet oxygen, which is a highly reactive product with cytotoxic effects, which leads to the death of the tumoral cells. In PDT singlet oxygen is obtained from the oxygen contained in the tumoral cell region, through energy transfer mechanisms derived from the reactions that the photosensitizer generates.

Light is necessary for the PS to generate singlet oxygen, and it can be from a laser, a LED or a lamp, depending on the photosensitizer used and the nature of the disease that needs to be treated.

We will discuss the PDT components in the following paragraphs, describing the properties that light should have in order for the therapy to be efficient, how PDT works and the characteristics of the PSs that have demonstrated to be promising for the therapy.

1.1.1 Light

It is very important to have a light source, since light triggers the reactions that lead to the formation of singlet oxygen. The light source should emit at an appropriate wavelength for an efficient treatment. In fact, the wavelength range to be used for PDT is approximately 650-1200 nm. The reason for this specific optical window is the absorption range of the main chromophores in the human cells. Chromophores are molecules, or part of a molecule, that absorb light of a particular wavelength range. In tissue the most relevant chromophores are water, oxyhemoglobin (HbO_2), deoxyhemoglobin, melanin and cytochromes, whose absorption spectra are reported in fig 1.1. The optical window for PDT falls exactly in the wavelengths for which the overall tissue absorption is the lowest. Actually, the acceptable optical range for PDT is further reduced to wavelengths below 850 nm, since the wavelength range in which PS molecules efficiently absorb and convert light energy into singlet oxygen.

As far as the light source is concerned, lasers, LEDs and lamps can be used for the therapy. Lasers are widely used in PDT, since they can be easily coupled into single optical fibers, which allow, for example, endoscopic light delivery. Moreover they are convenient and reliable, and their monochromaticity gives the maximum efficiency of photoactivation. However, being single wavelength devices is also their main limitation, since different photosensitizers require different wavelengths to be excited, hence a separate laser unit is needed for each PS. Lamps, instead, can be spectrally filtered to match any photosensitizer, and they also have a flexible geometry. On the other hand, they can be efficiently coupled only into optical fiber bundles or liquid light guides, hence the endoscopic use is not possible. LEDs have been recently adopted in PDT, and they are mainly used for irradiation of tissue surfaces that are easily accessible. They are low cost, easy to be configured in arrays to achieve different irradiation geometries, and they can be arranged in linear arrays for endoscopic use. However LEDs are not very efficient

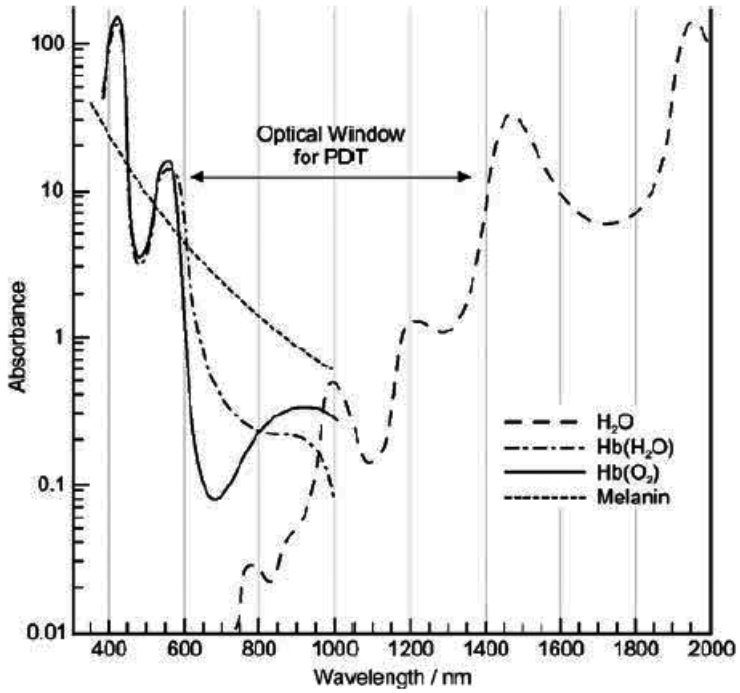

Figure 1.1: *Absorption spectra of the most important chromophores in human tissue, which define the optical window for PDT.*

in electrical-to-light conversion, hence generated heat must be removed. Moreover, as lasers, they are monochromatic, but their cost per Watt is much smaller, which makes using different sources for each PS less problematic.

1.1.2 Singlet oxygen and working principle

After the injection of the PS in the tumoral region, the area is subject to irradiation of light of the appropriate wavelength. Photon absorption takes a photosensitizer molecule from the ground state to an excited state. The excited molecule is unstable, hence it transfers its energy through different possible mechanisms. For example, it could lose it as heat or as fluorescence, but the most interesting energy transfer for PDT is intersystem crossing, through which the excited molecule passes in a stable triplet state. The PS in this state may undergo a non-radiative decay to the ground state or, more likely, it may transfer its energy to the molecular oxygen present in the tumoral region, through a Type II redox reaction. Molecular oxygen is a triplet in its ground state, and the energy transfer from the PS molecule makes it become singlet oxygen, which is highly cytotoxic. Other types of reactions may occur after intersystem crossing, like Type I redox reactions, which are

able to produce radical species that are also toxic for cells. However it is believed that these processes are much more unlikely than Type II reactions.

The main photosensitization processes in PDT are summed up in the Jablonski diagram in figure 1.2.

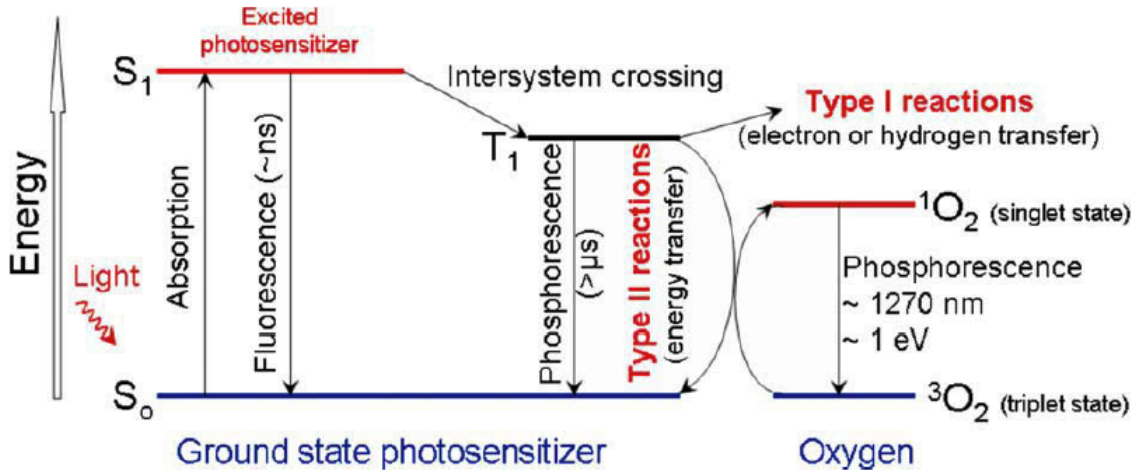

Figure 1.2: *Modified Jablonski diagram of the main energy transfer processes that involve the photosensitizer molecule and that lead to the formation of singlet oxygen.*

The mean lifetime of singlet oxygen is quite short, from 10 to 320 nanoseconds, therefore its diffusion is very limited in cells, from 10 to 55 nm. This determines the locality of PDT, as the photodynamic damage occurs very close to the region where the photosensitizer is excited.

1.1.3 Photosensitizer

Photosensitizers are another key factor in PDT. PSs can be categorized based on their basic structure, which can be porphyrin, chlorin, cyanine and other dyes, but also by different generation. The PSs of the first generation were hematoporphyrin and its derivatives, they were used extensively to clinically treat tumors, but they also had some limitations, as for example poor chemical purity, high photosensitive toxicity, given by a long lifetime and a high accumulation in normal tissues, and a short absorption wavelength. Photofrin was the first PS to be clinically approved in 1995, and it is still used nowadays to treat some types of cancers, like lung cancer and bladder cancer [7]. However, this PS is an

inefficient singlet oxygen producer [8] and its phototoxicity is a concern.

In this work we will focus only on some of the PSs of the second generation, since these PSs are more effective and technologically superior with respect to first generation ones. Indeed, second generation PSs were improved in purity, tumor selectivity, phototoxicity and longer absorption wavelength, which allows for a deeper tissue penetration and higher PDT efficiency. Among the second generation PSs the ones that are going to be considered in this work are methylene blue, indocyanine green, chlorin e6 (Ce6), Verteporfin (Visudyne®), Motexafin Lutetium (Lu-Tex®) and Palladium bacteriopheophorbide (Tookad®), of which the first four have been clinically approved, while the other two are still under clinical trial.

However, also second generation PSs have some issues, such as their poor water solubility and their poor tumor selectivity. In fact, some research has been conducted to achieve third generation PSs to solve these limitations. The idea is to conjugate or encapsulate second generation PSs with carriers that increase their accumulation in the site of interest, such as the tumoral region, but it is still in the development phase.

Considering now what concerns an ideal PS, there are several characteristics that it shall have to be considered successful for PDT, but just the main important ones related to PDT efficiency are going to be mentioned.

One feature is considered to be the ability of the PS to produce a Type II redox reaction [8], which leads to the singlet oxygen formation and so to the cell death.

Another important characteristic for an effective PS is to have a high absorption at the wavelengths effective for PDT, better if they are the highest possible, so at approximately $700 - 850$ nm, which corresponds to the frequency range $350 - 430$ Hz, in order to maximize the penetration depth of light [9]. It is important for the PS to have a high absorption in the spectral region of PDT, since the absorption of the tissues surrounding the tumor or the lesion to be treated is smaller with respect to other frequencies. This is of interest because the more energy the PS is able to absorb, the more probable the reactions that lead to the singlet oxygen formation will be. Hence, the singlet oxygen generation will be much higher when the PS is subject to a light source emitting at the frequency at which the PS absorption peak is located.

More details and other characteristics for a clinically successful PS, with a particular

attention for the ones oriented towards the wellness of the patient, can be found in Allison [8].

The PSs considered in this work are either the most clinically successful or the most promising in terms of efficiency of PDT. Their properties will be discussed below, together with their description and their usage.

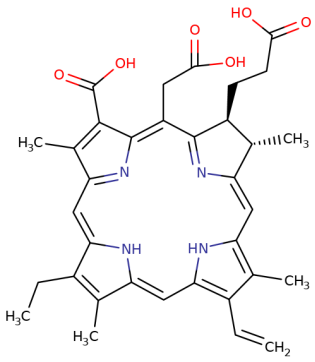

(a) *Structural formula diagram of chlorin e6. (PubChem online)*

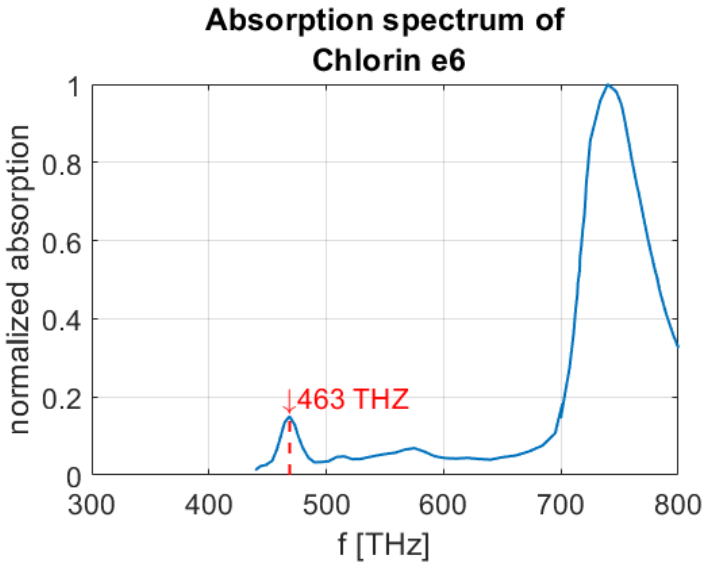

(b) *Absorption spectrum of chlorin e6 in ethanol (Scott Prahl online).*

Figure 1.3: *Molecule diagram (**a**) and absorption spectrum (**b**) of chlorin e6.*

Chlorin e6

Chlorin e6 belongs to the chlorins family. Its chemical structure is reported in Fig.1.4a. It is highly hydrophobic, but it shows a high accumulation in tumoral regions. This seems to be related to hydrophobicity, making hydrophobic PSs more interesting for clinical applications with respect to hydrophylic ones [10]. The drug has a high absorption in the red and in the UV regions of the spectrum, as shown in figure 1.3b with ethanol as solvent. However, since PDT requires the use of wavelengths larger than 650 nm, only the peak in the red region will be considered, as illustrated in Fig.1.3b. Hence the activation frequency for this PS is around 460 THz, which corresponds to a wavelength of approximately 650 nm. Chlorin e6 has been used in PDT to treat cancer, e.g. breast tumors [11], and heart diseases.

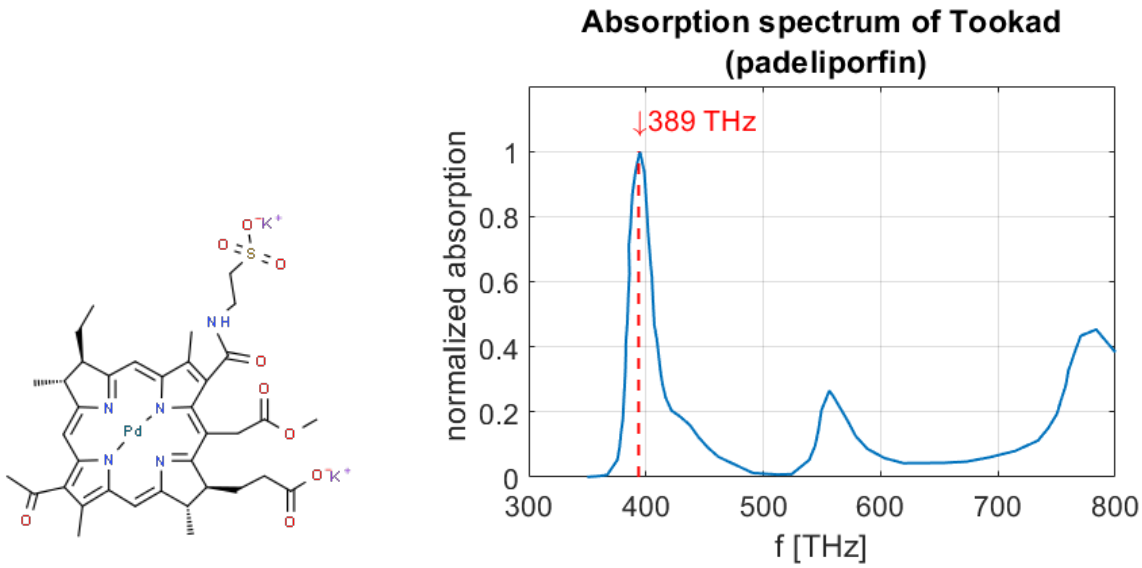

(a) *Structural formula diagram of Tookad. (PubChem online)*

(b) *Absorption spectrum of Tookad in aqueous micellar solution (Francois Brole).*

Figure 1.4: *Molecule diagram (**a**) and absorption spectrum (**b**) of Tookad®.*

Tookad

Padeliporfin (Tookad®) is a bacteriophorbide derivative of bacteriochlorophyll. It is hydrophobic, therefore it needs a carrier to be administrated. The human system disposes of it quite rapidly, hence the drug is generally illuminated shortly after being infused. Moreover the photosensitivity of Tookad results to be limited to three hours. The lesions induced by the drug after illumination have appeared to be vascular targeted, characterized by hemorrhagic necrosis. The therapy with this PS is well tolerated, so it can be performed also in an outpatient environment. As far as its optical properties are concerned, in figure 1.4b the absorption spectrum of this compound in water is reported. It is activated at 389 THz, which correspond to a wavelength of 771 nm, so it allows for deep penetration in tissues. The frequency of activation is intended here as the frequency at which the absorbance of the PS is maximum in the range of application of PDT. Tookad has been mainly studied for prostate cancer, however there is still poor understanding of its dosimetry in PDT, making the therapy application premature and requiring further investigation.

Lu-Tex

Motexafin Lutetium (Lu-Tex®) belongs to the porphyrins family and has been used

to treat prostate cancer. It is hydrophylic and it can be delivered intravenously. It is disposed rapidly and it has no photosensitivity after 24 hours. Most of the drug accumulates in regions in which there is an abnormal formation of blood vessels, typical of tumoral lesions. The treatment time with this PS is in the order of minutes, since it is an excellent singlet oxygen producer.

The absorption spectrum of Lu-Tex in human breast is shown in figure 1.5b. It is activated at 403 THz, corresponding to 745 nm, allowing deep tissue penetration. Moreover is has fluorescent capabilities, which make it useful not only for diagnostic purposes, but also for dosimetry monitoring.

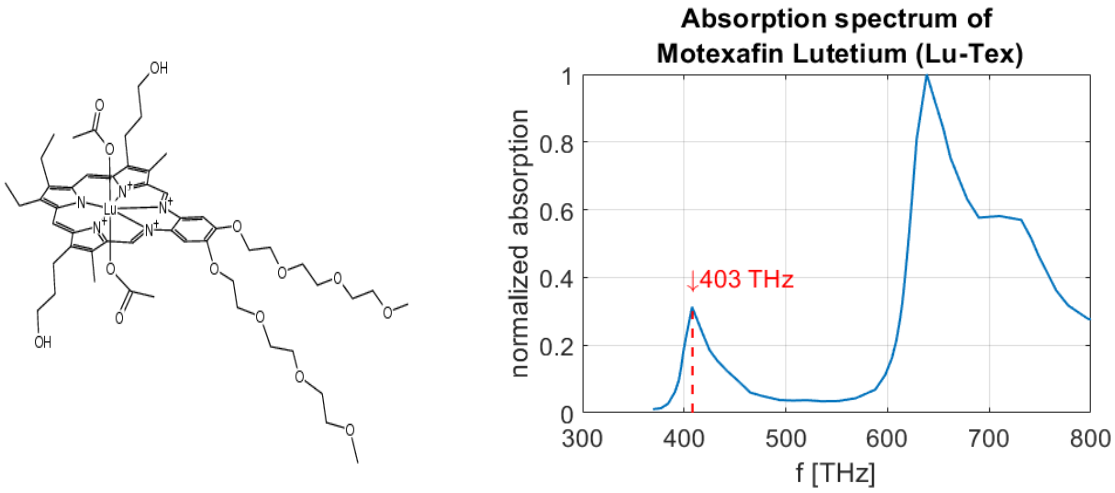

(a) *Structural formula diagram of Lu-Tex®. (PubChem online)*

(b) *Absorption spectrum of Lu-Tex®(Motexafin Lutetium) in human breast (Scott C Davis OSA publishing).*

Figure 1.5: *Molecule diagram (**a**) and absorption spectrum (**b**) of Lu-Tex.*

Verteporfin

Verteporfin is a derivative of benzoporphyrin. It is hydrophobic, so it is usually delivered with liposomes. This PS is cleared quite rapidly and it is photosensitive for just a couple of hours, so the treatment shall initiate within 30 minutes from its infusion. The drug acts on the vascular system and it is able to treat lesions with high formation of new blood vessels. In particular, Verteporfin-based PDT has been widely used in the treatment of macular degeneration related to age, an eyes disease that leads to blindness because of leakages from newly formed blood vessels in the eye. The activation of the PS in water occurs at 428 THz , i.e. 700 nm , as can

be seen in figure 1.6b .

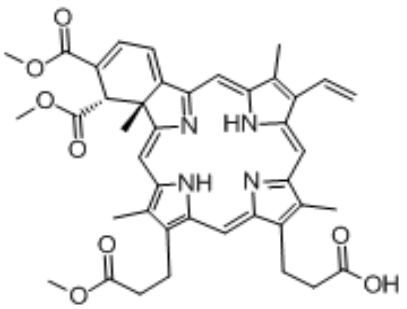

(a) *Structural formula diagram of verteporfin. (PubChem online)*

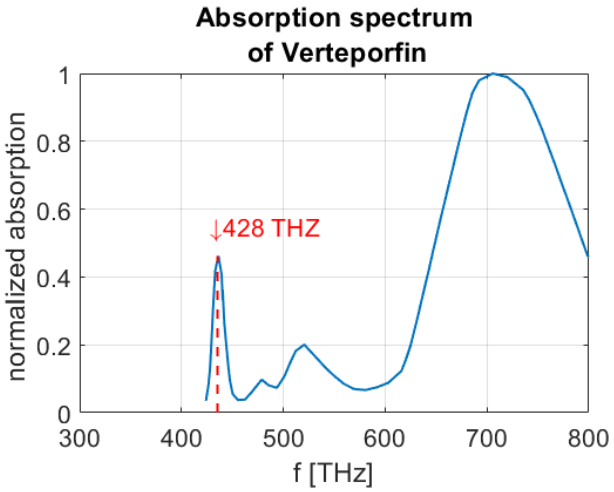

(b) *Absorption spectrum of verteporfin in water (Diogo Pellosi).*

Figure 1.6: *Molecule diagram (**a**) and absorption spectrum (**b**) of verteporfin.*

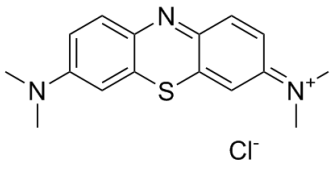

(a) *Structural formula diagram of methylene blue. (PubChem online)*

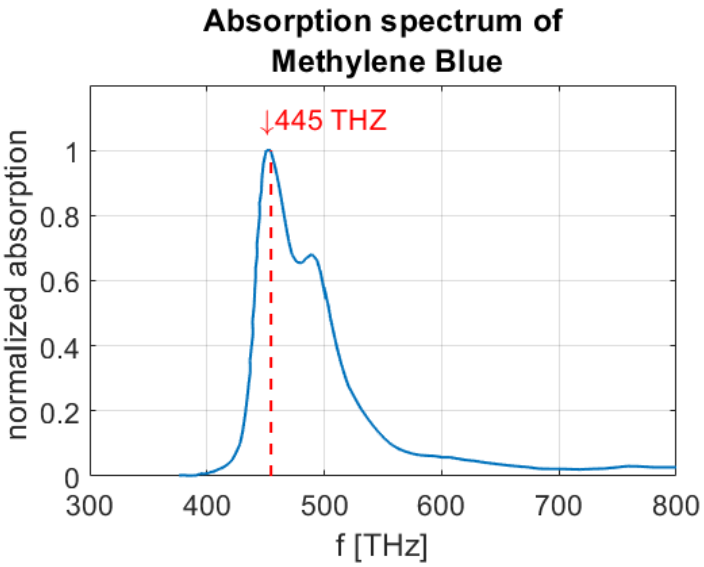

(b) *Absorption spectrum of methylene blue in distilled water (Van-Phuc Dinh).*

Figure 1.7: *Molecule diagram (**a**) and absorption spectrum (**b**) of methylene blue.*

Methylene blue

Methylene blue (MB) is a hydrophobic phenothiazine derivative that has been extensively used in medicine. In PDT, early reports suggest that tumor selectivity of

MB is low when injected and that it highly depends on the nature of the lesion [12], but direct application of MB on the tumor site may result in accumulation within tumor cells [13]. The drug is able to produce both singlet oxygen species, through a Type II redox reaction, and radical species, with a Type I redox reaction. This makes MB suitable also to treat tumoral lesions with hypoxic regions, where Type II reactions are inefficient [12]. Moreover, studies have shown that the drug is able to damage several different kinds of cells, tissues and organisms, making it useful to treat many cancerous and non-cancerous diseases [12]. The absorption of this PS in water is reported as function of the light frequency in figure 1.7b, where it can be seen that it is activated at 445 THz, so at 674 nm.

Many experiments have been made on the use of methylene blue in PDT to treat numerous diseases, like osteomyelitis, AIDS-related Kaposi's sarcoma and malignant melanomas [14]-[15].

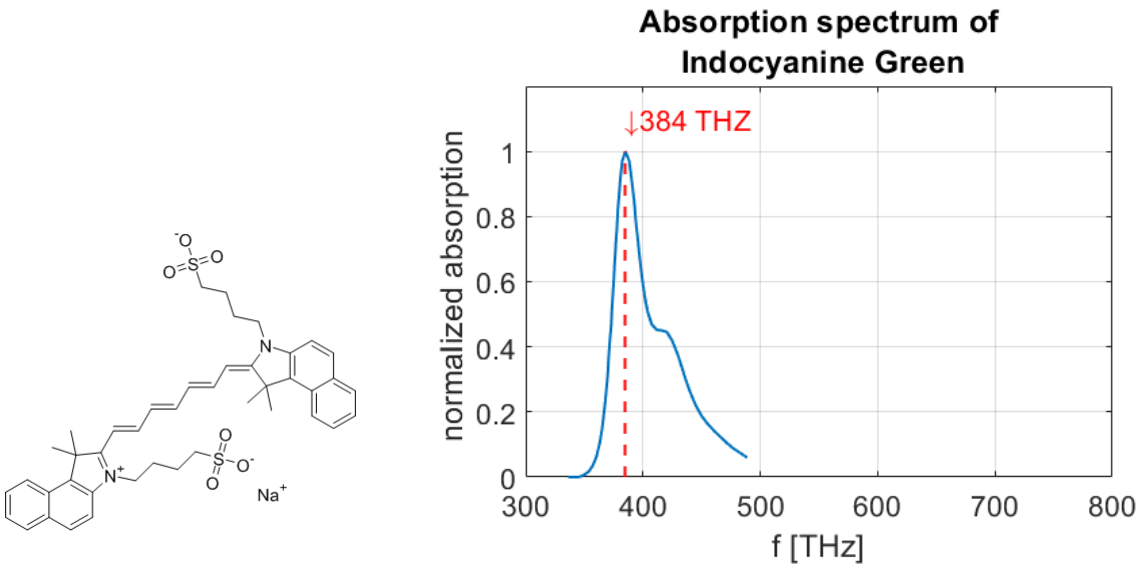

(a) *Structural formula diagram of indocyanine green. (PubChem online)*

(b) *Absorption spectrum of indocyanine green in water (Scott Prahl online omlc).*

Figure 1.8: *Molecule diagram (**a**) and absorption spectrum (**b**) of indocyanine green.*

Indocyanine green

Indocyanine green (ICG) is a water-soluble cyanine dye which has been widely used in the medical field for different kind of treatments. It is believed that the main

cytotoxic effect of ICG is not the production of singlet oxygen, but it is due to its decomposition products[16]. It is rapidly disposed after intravenous injection, its half-time is reported to be of 2 to 4 minutes [17].

It has a high capability of conversion of energy into heat, making it interesting for photothermal therapy, which is an extension of PDT based on heat release to kill cancer cells. Moreover the fluorescence properties of this drug make it also useful for bioimaging purposes.

The toxicity of ICG is classified as low and severe adverse reactions are rare. Therefore it has been widely investigated to be used in PDT for the treatment of, for example, oral caner[18]. However, its quick degradation in moist environment, its poor tumor specificity and its poor ability to produce singlet oxygen make its use in clinical applications very limited[17].

For what concerns the optical properties of the drug, its absorption peak is in the NIR region of the spectrum, at 384 THz in water (780 nm), as shown in figure.

1.1.4 Advantages and limits of PDT

PDT has a lot of advantages with respect to surgery, chemotherapy and radiotherapy in cancer treatment. In fact it is minimally invasive, has less side-effects, it is more affordable and it can be done in an outpatient environment.

PDT is also selective and local, which means that it is able to treat a very specific target, and this capability depends both on the PS ability to localize in the tumoral cell region and on the precision of the delivery of light to the site.

Moreover, PDT can be repeated in the same region if needed, unlike other therapies, hence it does not compromise further treatment options, and it can be performed on patients that cannot be treated with other techniques.

However, PDT has also limitations. Its localized nature is both one of its advantages and one of its current main problem. In fact, locality becomes a limit in the case of tumor metastis, which is the most frequent cause of death in cancer patients, since the tumor spreading in different parts of the body makes the treatment with PDT unsuccessful.

Dosimetry of the PS is also an issue, since there is no precise knowledge of the PS

doses that make PDT efficient. The use of PSs with fluorescent capabilities has been proposed by some authors for real-time monitoring of the drug distribution and of the tumoral cells destruction.

Another great limitation in PDT is the possible presence of severe local lack of oxygen (hypoxia) in the tumor region, which makes the technique very inefficient. In fact, the efficiency of PDT lies mainly in the cytotoxic effects of singlet oxygen, therefore the presence of oxygen is a necessity.

As already mentioned, also the PSs that have been proposed so far present some issues, like the poor tumor selectivity, the poor solubility in water and, in some cases, their too fast degradation, making evident the need of new PSs or of carriers which can provide the required properties of an ideal PS.

A lot of research has been carried to increase the efficacy of PDT, and nanotechnology has been proved to be very useful. In particular, nanostructures complexed with PSs on their surface have been extensively studied and used to promote the accumulation of the drug in the tumor cells, together with the enhancement of singlet oxygen production.

In this work we are going to consider just gold nanostructures, since this material has a very good biocompatibily and revealed to be very useful and efficient in the enhancement of PDT efficacy.

1.2 Plasmonics

Metallic nanostructures are able to host non-propagating electromagnetic modes, called localized surface plasmons (LSPs). These are excitations of the conduction electrons of the nanostructure due to the presence of an oscillating electromagnetic field, with wavelength comparable to electric size of the nanostructure.

An important consequence of LSPs is the field amplification that can arise in the near-field region of the metal. This electromagnetic near-field enhancement mechanism of plasmonic nanostructures has been widely investigated to achieve singlet oxygen generation control. In fact, when there is an overlap between the localized surface plasmon resonance (LSPR) band and the absorption band of the near photosensitizer molecules, the absorption of the PS is remarkably enhanced by the local electric field, greatly increasing the production of singlet oxygen.

Lots of experiments have been made about the PDT efficacy in the presence of metal nanoparticles, and the results showed clearly that, when combined with PSs molecules, they are able to highly enhance PDT damages to the tumoral cell[19].

1.2.1 Localized surface plasmon theory: electrostatic approximation

In metallic nanostructures, i.e. with size comparable to the metal skin depth, the electric field of incident light can penetrate the metal and interact with the conduction electrons. The displacement of electrons from the positively charged lattice generates a restoring force that pulls the polarized electrons back to the lattice, leading to a coherent oscillation of the conduction electrons. This collective oscillation of free electrons is called a plasmon, which corresponds to a quantum of plasma oscillation. Therefore, the plasmon in a nanostructure can be intuitively thought as a mass-spring harmonic oscillator, where the electron cloud oscillates like a dipole in the same direction of the applied electric field, as can be seen in figure 1.9. It is to be noticed that, in order for light to excite the plasmon, its frequency must be in resonance with it.

In nanostructures, plasmons are non-propagating excitations, called localized surface

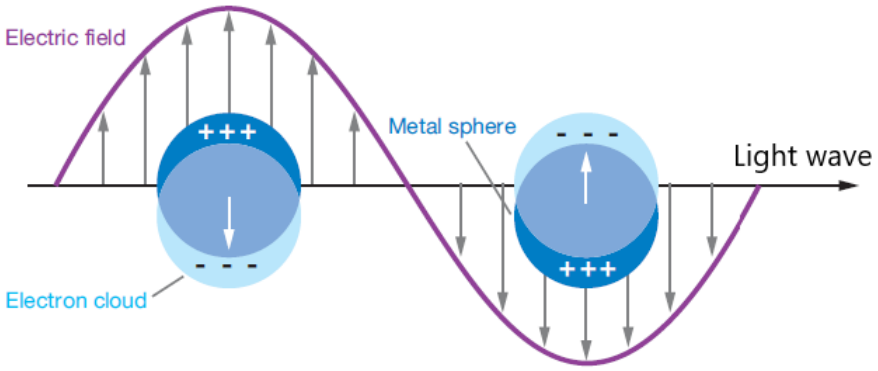

Figure 1.9: *Illustration of a localized surface plasmon (electrons oscillation) in a metal nanostructure due to impinging light[20].*

plasmons (LSPs). A good description of the problem in the near field region of the structure, if its size is much smaller than the light wavelength, can be obtained through the electrostatic approximation, for which the nanostructure is considered to be in a static electric field of the form $\boldsymbol{E_0} = E_0\hat{z}$. In this case, the distortion of the electron cloud in response to the electric field can be expressed by the nanoparticle polarizability α as:

$$\alpha = (1+\chi)\,\varepsilon_0\,\varepsilon_d(\omega)\,V_{ns}\,\frac{\varepsilon_m(\omega)-\varepsilon_d(\omega)}{\varepsilon_m(\omega)+\chi\varepsilon_d(\omega)} \quad , \tag{1.1}$$

where ω is the frequency of light, which tends to 0 in the static approximation , ε_d is the relative permittivity of the non-absorbing surrounding medium (Im[ε_d] = 0), V_{ns} is the nanostructure volume, χ is a geometrical factor, and $\varepsilon_m(\omega)$ is the complex relative permittivity of the metal, which has general form:

$$\varepsilon_m(\omega) = Re[\varepsilon_m(\omega)] + iIm[\varepsilon_m(\omega)] \quad . \tag{1.2}$$

A scheme representing a metallic nanosphere of radius a in a static electric field of intensity E_0 is shown in figure 1.10 for a better understanding of the geometry, where θ is the angle between the static electric field and the position vector $\boldsymbol{r}$ at point P.

With the electrostatic approach the distribution of the potential ϕ outside and inside the nanostructure can be found as the solution to the Laplace equation $\nabla^2\phi = 0$, while the electric field can be found as the gradient of the potential ($\boldsymbol{E} = -\nabla\phi$). All the calculations can be found in any textbook of classical electrodynamics, e.g. Plasmonics: Fundamentals

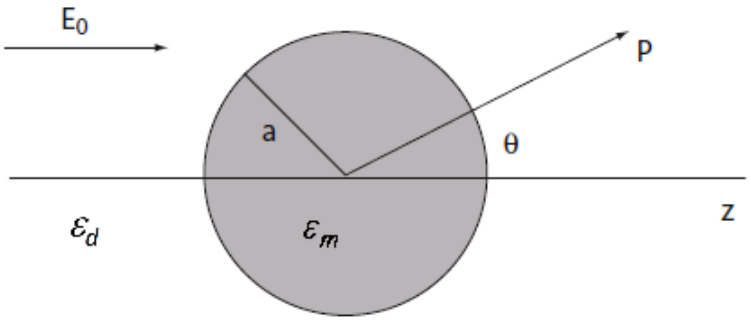

Figure 1.10: *Schematic representation of a metallic homogeneous sphere of radius a immersed in a dielectric homogeneous material, in the presence of an electrostatic field of intensity E_0. The quantities ε_m and ε_d are the relative permittivities of the metal sphere and of the surrounding background, respectively, and θ is the angle between the z-axis and the position vector at point P.*

and Applications (2007) [21]. The resulting expressions of the electric field distribution inside and outside the nanostructure are, respectively:

$$\boldsymbol{E_{in}} = \frac{(1+\chi)\,\varepsilon_d}{\varepsilon_m + \chi\varepsilon_d}\,\boldsymbol{E_0} = \frac{\alpha}{\varepsilon_0(\varepsilon_m - \varepsilon_d)V_{ns}}\,\boldsymbol{E_0} \tag{1.3}$$

$$\boldsymbol{E_{out}} = \boldsymbol{E_0} + \frac{\boldsymbol{n}(\boldsymbol{n}\cdot\boldsymbol{p}) - \boldsymbol{p}}{V_{ns}\varepsilon_0\varepsilon_d} = \boldsymbol{E_0} + \alpha\,\frac{\boldsymbol{n}(\boldsymbol{n}\cdot\boldsymbol{E_0}) - \boldsymbol{E_0}}{V_{ns}\varepsilon_0\varepsilon_d} \quad , \tag{1.4}$$

with $\boldsymbol{n} = \boldsymbol{r}/r$ being the radial unit vector.

It can be noticed that both the fields are proportional to the polarizability α, which experiences a resonant enhancement when $|\varepsilon_m + \chi\varepsilon_d|$ is a minimum, as can be seen in equation 1.1. In the case of a small or slowly-varying $Im[\varepsilon_m(\omega)]$ around the resonance frequency, the condition can be written as:

$$Re[\varepsilon_m(\omega)] = -\chi\varepsilon_d(\omega) \quad . \tag{1.5}$$

Equation 1.5 is referred to as the Fröhlich condition, and the dipolar associated mode, in an oscillating field, is called the surface plasmon of the metal nanostructure (LSPR).

Another interesting consequence of the polarizability resonance, especially from an optics point of view, is the enhancement of the absorption and the scattering efficiencies of the nanostructure. The corresponding absorption and scattering cross sections result

to be, respectively [22]:

$$C_{abs} = \frac{k\, Im(\alpha)}{\varepsilon_0\, \varepsilon_d} \tag{1.6}$$

$$C_{sca} = \frac{k^4 |\alpha|^2}{6\pi(\varepsilon_0\, \varepsilon_d)^2} \quad , \tag{1.7}$$

with $k = 2\pi/\lambda$.

The nanostructure can therefore be seen as an electric dipole, which absorbs and scatters electromagnetic fields, resonating at a specific wavelength. However, only if the size of the structure is very small compared to the light wavelength, its representation as an ideal dipole and quasi-static regime are verified, so for electromagnetic fields varying with time but with negligible retardation effects of the field over the structure volume. In fact, this theory of plasmon resonance by a dipole structure results to be a reasonably good approximation just for very small structures, with dimension much below 100 nm.

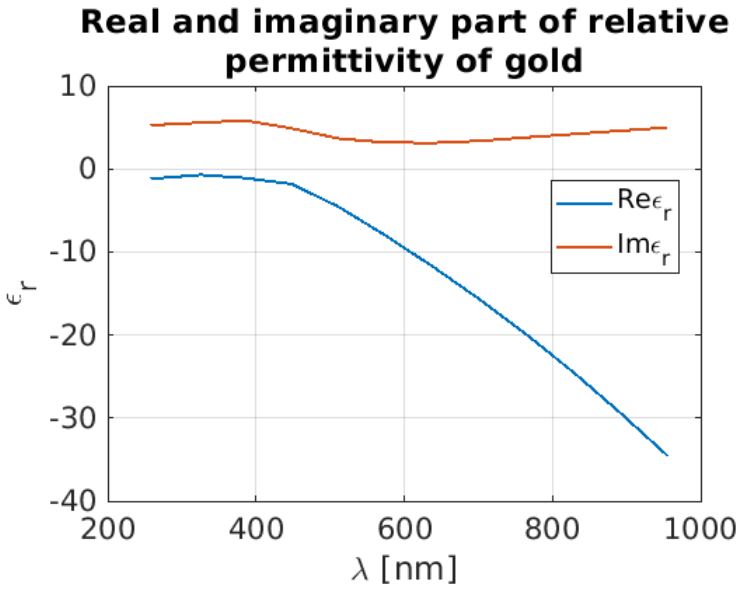

Figure 1.11: *Real and imaginary part of the complex relative permittivity of gold, according to a Drude-Lorenz model that fits experimental data.*

A demonstration of the limit of this approximation can be obtained calculating the two cross sections of a gold nanoparticle of radius 90 nm using the equations 1.6 and 1.7, and comparing the results with the ones computed through the COMSOL Multiphysics® software. As far as the relative permittivity $\varepsilon_r = \varepsilon_m/\varepsilon_0$ of gold is concerned, its value was

computed from the complex refractive index $r = n - i\kappa$ as:

$$\varepsilon_r = (n - i\kappa)^2 \qquad . \tag{1.8}$$

The values considered for n and κ of gold were retrieved from a of Lorenz-Drude model that fit experimental data; in figure 1.11 the real and imaginary part of ε_r are represented as function of the wavelength in nm.

The resulting theoretical absorption cross section for an isolated gold nanoparticle of radius 90 nm is shown together with the absorption cross section computed through simulations in COMSOL Multiphysics® in figure 1.12, while the results for the scattering cross section are presented in figure 1.13.

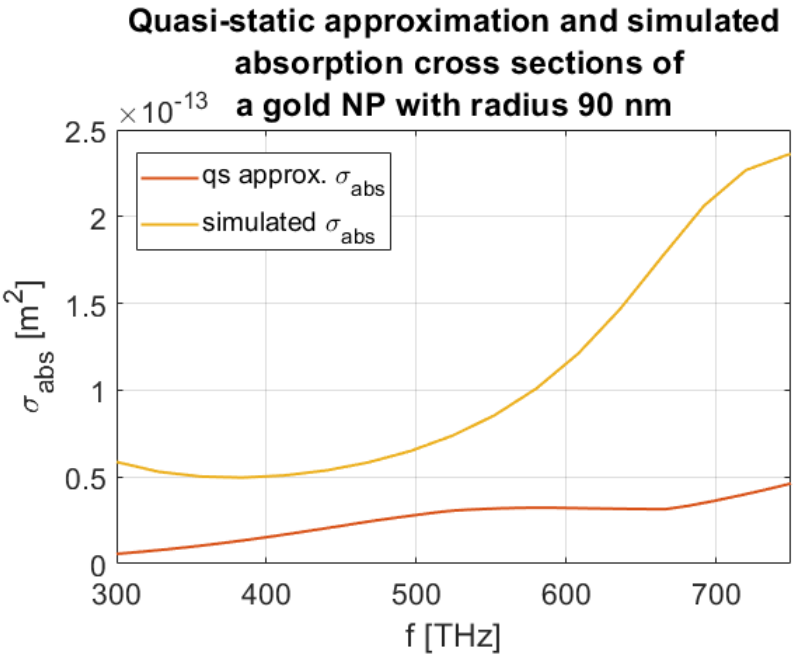

Figure 1.12: *Comparison between the quasi-static approximation absorption cross section and the one simulated with COMSOL®.*

It can be seen that the theoretical curves do not approximate the simulated ones very well, which can be explained by the fact that the dipole theory for nanostructures is not sufficient when these are no longer very small in size with respect to the light wavelength, which is the case for a nanoparticle of radius 90 nm.

Hence, a full-wave approach is needed for a better understanding of the plasmon resonance behaviour in larger nanostructures. First, we are going to take into account

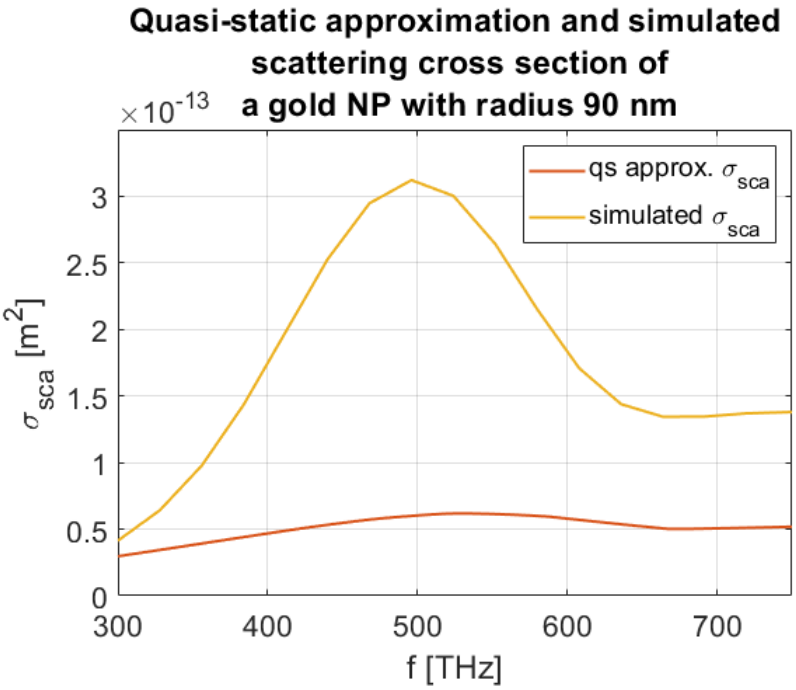

Figure 1.13: *Comparison between the quasi-static approximation scattering cross section and the one simulated with COMSOL®.*

Mie's electrodynamic theory for spherical nanostructures, discussing how the size of the structure affects the plasmon resonance condition. Then, we are going to describe the size effects on the LSPR spectral position also for rod-shaped structures.

1.2.2 Mie theory

In 1908 Gustav Mie developed through an electrodynamic approach a complete theory for the absorption and scattering of electromagnetic radiation by a sphere.

For non sufficiently small particles the quasi-static approximation is no longer valid because of retardation effects of the electromagnetic field, where retardation is due to the phase difference between the field propagating from two different regions of the nanoparticle.

In particular, beyond the quasi-static regime, two competing processes that modify the plasmon resonance can be identified: a radiative damping process, which dominates for large nanoparticles, and absorption, which is instead predominant in smaller ones.

A better understanding of this can be obtained analyzing the terms of the expression of the polarizability α, for a nanosphere of volume V, obtained from the expansion of the

first transverse magnetic mode of Mie theory [21]

$$\alpha = V \frac{1 - \frac{1}{10}(\varepsilon_m + \varepsilon_d)\, x^2 + O(x^4)}{\left(\frac{1}{3} + \frac{\varepsilon_d}{\varepsilon_m - \varepsilon_d}\right) - \frac{1}{30}(\varepsilon_m + 10\varepsilon_d)\, x^2 - i\frac{4\pi^2\, \varepsilon_d^{3/2}\, V}{3\, \lambda_0^3} + O(x^4)} \quad , \tag{1.9}$$

where again ε_m and ε_d are the relative permittivities of the metal nanosphere and of the dielectric background, respectively. The quantity λ_0 is the free-space wavelength, while the parameter $x = \frac{\pi r}{\lambda_0}$ is the so called size parameter, with r being the radius of the sphere.

The term x^2 at the numerator includes the retardation effects of the exciting electromagnetic field over the volume of the structure, and it yields to a shift in the frequency of plasmon resonance. The factor x^2 at the denominator accounts instead for the retardation of the depolarization field inside the sphere, which is the field that arises inside the structure in opposition to the incident field, leading to a shift in the resonance peak too.

The resulting overall shift for gold and noble metals in general is towards lower frequencies, hence a red-shift in the plasmon resonance can be observed as the nanoparticle size increases. This shift can be explained in an intuitive way by the fact that for larger nanoparticles the distance between charges at opposite sides is increased, which leads to a smaller restoring force and to a lower photon energy needed to excite the plasmon.

Radiation damping is accounted for in the third purely imaginary term of the denominator of α in equation 1.9. It is a radiative decay process of electrons into photons, for which the energy of moving electrons is converted into electromagnetic energy and emitted in the form of, for example, visible or infrared light, and it is the main reason for the decrease of the plasmon resonance strength as the particle size increases.

In addition, a broadening of the plasmon resonance occurs for larger volumes: the standard purely classical interpretation of this broadening is that it is due to losses by light reemission (scattering) from the conduction electrons on the particle surface, which cause a damping of the electrons oscillation [23].

Hence, in summary, for larger particles the resonance peak shifts to smaller frequencies, it decreases in intensity and it is significantly broadened. More details about the theories

behind the behaviour of the plasmon resonance for increasing nanoparticles size were discussed by Wokaun et al., 1982 [24].

The considerations made so far were for a spherical nanoparticle, but for different shapes, like nanorods, a different behaviour sets in.

Experiments were made by Juvé et al. [23] with gold nanorods covered with a silica shell. It was found that the main resonance is due to the longitudinal LSPR, the one excited by light polarized along the rod long axis, and that its spectral position is red-shifted for an increasing aspect ratio, where the aspect ratio is defined as the ratio of the length of the nanorod and its diameter.

But still no clear evidence has been found in literature on how the length, the radius and the material alone of a nanorod, or any other shape, affect the resonance peak, and, to our knowledge, the so far proposed classical and simple quantum mechanical models fail to predict the LSPR spectral position scaling, making evident the need of a more accurate modeling.

Hence, another perspective has been used: nanostructures can be seen and discussed as nanoantennas, whose plasmonic properties, which depend on the size and geometry of the structure, have been extensively studied.

1.2.3 Nanostructures as nanoantennas

Antennas are widely used to convert electromagnetic radiation in the radiofrequency and in the microwave regions into localized energy, and the other way around.

In classical antenna theory, the characteristic length of the antenna is related to the wavelength of incident radiation by a linear relationship. For example, for a half-wave dipole antenna, which has a rod shape, its resonant length is given by $L = \lambda/2$, with λ being the light wavelength.

However, experiments have shown that at optical frequencies the resonant length of a dipole antenna is smaller than half the wavelength of incident light. In fact, in the optical regime radiation penetrates into the metal and generates oscillations of the free-electron gas, i.e. surface localized plasmons.

Novotny investigated the scaling of the spectral position of the LSPR with the size of a

rod shaped nanoantenna [25], stating that at optical frequencies the resonant length of a nanoantenna is no longer related to the wavelength of incoming radiation by $L = \lambda/2$, but by a more complex relationship that includes material properties and size of the structure.

For simplicity, the author defined an *effective* wavelength, λ_{eff}, that depends on the material properties of the structure and its size, and that is related to the resonant length of the rod by $L = \lambda_{eff}/2$, and studied its dependence on the antenna geometry and material.

The law that the author derived for λ_{eff}, that shows how it is related to the wavelength of incident light λ, is the following:

$$\lambda_{eff} = n_1 + n_2 \left(\frac{\lambda}{\lambda_p}\right) \quad , \tag{1.10}$$

where n_1 and n_2 are two coefficients that are related to the geometry of the structure and to the material properties and λ_p is the plasma wavelength of the antenna material. For gold, $\lambda_p \approx 138$ nm.

The model reported was obtained considering the nanoantenna as composed by rod shaped segments of radius $R << \lambda$ and analyzing just one of them, of length L, radius R and relative permittivity $\varepsilon(\lambda)$, and immersed in a material with dielectric constant ε_s.

The scheme in figure 1.14 shows the nanorod segment considered by Novotny with incident electric field of intensity E with propagation direction identified by the wavevector $\boldsymbol{k}$, and also the subsequent material surface charges oscillation.

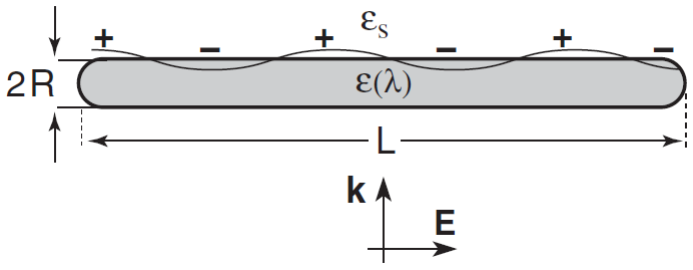

Figure 1.14: *Representation of the nanorod element analyzed by Novotny, of length L, radius R and relative permittivity $\varepsilon(\lambda)$, immersed in a material with dielectric constant ε_s and under the action of an electric field $\boldsymbol{E}$ whose direction of propagation is identified by the wavevector $\boldsymbol{k}$.*

Other considerations and assumptions that were made concern the relative permittivity of the rod element: since the dispersive properties of the antenna are of interest, just the real part of the rod relative permittivity, $\varepsilon' = Re\{\varepsilon\}$, was taken into consideration; moreover, the rod material was modeled as a free-electron gas according to Drude theory, leading to an expression for ε' given by Drude formula

$$\varepsilon' = \varepsilon_{\text{inf}} - \left(\frac{\lambda}{\lambda_p}\right)^2 . \tag{1.11}$$

In the formula, $\varepsilon_{\text{inf}} = \varepsilon'(\lambda \to 0)$ is the relative permittivity at infinite frequency, and it quantifies the deformational electric polarization, which arises when there is a displacement of negative and positive charges in a molecule from their equilibrium positions due to the action of an external field. For gold, $\varepsilon_{\text{inf}} \approx 11$.

Theoretical developments and numerical evaluations led the author to the following expressions for the coefficients n_1 and n_2 presented in equation 1.10:

$$n_1 = 2\pi R \left[13.74 \; - \; 0.12 \; \frac{\varepsilon_{\text{inf}} + \varepsilon_s \, 141.04}{\varepsilon_s}\right] - 4R \tag{1.12}$$

$$n_2 = 2\pi \, R \; \frac{0.12 \sqrt{\varepsilon_{\text{inf}} + \varepsilon_s \, 141.04}}{\varepsilon_s} \qquad . \tag{1.13}$$

The details about the calculations and considerations that were made can be found in Novotny (2007).

Hence, the resonant length L of a nanorod of radius R corresponds to an incident wavelength λ given by:

$$\lambda = \frac{(2L - n_1) \, \lambda_p}{n_2} \qquad , \tag{1.14}$$

with n_1 and n_2 given by expressions 1.12 and 1.13.

The wavelength in 1.14 can be interpreted also as the wavelength at which the LSPR is spectrally located, where the spectral position of the resonance depends on the radius of the rod R, on its length L, on its material and on the surrounding background. It can be noticed that the relation between L and λ still remains linear.

What can be deduced from these results is that, for an increasing length L of the

nanorod, the resonance wavelength linearly increases, so a red-shift can be observed, and the same occurs for an increasing radius R.

All these considerations about the LSPR spectral position for a nanostructure are going to be taken into account in the attempt of engineering the nanoparticle, to achieve a superposition between its resonance peak and the absorption peak of the PSs that we have considered. In this way, the singlet oxygen production originated by the reactions that the PS initiates will be highly enhanced, as experiments have shown, leading to great enhancement of PDT efficacy.

Chapter 2

Methods and simulations

In order to investigate how the LSPR spectral position of a gold nanostructure varies depending on its size and geometry, the COMSOL Multiphysics software® was used.

In this chapter we will show in detail the settings that were used to simulate gold nanostructures in a non absorbing medium and to compute quantities we were interested in for this work, as the absorption and scattering cross sections and the scattered electric field on the nanoparticle surface. Moreover, we will also show how to simulate a PS shell around the gold nanoparticle and how to insert materials that are not present in the COMSOL ® library. A PS nanoparticle will also be simulated in order to compare the absorption cross section of a PS in the presence and in the absence of a metallic nanostructure, to demonstrate the absorption enhancement provided by the nanoparticle, which is crucial to improve PDT efficiency.

The aim of this chapter is to be a guide for the use of COMSOL Multiphysics® as a tool for optimizing PDT, in particular to simulate light interaction with metallic nanoparticles of different shapes and sizes and PSs shells.

2.1 A detailed guide on how to simulate scattering from nanoparticles

2.1.1 Preparing the file

Open COMSOL® and create a new file. Select "Model Wizard".

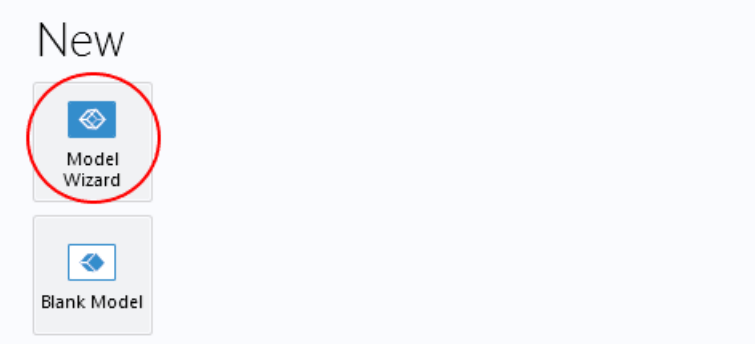

Then select "3D" as Space Dimension.

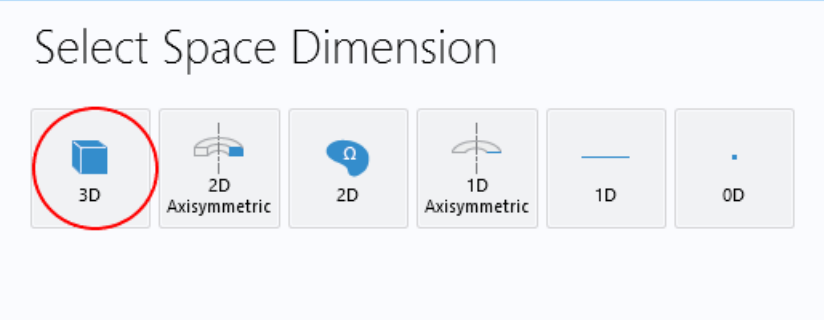

In "Select Physics", under "Optics/Wave Optics", double click "Electromagnetic Waves, Frequency Domain (ewfd)": it will be added to "added physics interfaces".

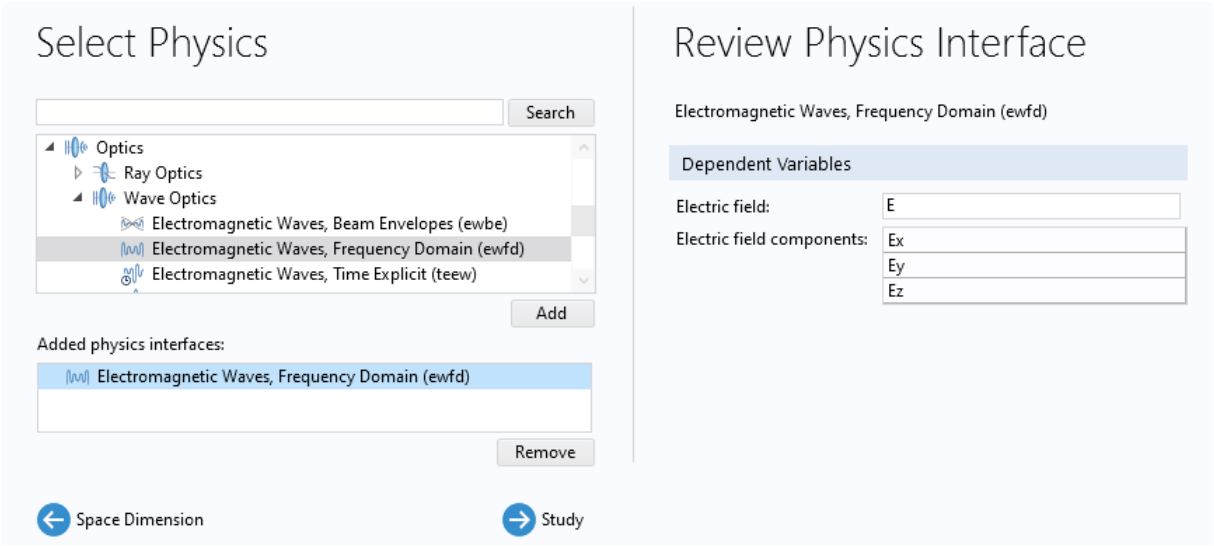

Click on done to proceed and the simulation interface will appear.

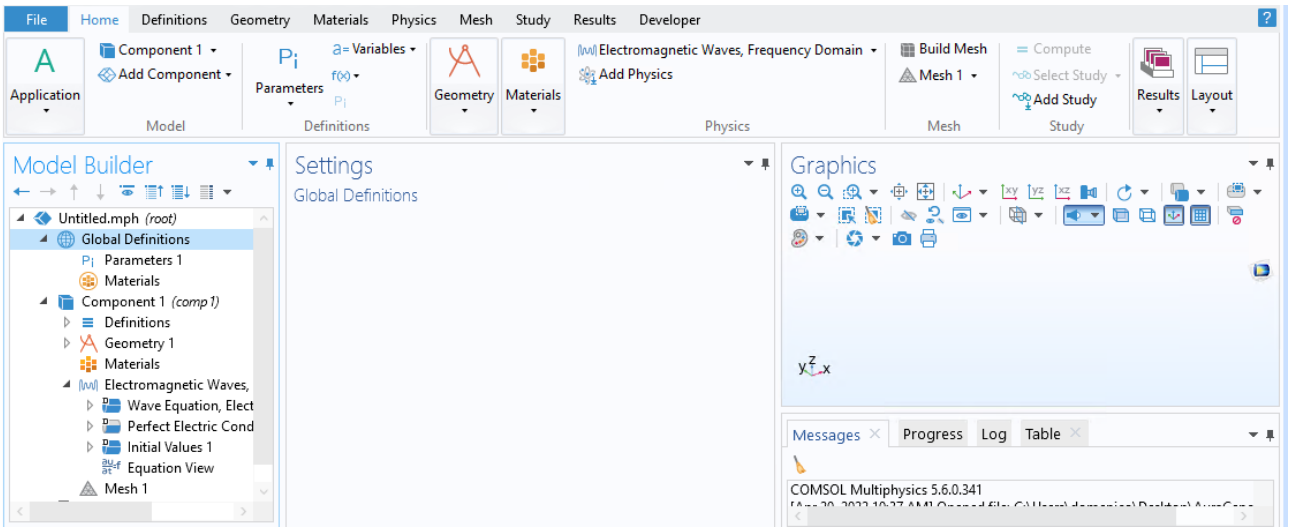

2.1.2 Configuring the geometry

Right-clicking on "Geometry" it is possible to build different already defined structures, like spheres or cubes. We will show the settings for a spherical nanoparticle to proceed in the explanation, since it is the most simple to be treated, but the settings are the same for any other structure to be chosen. Hence, select "Sphere" to build the spherical nanoparticle.

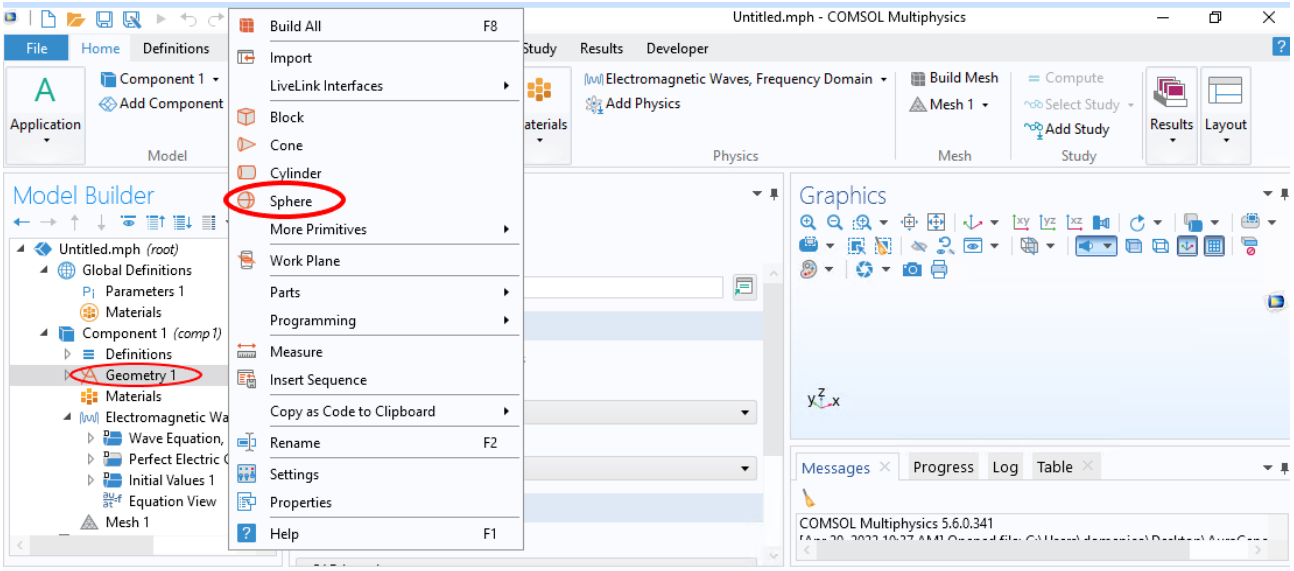

In the settings of the structure just built, it is possible to choose a label for it, in our case we will name it "nanoparticle", and we can set here the radius for it: under "Size" in "Radius" set the value, in meters, that was chosen. In our case we decided to build a nanoparticle of radius 50 nm. It is also possible to decide the position of the center of the nanoparticle, by setting its xyz coordinates, but we will keep it to the center of the coordinates system, so (0 0 0).

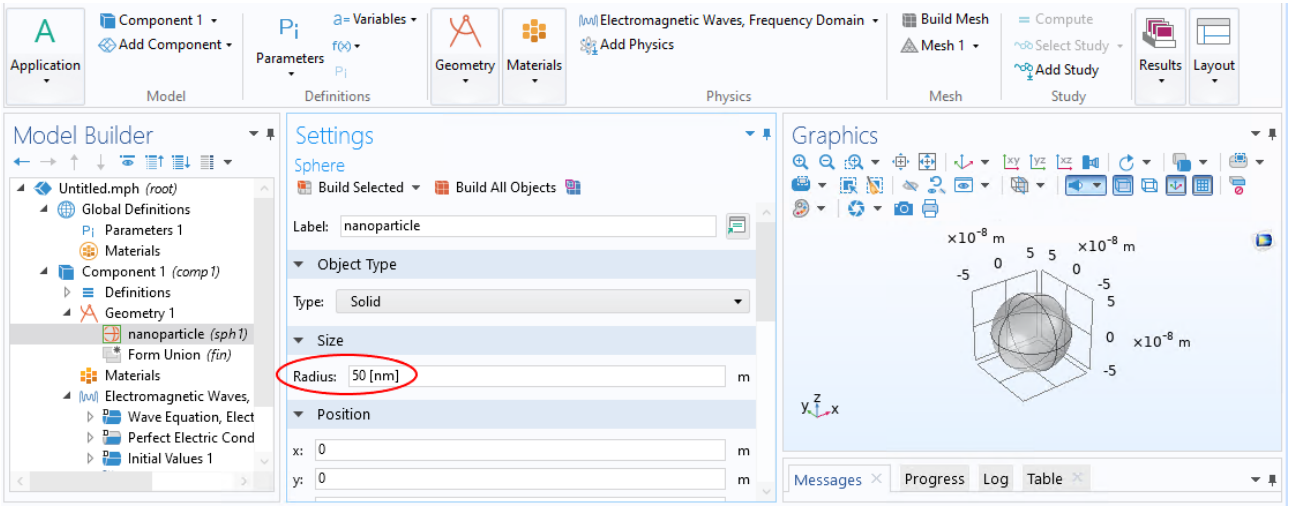

The radius of the nanoparticle can also be set as a parameter: in "Global Definitions" click on "Parameters" and in its settings simply add the variable name that needs to be defined and the value to be attributed to it. In our example, we chose as variable name for the nanoparticle radius r_{np} and as value the one inserted before 50 nm. Once the

variable has been defined, in the nanoparticle settings insert the chosen label for it in the field dedicated to the radius.

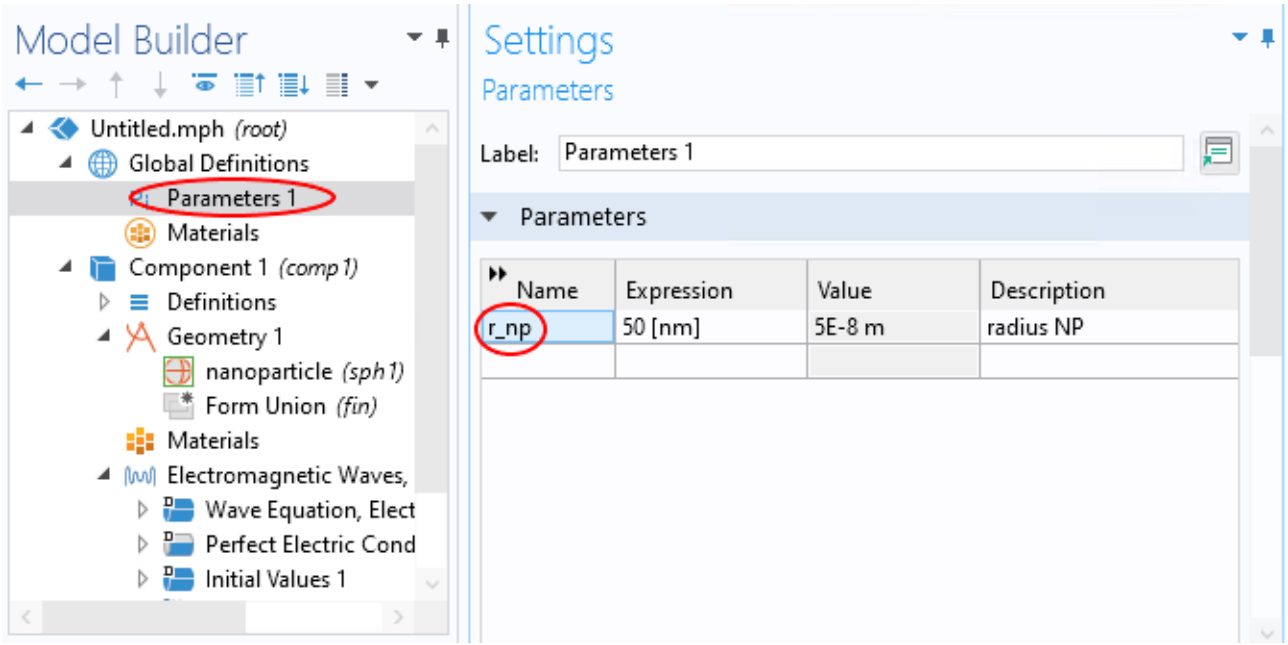

To build the nanoparticle, click on "Build Selected", and it will appear in the Graphics space.

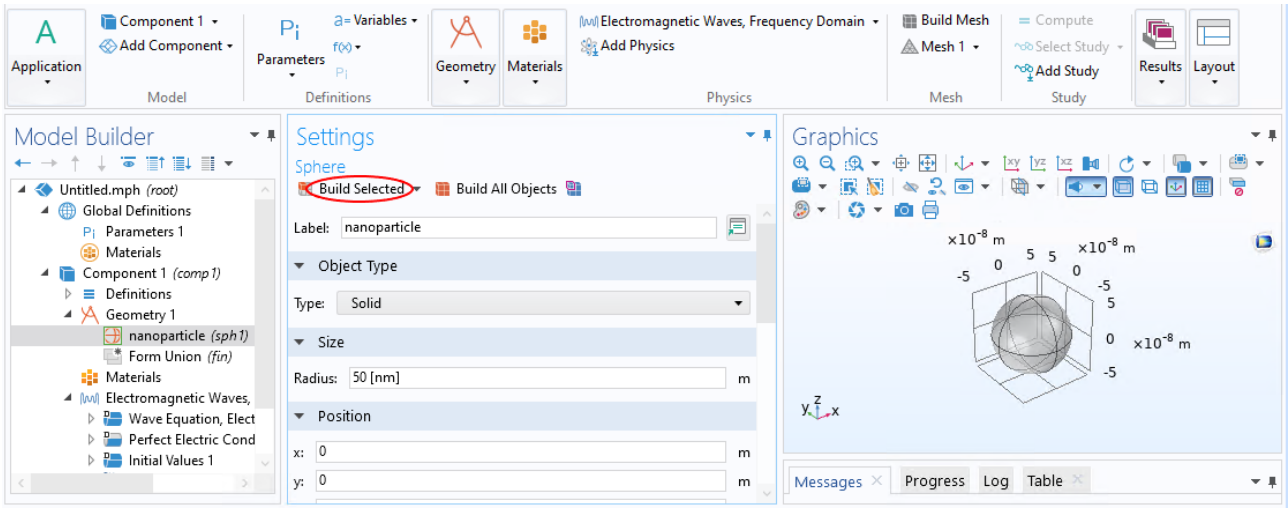

To simulate the medium surrounding the nanoparticle, a second sphere can be built with a sufficiently large radius, e.g. 200 nm for a plasmonic nanosphere of radius 50 nm. For simplicity, a spherical background was chosen for every plasmonic nanostructure investigated, so also for the ones with shapes different from a sphere. The parameters for

the background sphere can be modified as done before for the plasmonic nanoparticle in its settings.

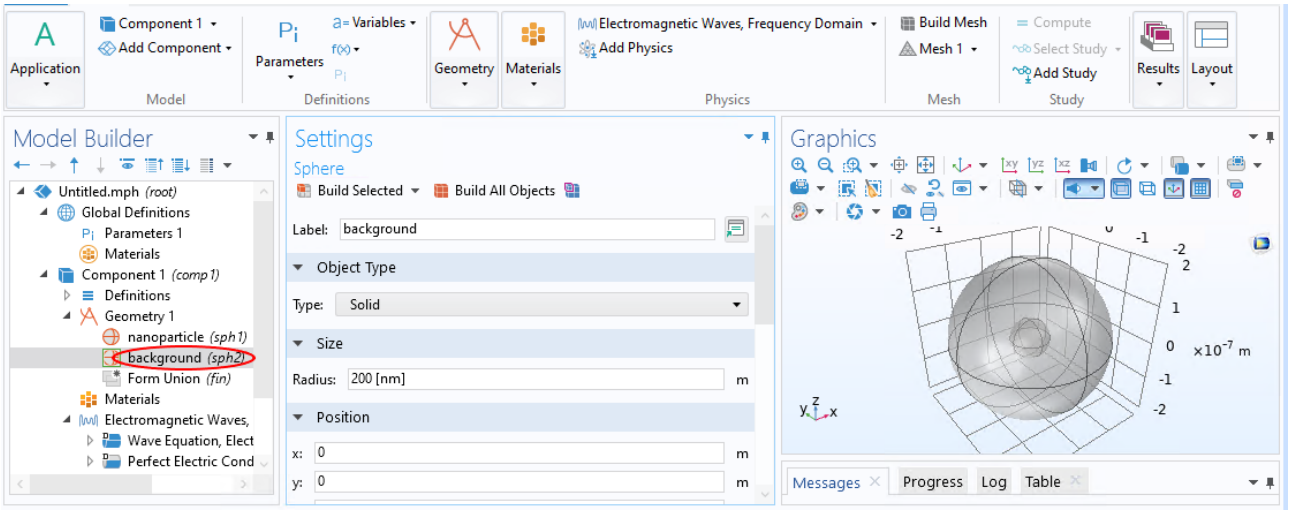

To insert absorbing boundary conditions and hence avoid the problem of reflections from the sphere surrounding the plasmonic particle, the background can be set to contain a perfectly matched layer (PML): this can be done by inserting a layer in the background sphere, by setting in "Layer" the thickness we want for the PML, in our case 50 nm.

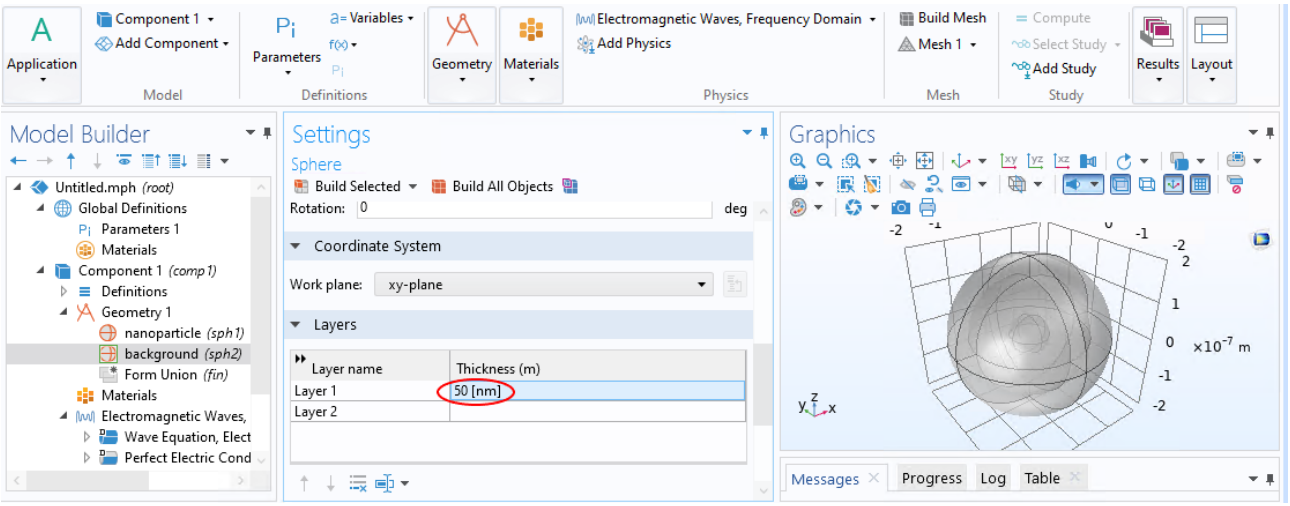

Hence, the PML is used as an absorbing boundary condition that absorbs incident light and minimizes the reflections, so that the numerical solutions will be more stable.

To complete the PML right select "Definitions" and choose "Perfectly Matched Layer".

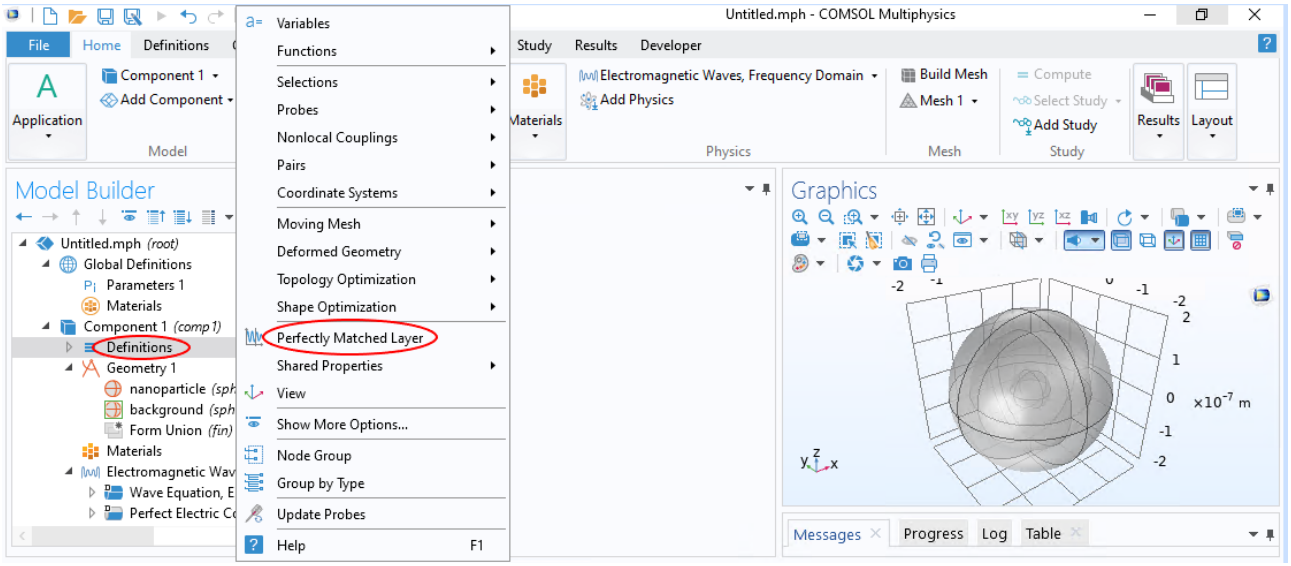

In the "Perfectly Matched Layer" settings, change the geometry type from cartesian to spherical.

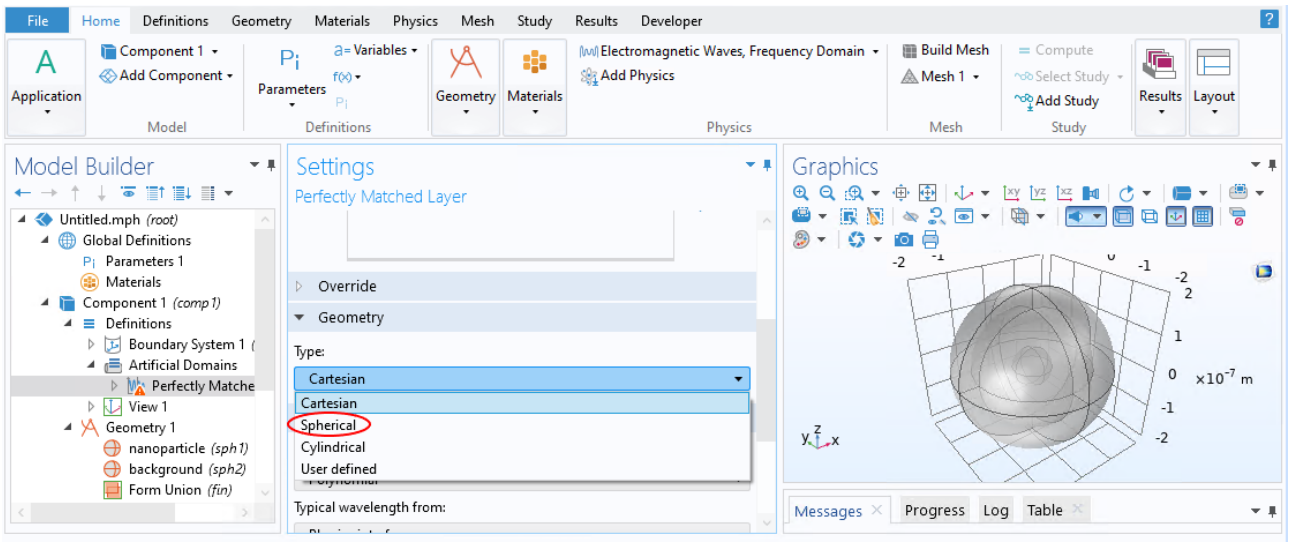

Then, in "Domain Selection", manually select with the mouse each of the eight parts of the outer shell that is going to constitute the PML. The selected parts appear of a darker blue with respect to the other ones.

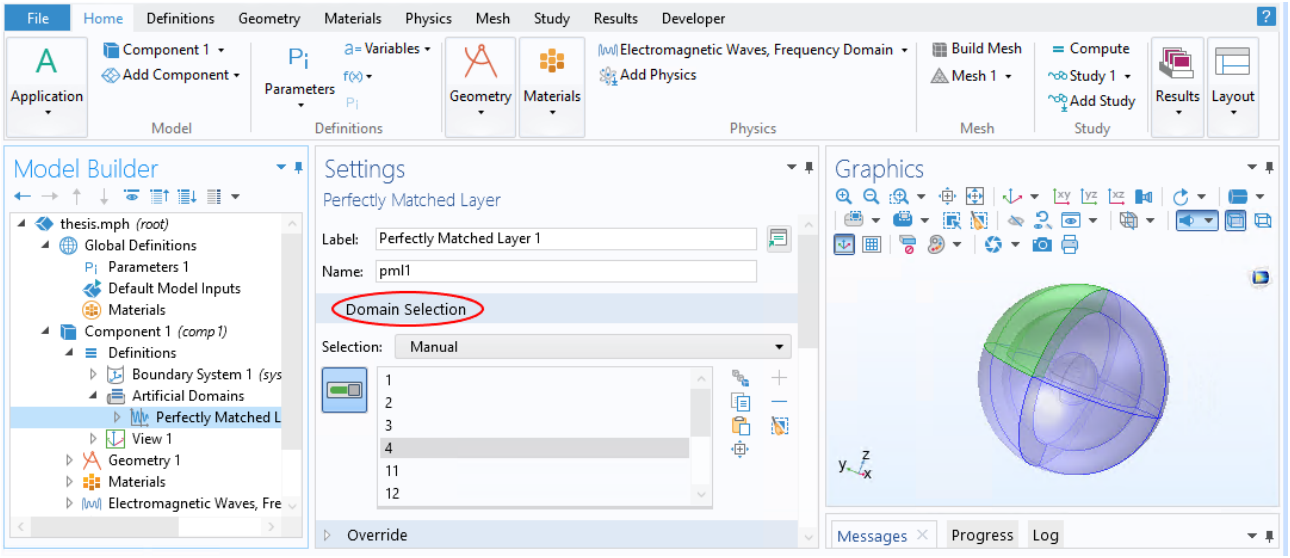

The choice of the materials for these three components is going to be explained in the following step.

2.1.3 Materials

To add the materials of interest, right click on "Materials" under "Component" and select "Add Material from Library".

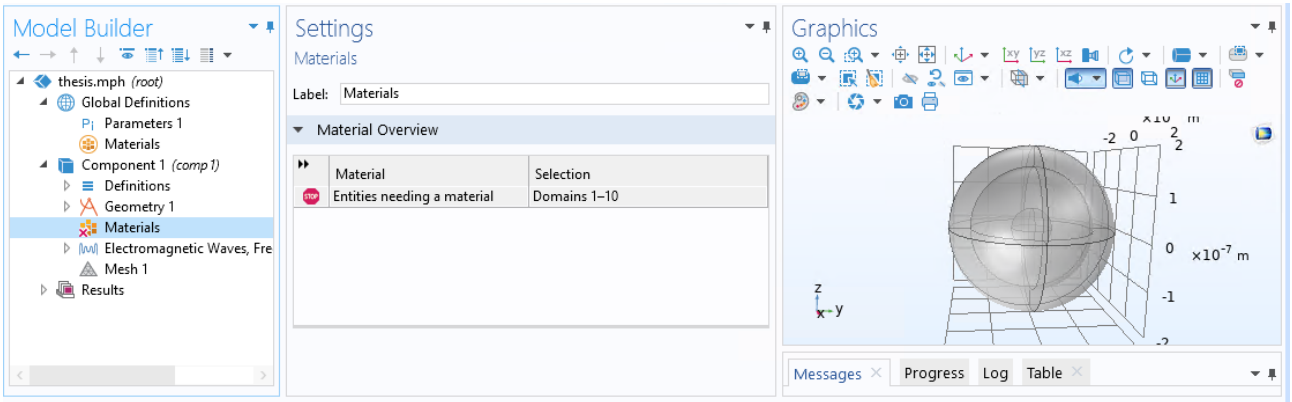

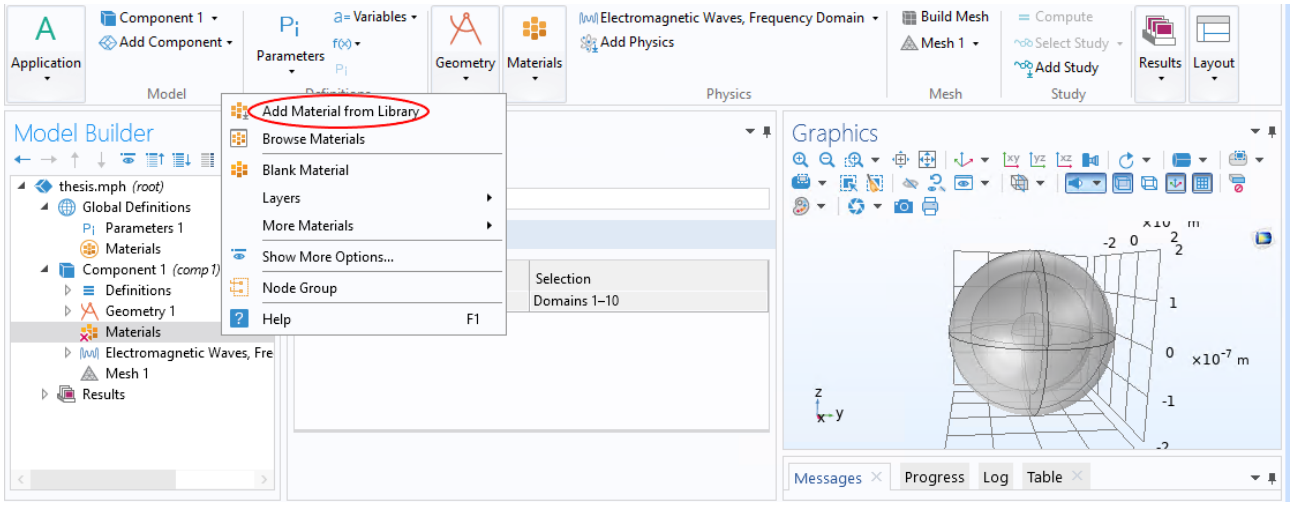

The COMSOL® library offers a wide range of materials to be used, among which metals, dielectrics and so on. For all the plasmonic nanostructures, we have considered gold, for its biocompatibility and great plasmonic properties: we used the Lorentz Drude model, which is a theoretical model that fits experimental values of the real and imaginary part of the refractive index of the metal, as described by Rakie et al [....]. This model can be found under "Optical/Inorganic Materials/Au-Gold/Models and Simulations".

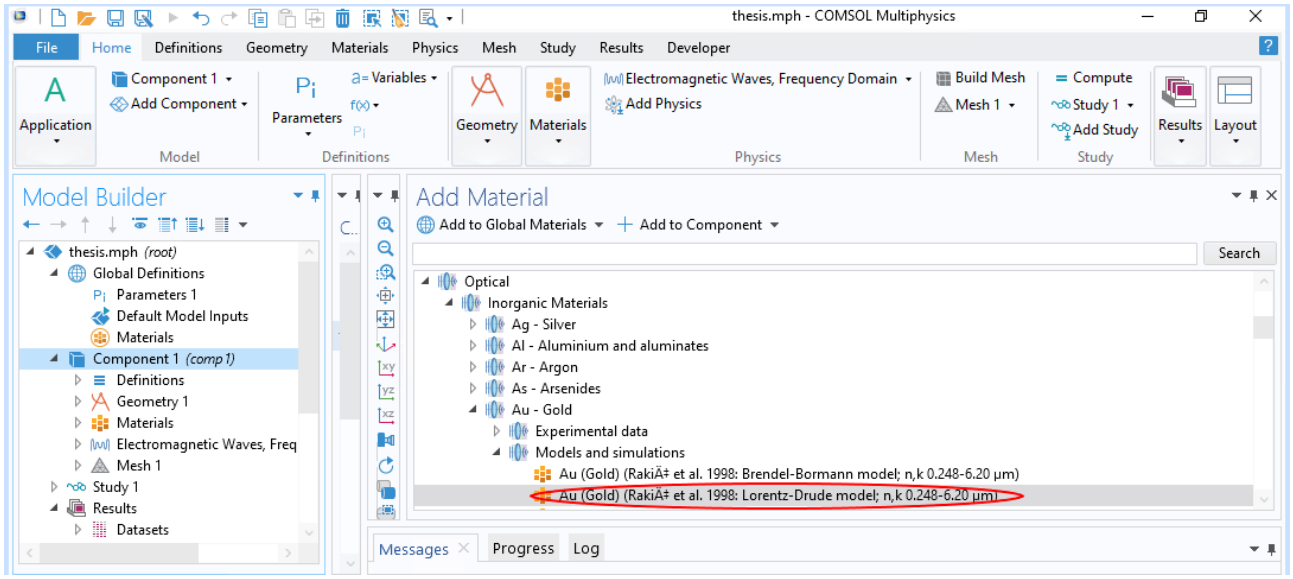

The materials can be added from the library to the component double clicking on them or clicking on "Add to Component".

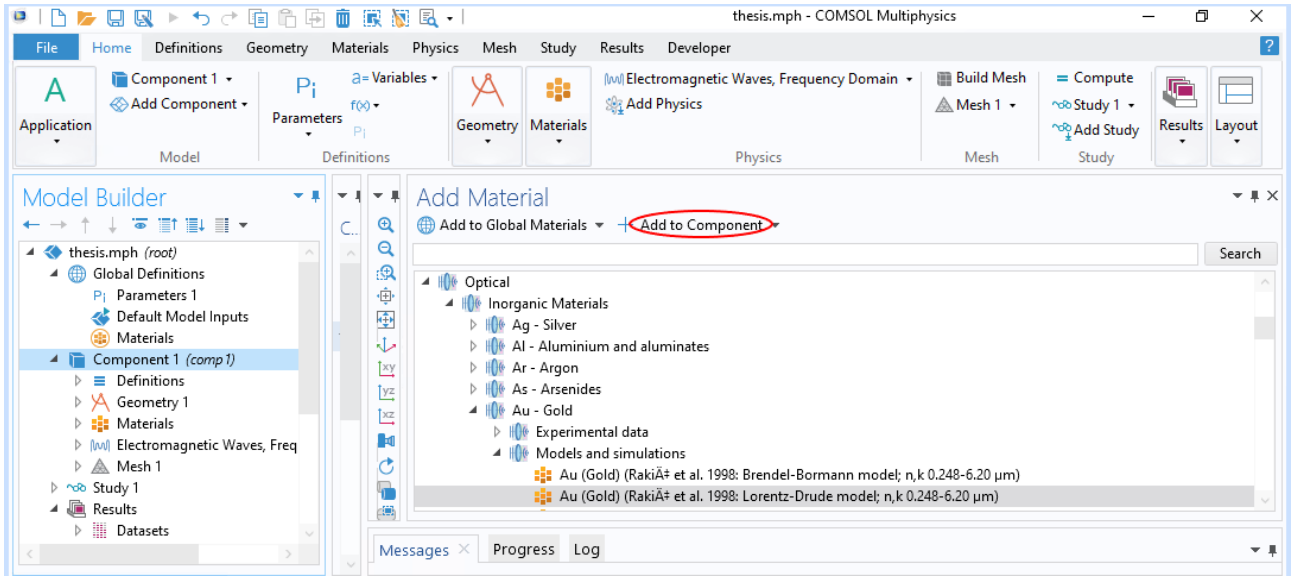

Once the material is added, it is possible to modify its properties if necessary and to select the domain to which it is associated. To associate the right domains to each material, a manula selection is required: this can be done from the material settings. In "Geometric Entity Selection" the selection has to be set to manual, then the elements associated to the material can be selected by clicking on them in the Graphics space.

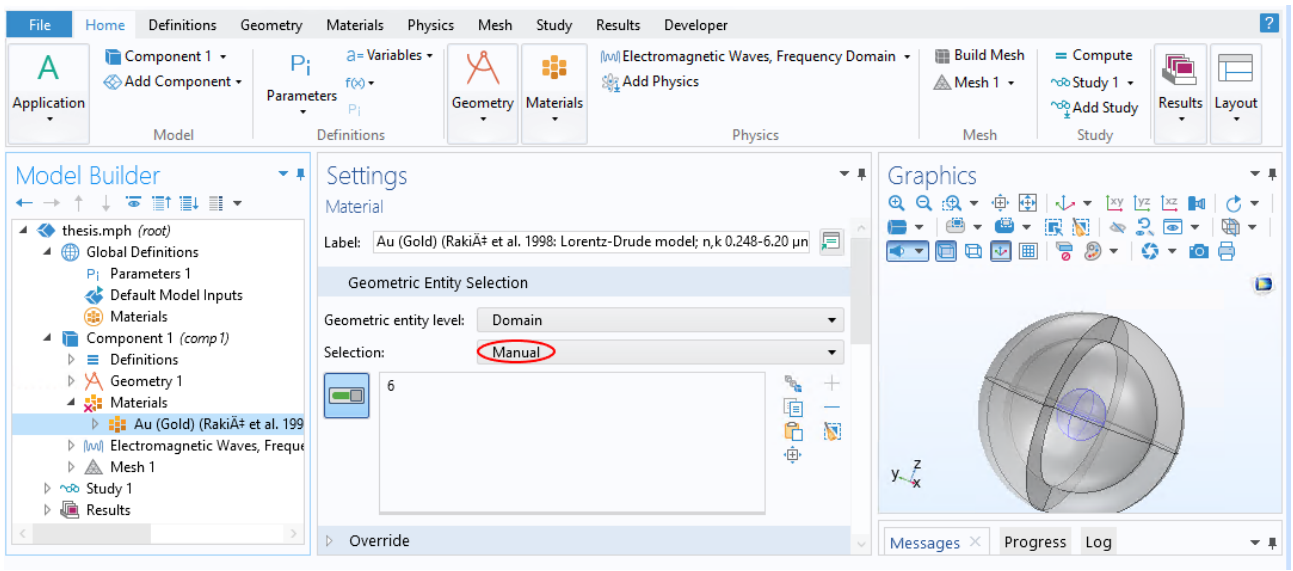

For the background and the PML we used water to simulate a human cell environment, in order to have results as close as possible as the ones that would be obtained in experiments, since cells, also tumoral ones, are mainly constituted by water. The model for liquid water can be found in the library under "Built-in materials/Water, liquid". Add

it to the component.

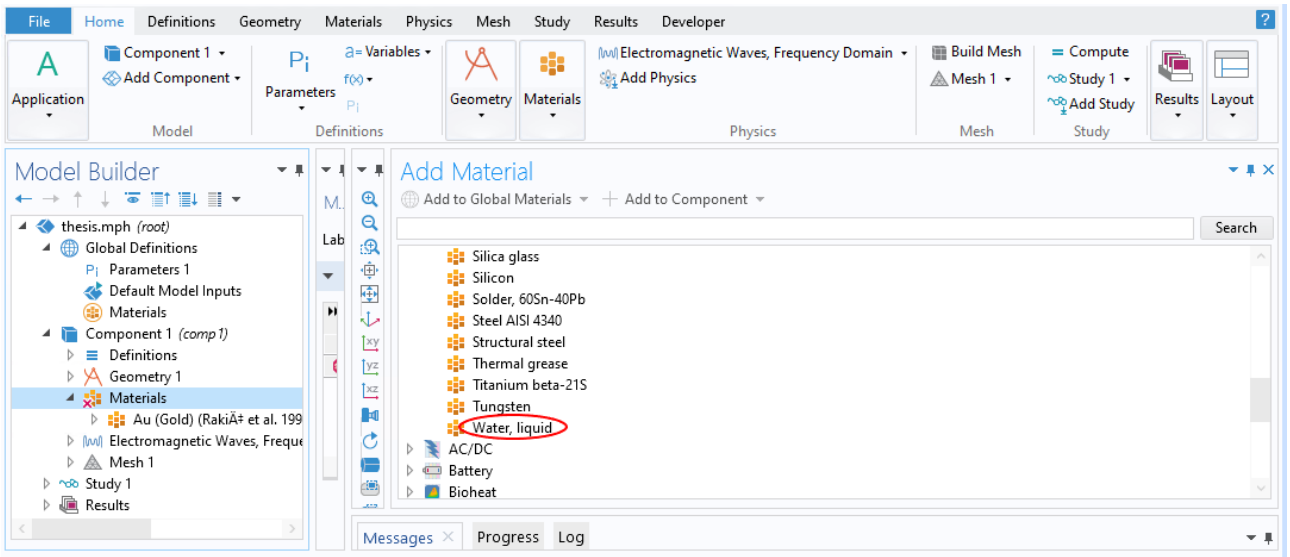

For the selected built in model of water, the real part of the refractive index has to be added manually in "Material Contents". We inserted the value 1.33, which is the real part of the refractive index of water for optical wavelengths, the ones we are interested in for PDT applications.

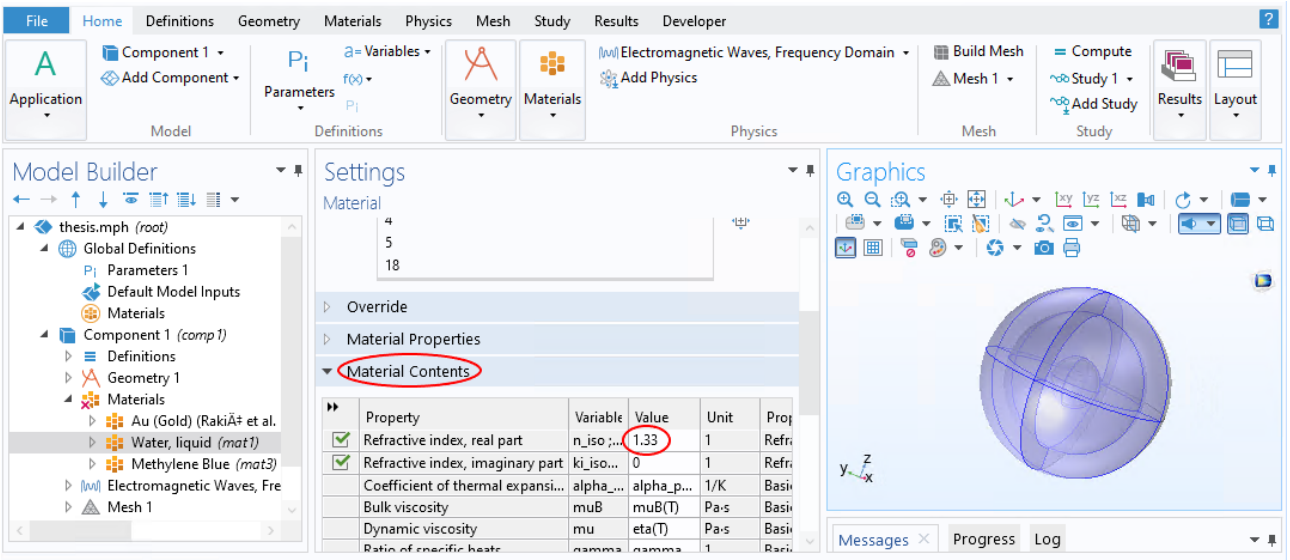

Then select the domains relative to water, which are the background and the PML.

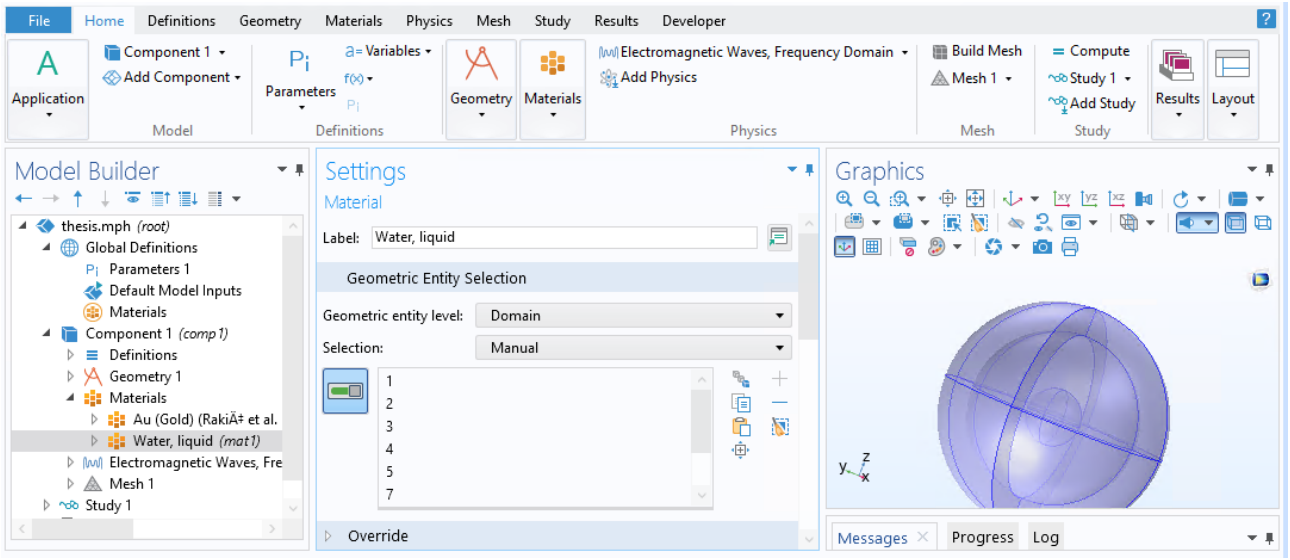

Finally if all the domains have an associated material this is what appears

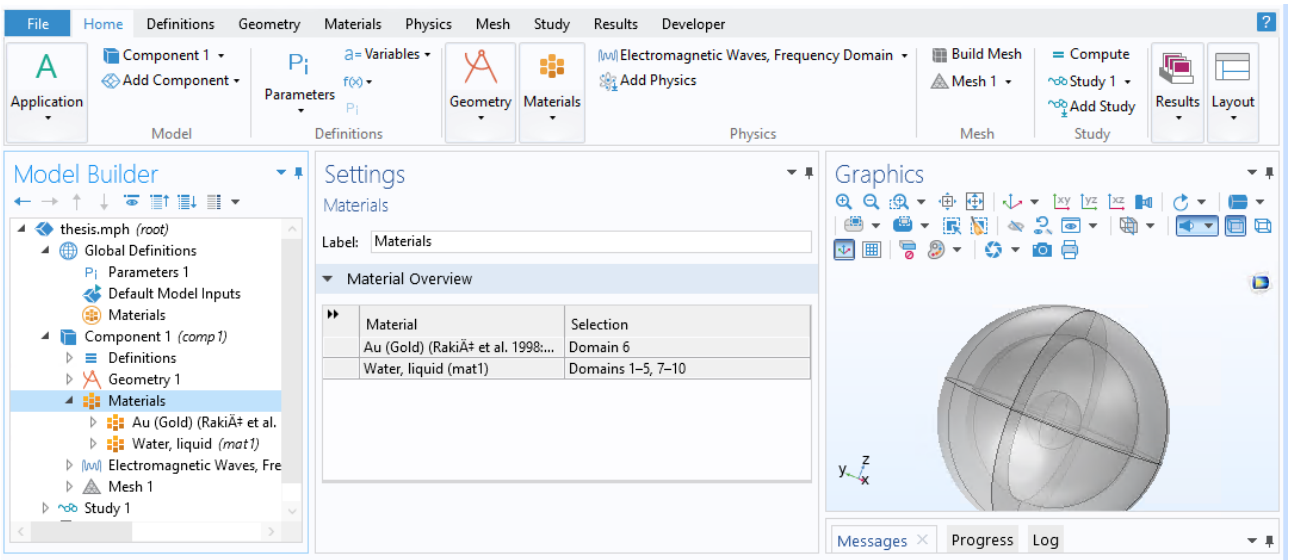

2.1.4 How to set the input electric field

We can now set the input electric field: we decided to use a simple plane wave $E = exp(-jkz)$, polarized along the x axis. To define it in COMSOL® go to "Electromagnetic Waves, Frequency Domain" settings and under "Formulation" change the selection from "Full Field" to "Scattered Field".

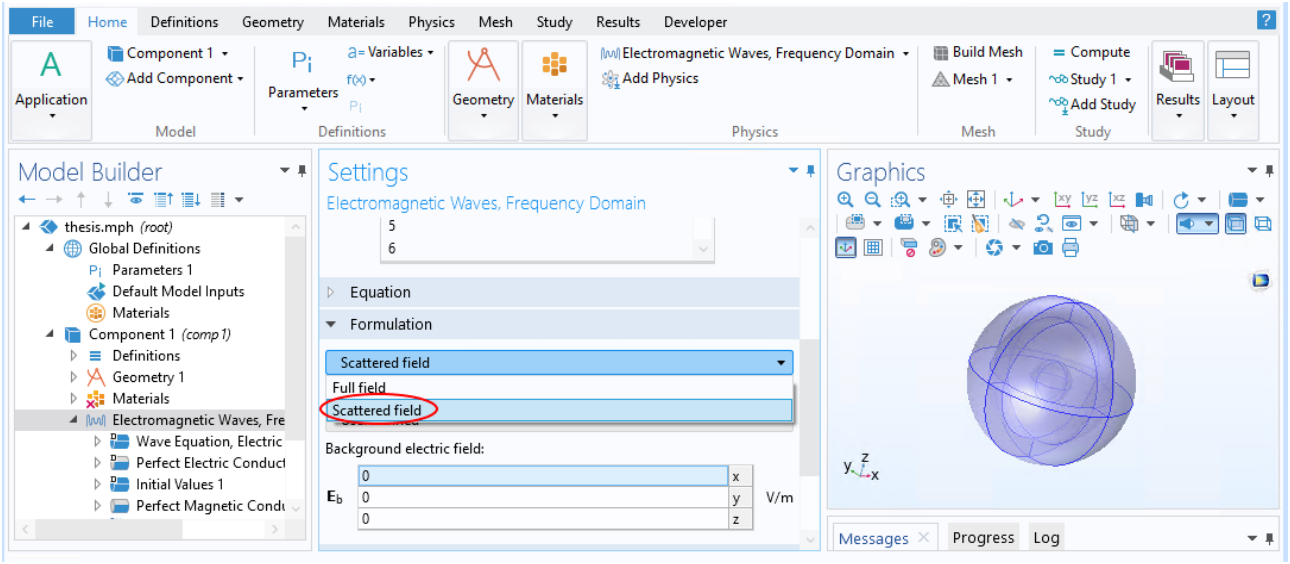

In this way, it is possible to define the background electric field through its components along the x, y, z axes. Since we use an x - polarized wave, we set the x-component as $E_x = exp(-jkz)$, and leave the other two equal to 0. Since we are studying a spherical nanoparticle in this example, the orientation of the linear polarization is not important. However, for asymmetrical structures, the polarization should be chosen oriented along the long axis of the nanostructure, since the main resonance is due to the longitudinal LSPR, the one excited by light polarized parallel to the long axis of the structure.

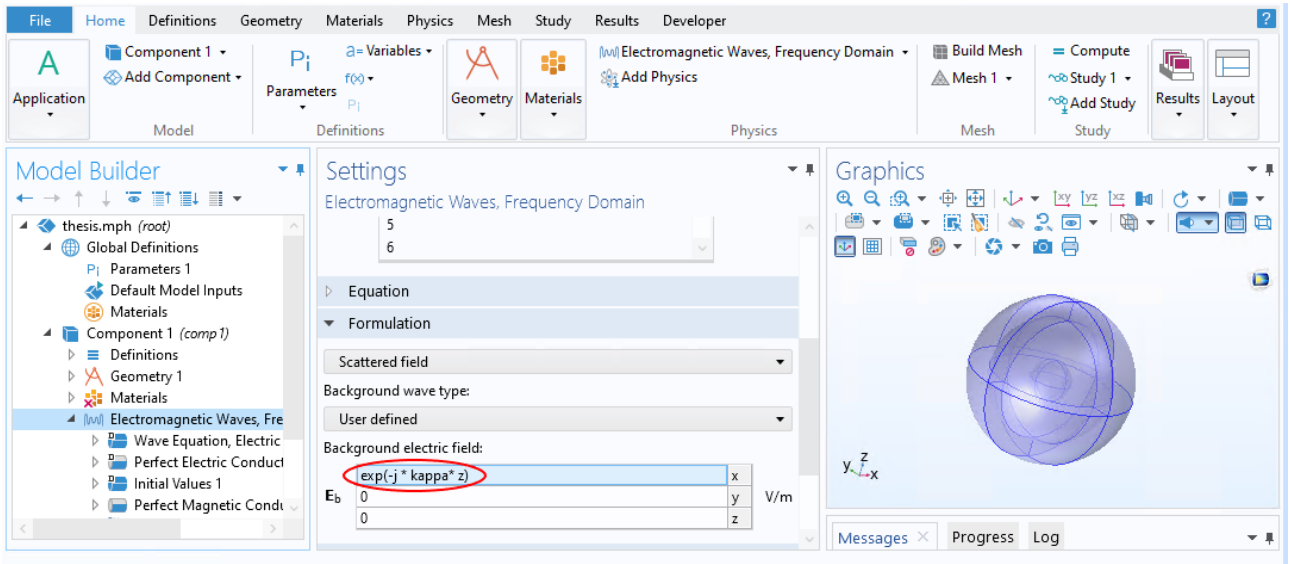

To define the quantities present in the expression we have written for the electric field, we need to define them in "Parameters" as $k_0 = 2pi/\lambda_0$, $\lambda_0 = c/f_0$, where f_0 can be

any frequency of interest, $k = n_b\, k_0$, with n_b is the refractive index of the background in which the metallic nanoparticle is immersed, equal to 1.33 in our example with water.

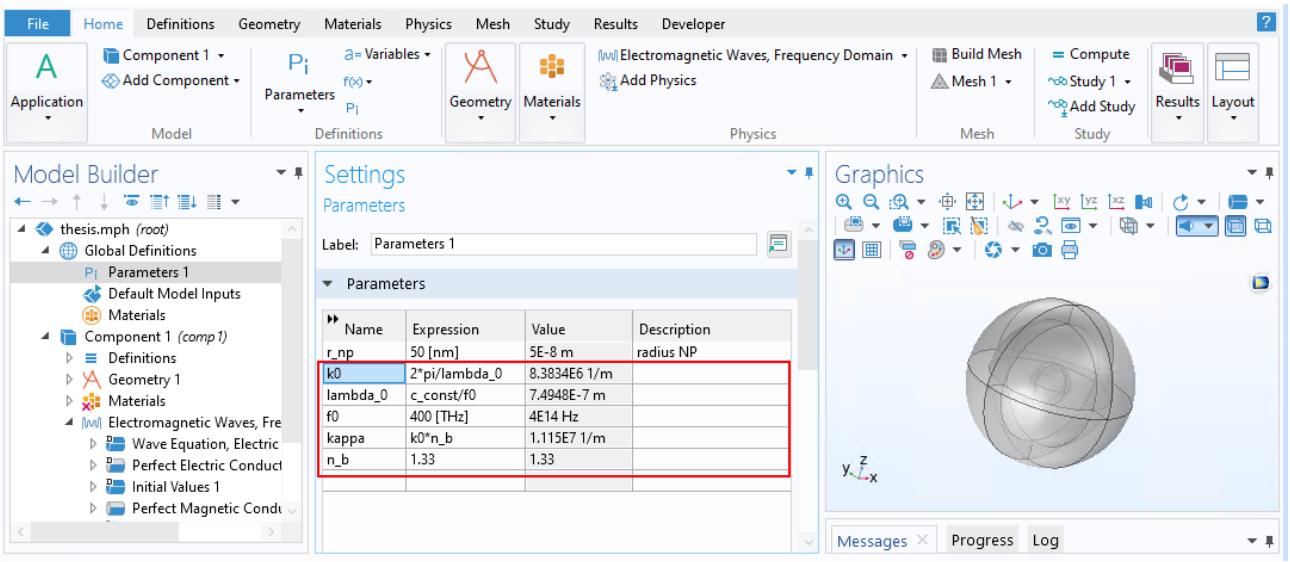

2.1.5 Solving Helmholtz equation

Comsol® is set to solve Helmholtz equation for homogeneous media for the electric field, whose solution will return the values of the scattered field:

$$\nabla \times \mu^{-1} (\nabla \times \boldsymbol{E}) - \omega^2 \varepsilon \boldsymbol{E} = j\omega \boldsymbol{J_f} \quad , \tag{2.1}$$

where $\boldsymbol{J_f} = \sigma \boldsymbol{E}$ is the free charge current, σ is the electric conductivity of the medium, $\varepsilon = \varepsilon_r \varepsilon_0$ is its permittivity, $\mu = \mu_0 \mu_r$ is its permeability. The frequency ω is related to the wavenumber k, for homogeneous media, by $\omega = \frac{k}{\sqrt{\mu\varepsilon}} = \frac{k_0\sqrt{\varepsilon_r}}{\sqrt{\mu\varepsilon}}$, where k_0 is the wavenumber in vacuum .

By rearranging the terms of Helmholtz equation, it can be rewritten as

$$\nabla \times \mu_r^{-1} (\nabla \times \boldsymbol{E}) - k_0^2 \left(\varepsilon_r - j \frac{\sigma}{\omega \varepsilon_0} \right) \boldsymbol{E} = \boldsymbol{0} \quad . \tag{2.2}$$

This equation can be found in COMSOL® in "Model Builder/Electromagnetic Waves, Frequency Domain" settings under "Equation".

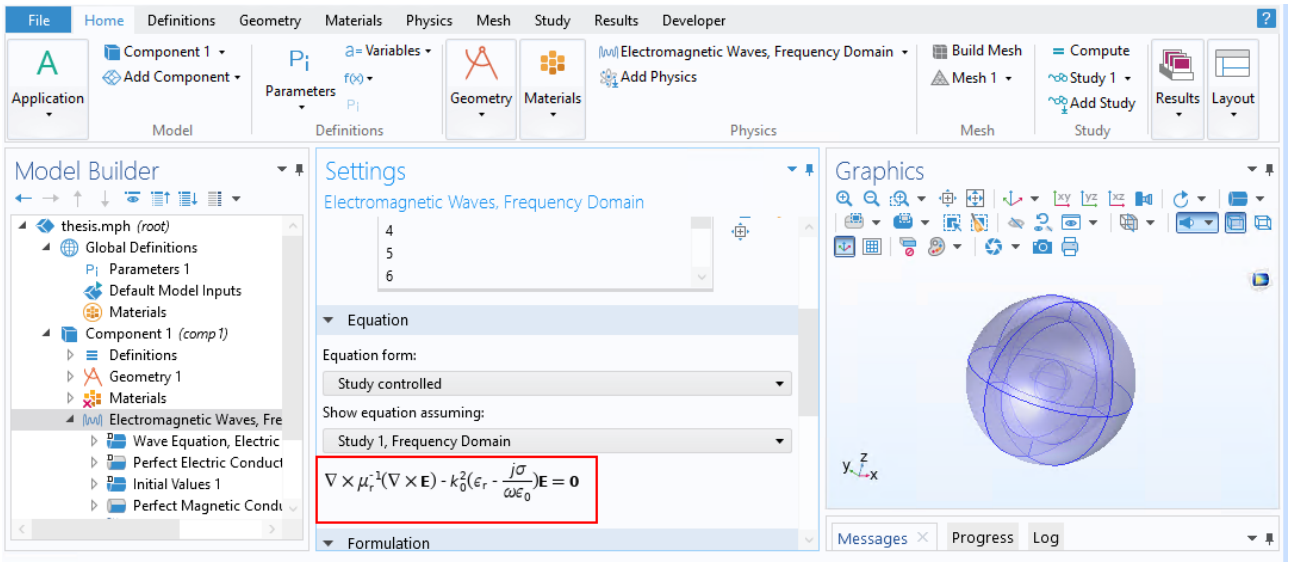

2.1.6 Increasing the speed of simulation: using symmetries

It is possible to increase the speed of the simulation by exploiting the symmetries of the structures we built. This can be done by building a cube with a side placed along the symmetry axis of the metallic nanoparticle. In our example, since we considered a nanosphere, we built a cube with a corner in the center of the nanoparticle to use both its axes of symmetry. The intersection of the cube and the other structures will return a part of them, in this way just an eighth of the nanoparticle and background will be studied.

The cube can be built from "Geometry", as the other objects, by selecting the "Block" element. Its predefined corner position is already set to the center of the system of reference, which in this case coincides with the metallic nanoparticle center. For what concerns the block size, its height, width and depth can be modified under the "Size and Shape" section. We kept all the three parameters equal to 1 µm, but it's sufficient for them to be bigger than the whole background sphere radius, including the PML.

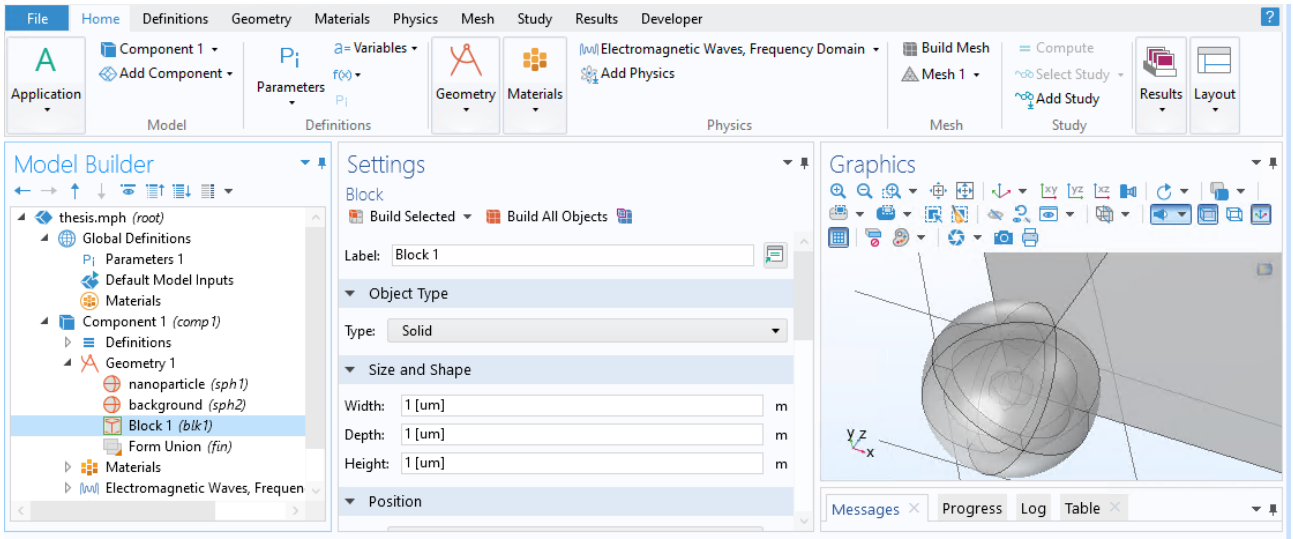

To obtain the intersection between the cube and the two spheres, first the nanoparticle and the background need to be united. To do this, right click on Geometry and select "Union" under "Booleans and Partitions".

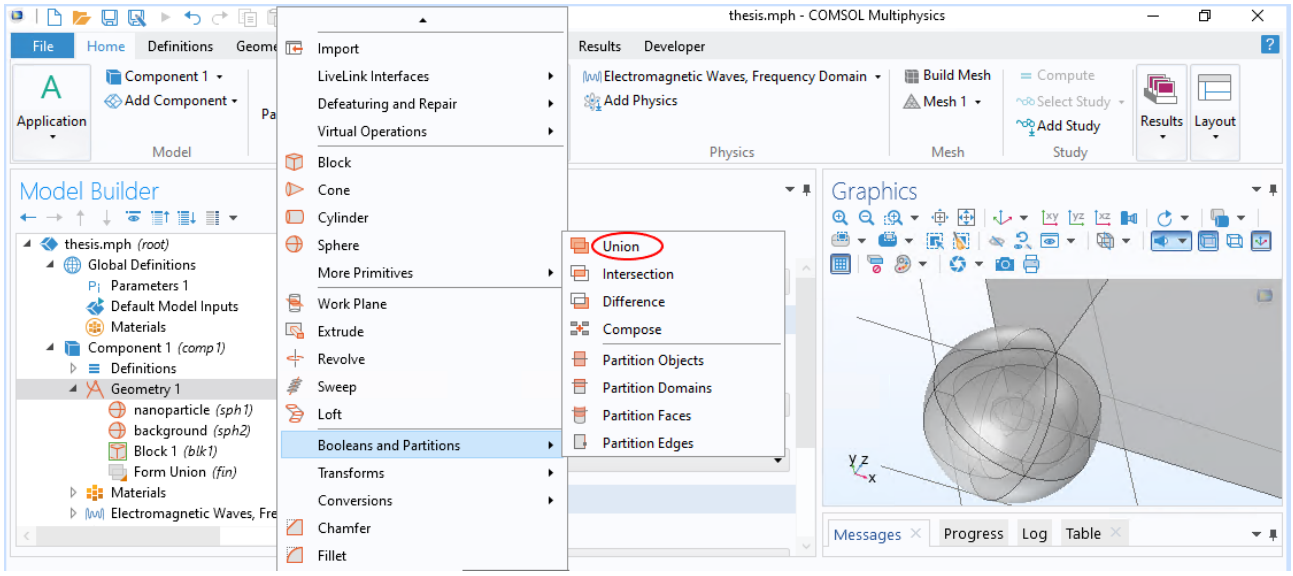

In the built union settings it is possible to select the input objects, which will be the background sphere and the nanoparticle. To select the nanoparticle from the Graphics space, the background sphere can be hidden by selecting the command "Click and Hide" in the Graphics tool bar. The union is completed selecting "Build selected". Then the hidden sections can be shown again selecting "Reset Hiding".

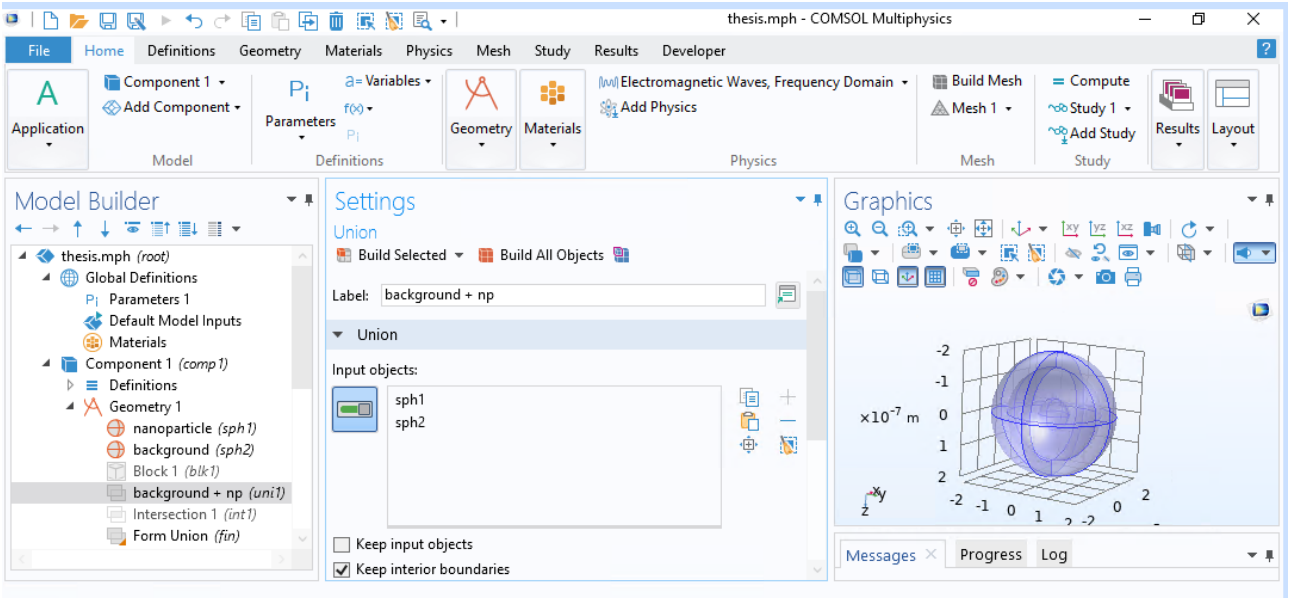

The second step is to right click again on "Geometry" and select "Intersection" under "Booleans and Partitions".

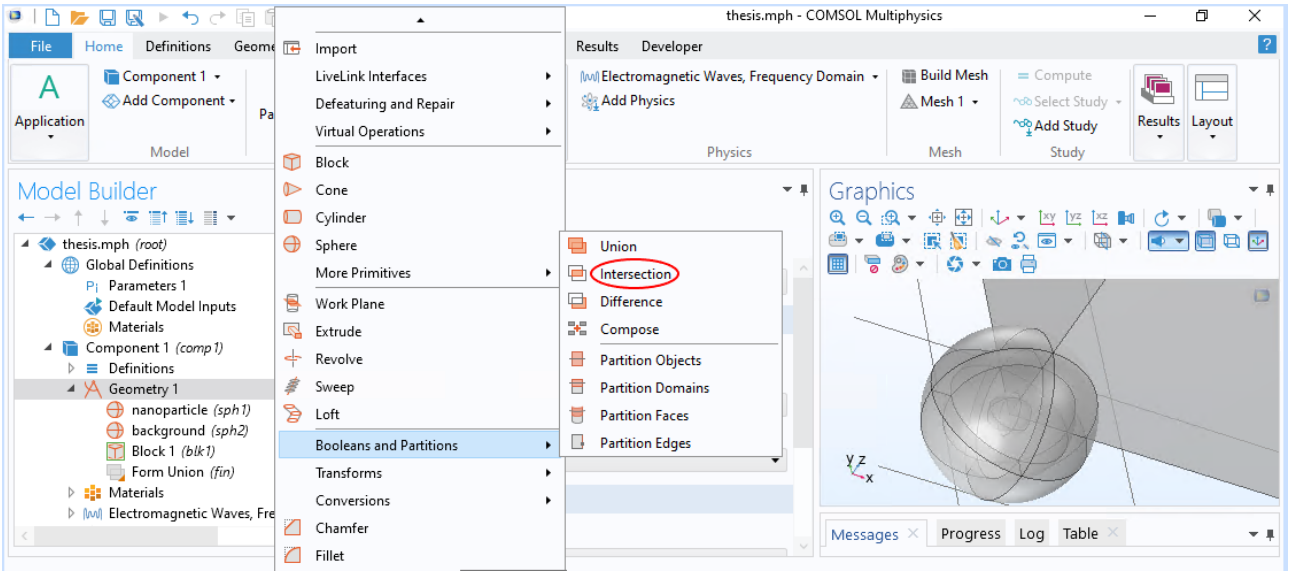

In the input objects section, the union and the block have to be selected. To select the union it is sufficient to click on the background sphere.

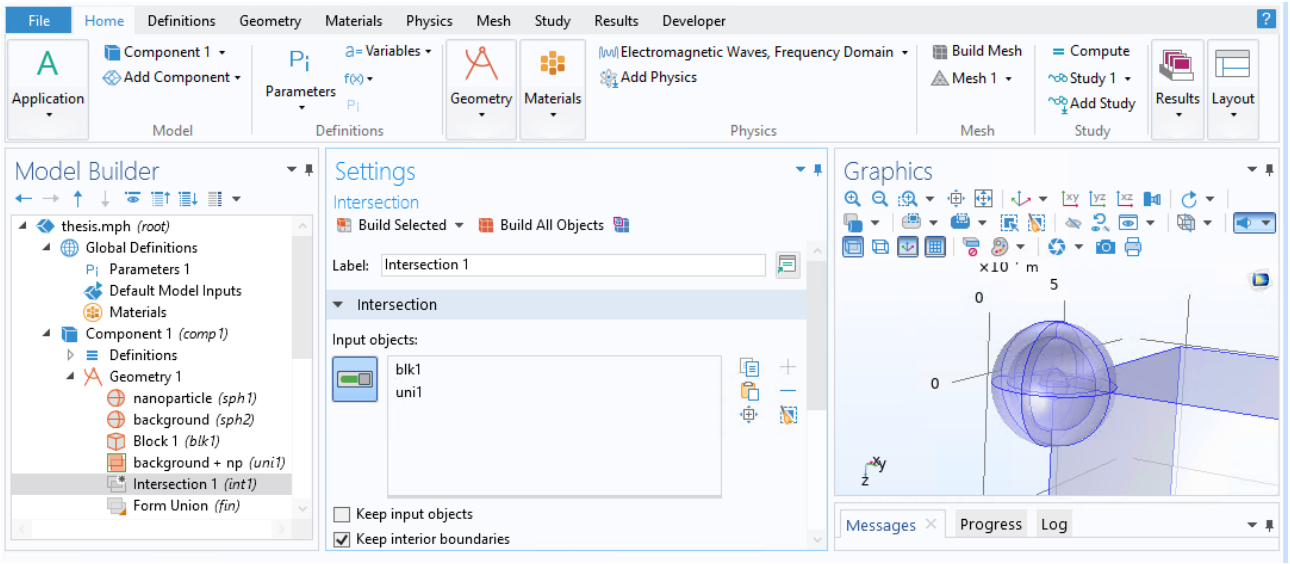

By the "Build All" command an eighth of the whole structure constituted by the nanoparticle, the background and the PML is obtained.

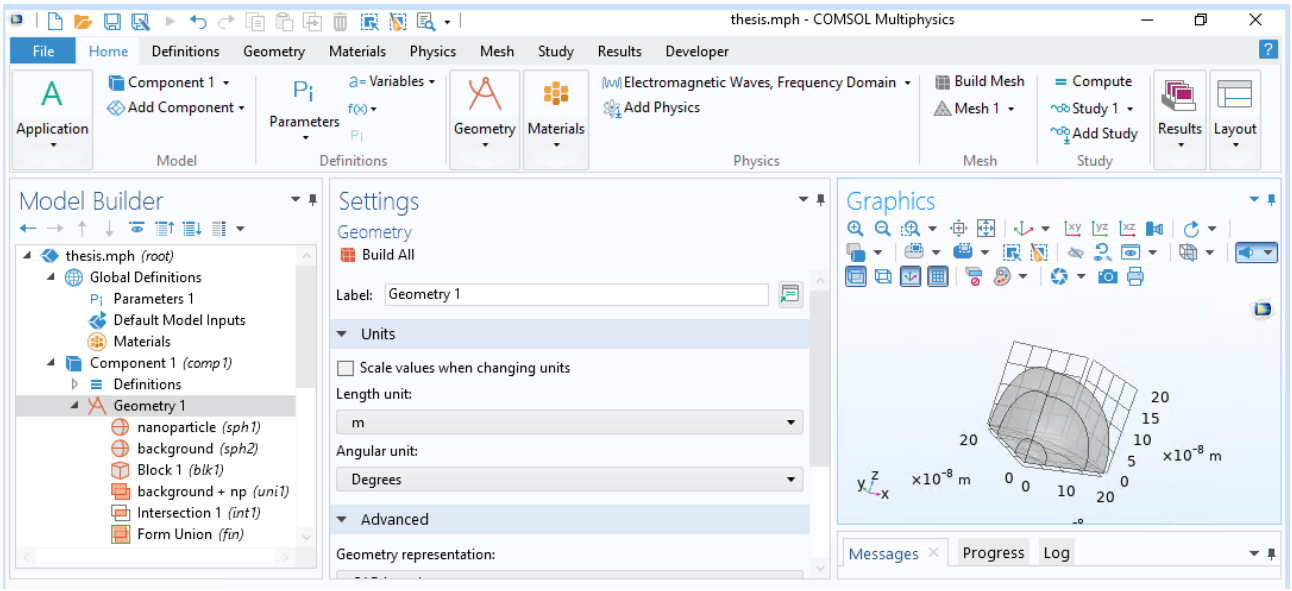

This division of the problem however requires some boundary conditions: we have to choose the perfect magnetic conductor (PMC) on the planes parallel to the magnetic field and perpendicular to the electric one, and the perfect electric conductor (PEC) for the planes parallel to the electric field and perpendicular to the magnetic one. The perfect electric conductor is already present by default, while to add the PMC right click on "Electromagnetic Wave" and select it from the the list.

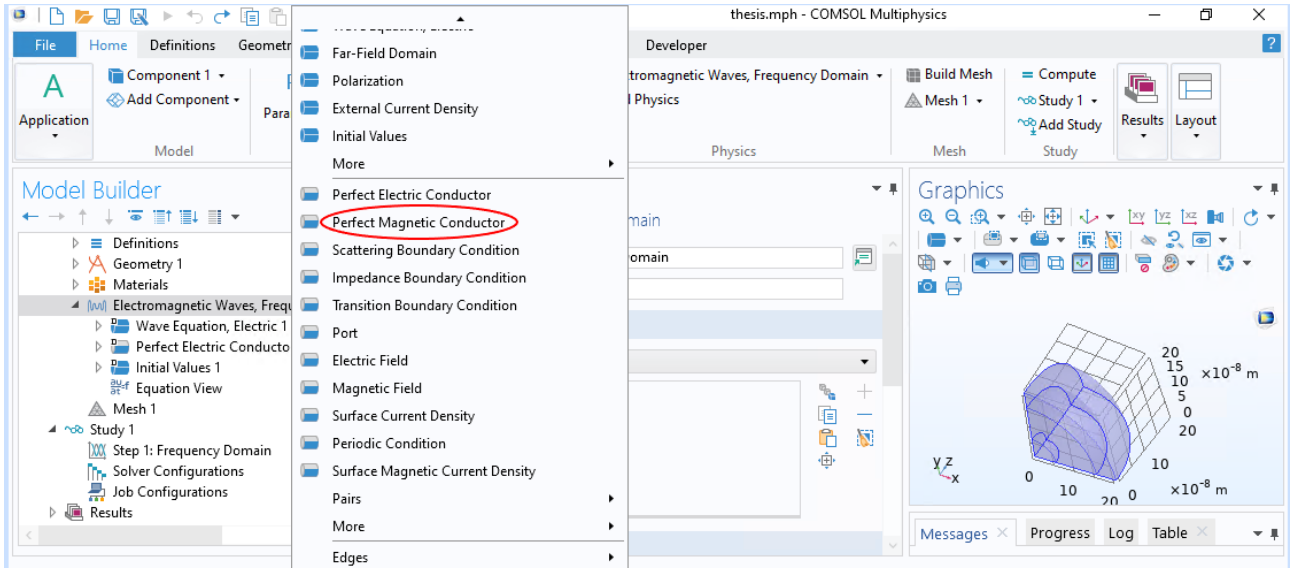

Then we have to manually select the domains. In our example we have chosen the electric field oriented along the x axis and the magnetic field oriented along the y one. Hence we should choose the zy plane as PMC.

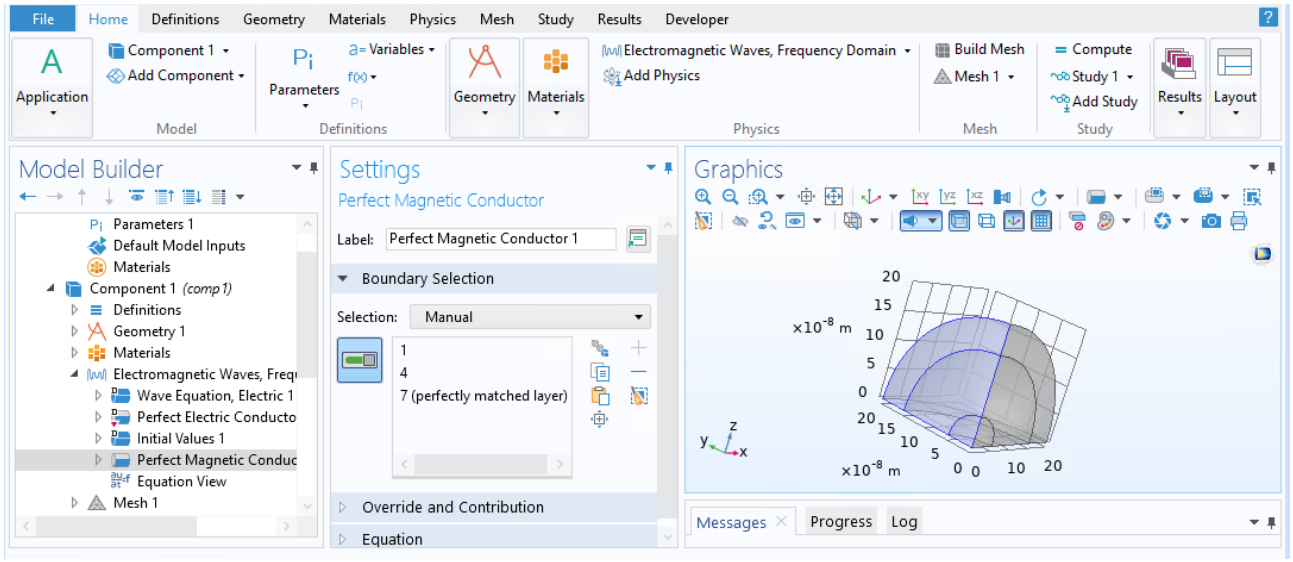

2.1.7 Increasing the speed of simulation: building a mesh

Now we have to build the mesh, which is a critical task to solve the Helmholtz equation, as it defines the number of finite elements that will constitute the objects we have built. The mesh quality, i.e. the size of each element, directly affects the computation time, the memory used to solve the problem and the accuracy of the solution. For larger elements

of the mesh the computation of the solution will be faster, but the solution will be less accurate, and the viceversa holds for smaller elements.

We start doing the mesh of the smaller objects. Right click on "Mesh" and select "Free Tetrahedral".

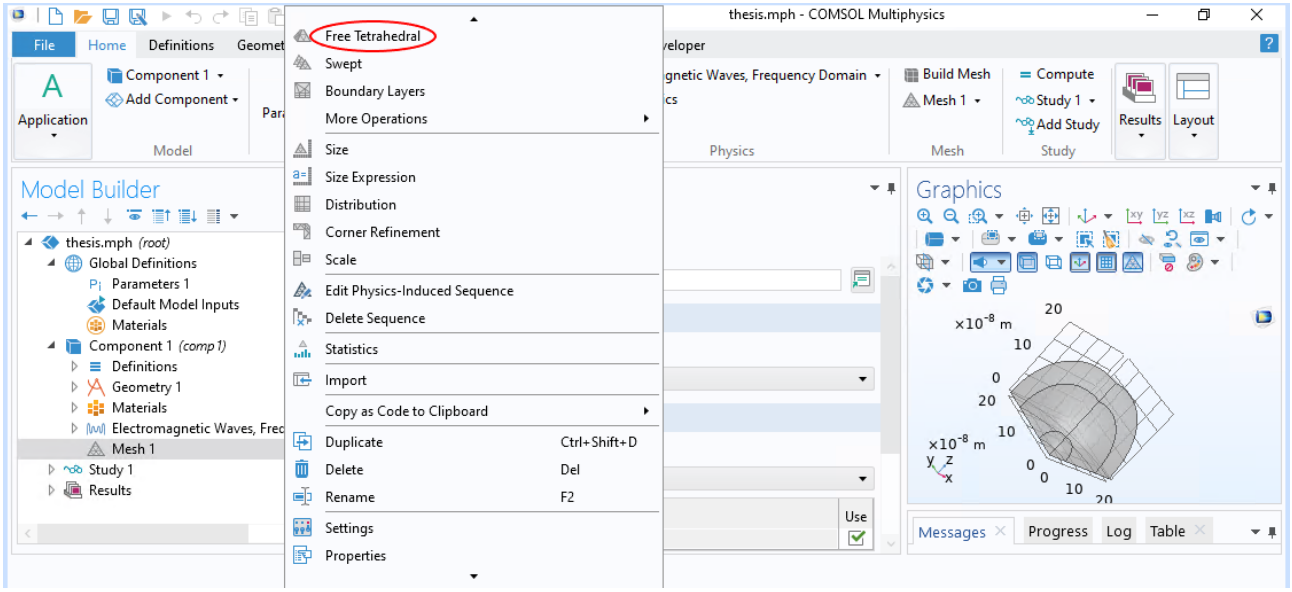

In the settings, under "Domain Selections" choose as "Geometric entity level" "Domain" and select the nanoparticle.

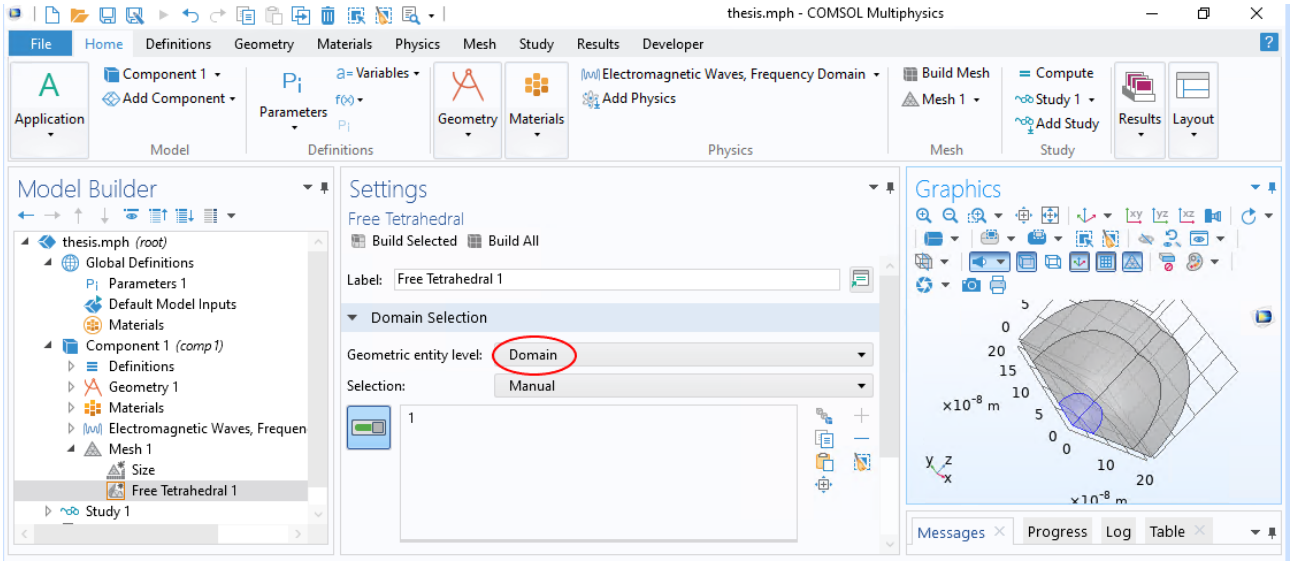

To modify the size of the mesh elements, right click on "Free Tetrahedral 1" and select "Size".

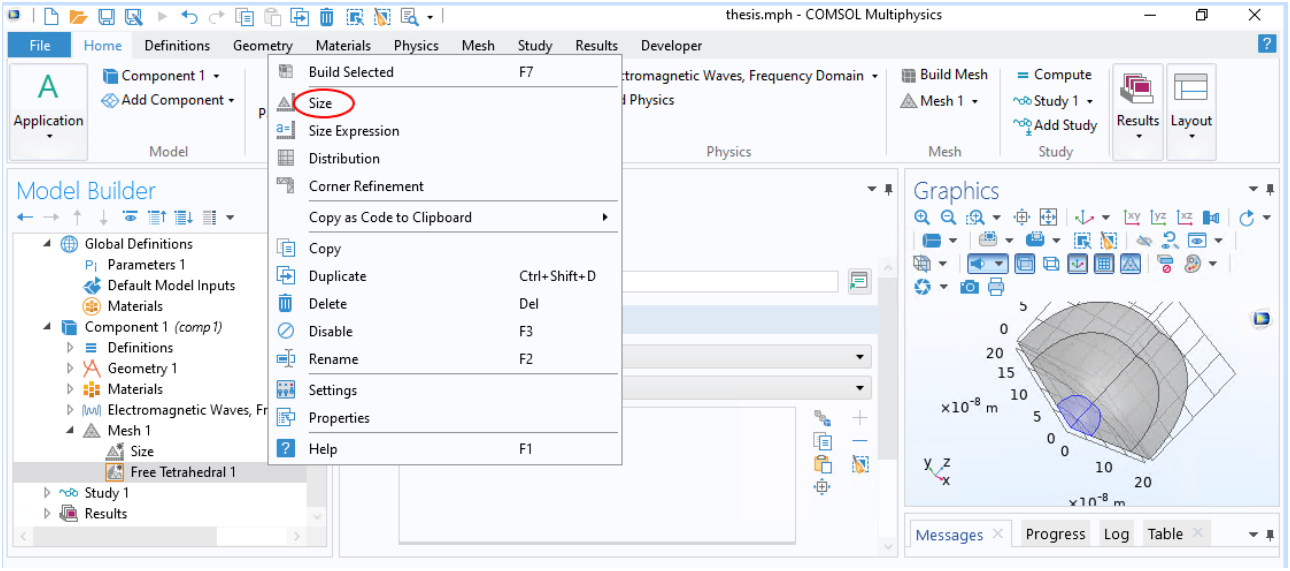

In the settings under "Element Size" select "Custom". Then in "Element Size Parameters" check the "Maximum Element Size" box and modify the predefined value. If the solution does not converge for the chosen values, they can be modified and reduced. For the 50 nm radius sphere we chose a maximum element size for the nanoparticle mesh elements of 15 nm. By clicking "Build Selected", the mesh will appear on the nanoparticle in the Graphics space.

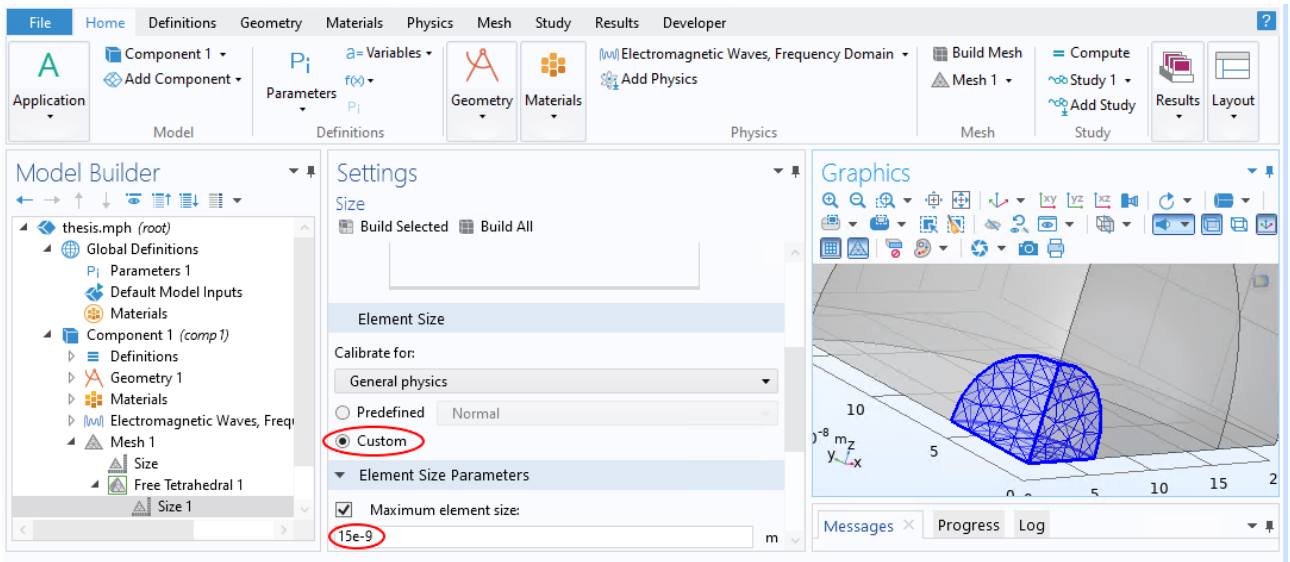

Next, to build the finite elements mesh for the background, PML excluded, right click on "Mesh" and select again "Free Tetrahedral". Select the domain around the nanoparticle, and then modify the maximum elements size as done before. We chose as value for the

background elements 90 nm.

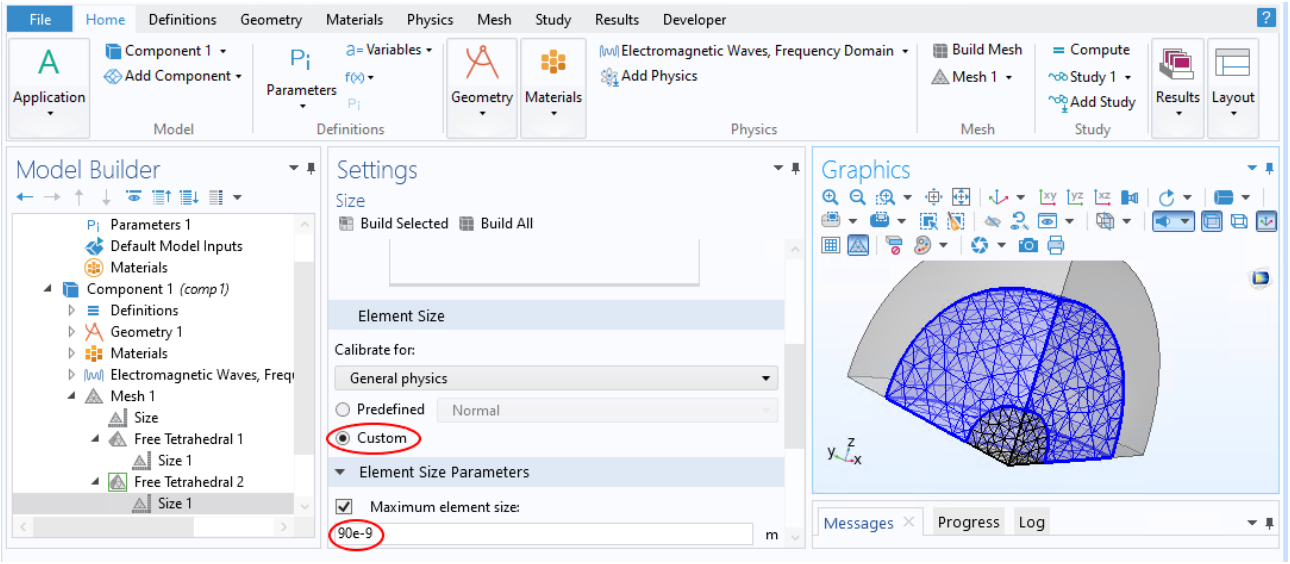

For the PML we are going to make a projection of the background surface onto the PML shell. To do this, right click on "Mesh" and select "Swept".

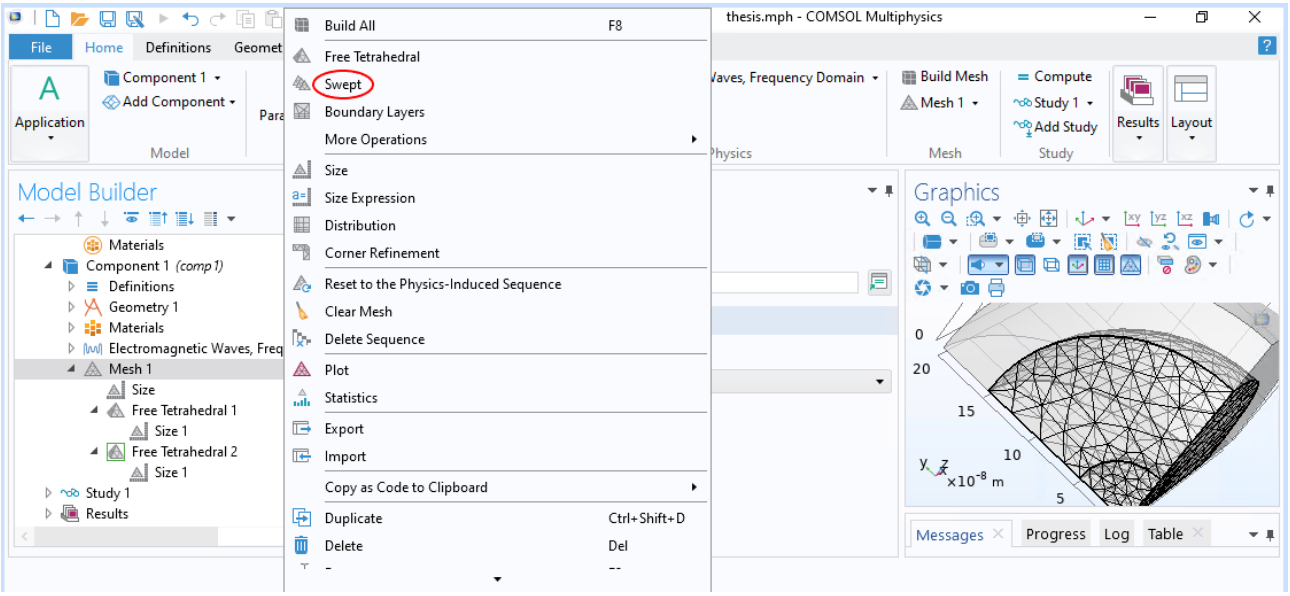

Under "Domain Selection" it is sufficient to select as "Geometric Entity Level" "Remaining".

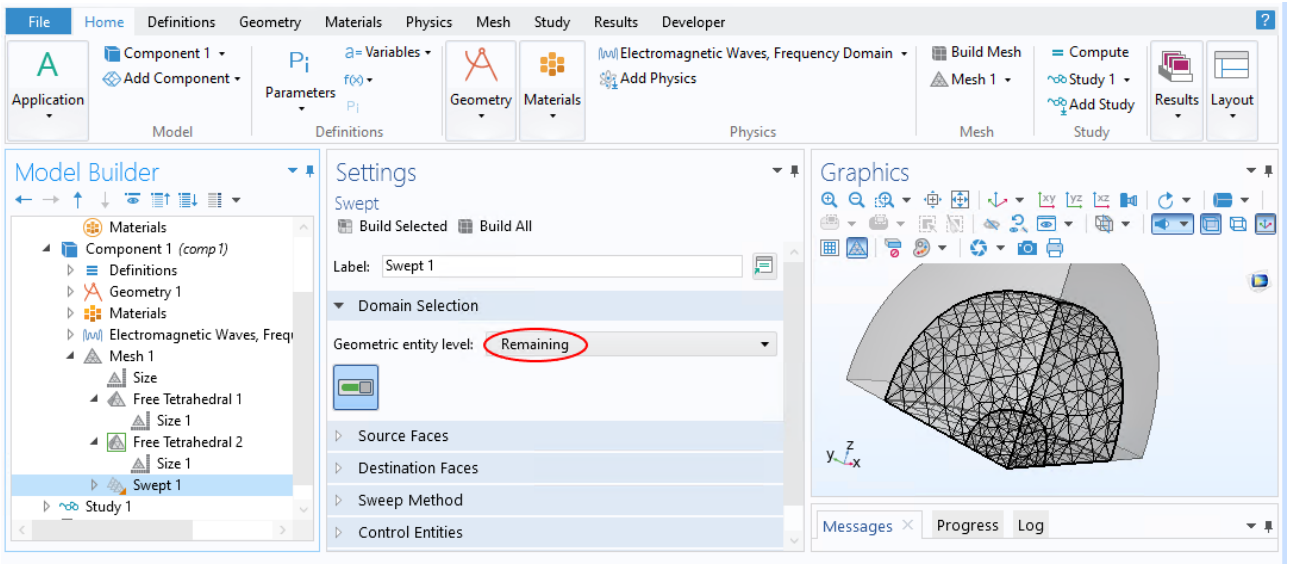

Then right click on "Swept" and select "Distribution", to specify on how many layers the PML should be divided into.

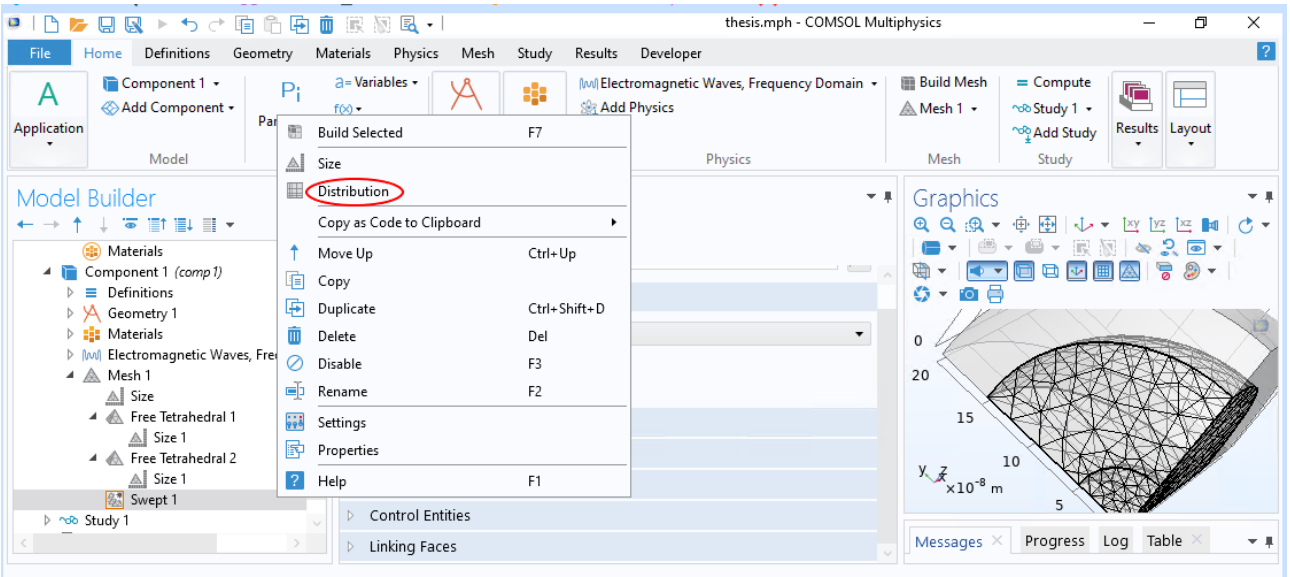

In the "Distribution" "Domain Selection" manually pick the PML domain and under "Distribution" the number of elements can be modified. It is recommended to use 6 to 8 layers for the PML, we used 8.

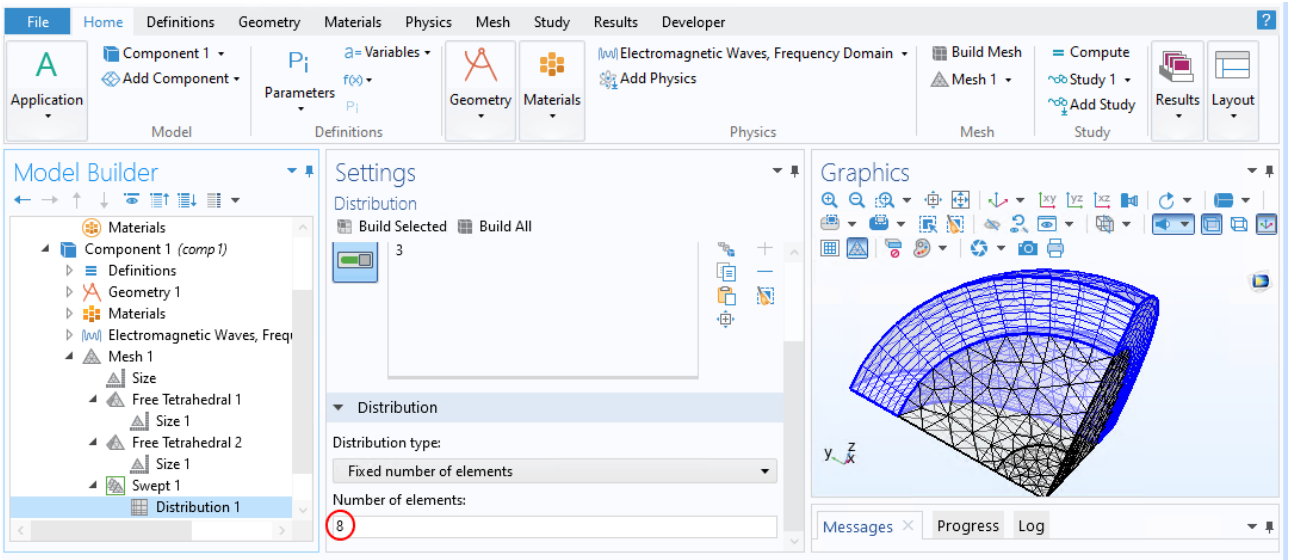

2.1.8 Setting the frequency range to study

The study that we want to make has to be added: click on "Add Study" in the "Home" tool bar.

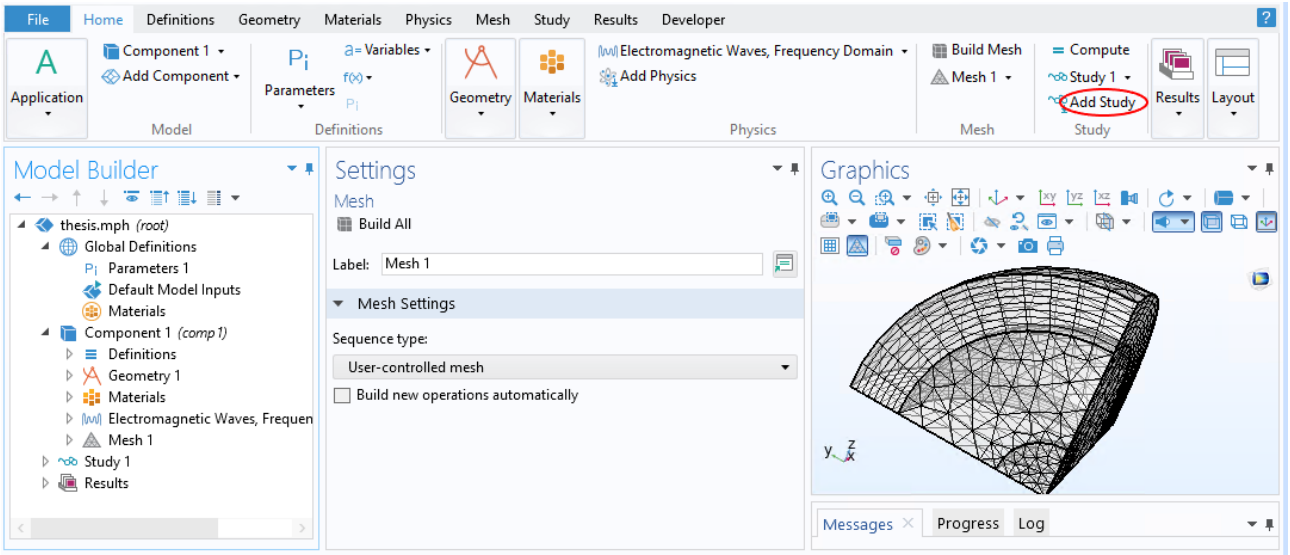

Then select, under "General Studies", "Frequency Domain" and click on "Add Study".

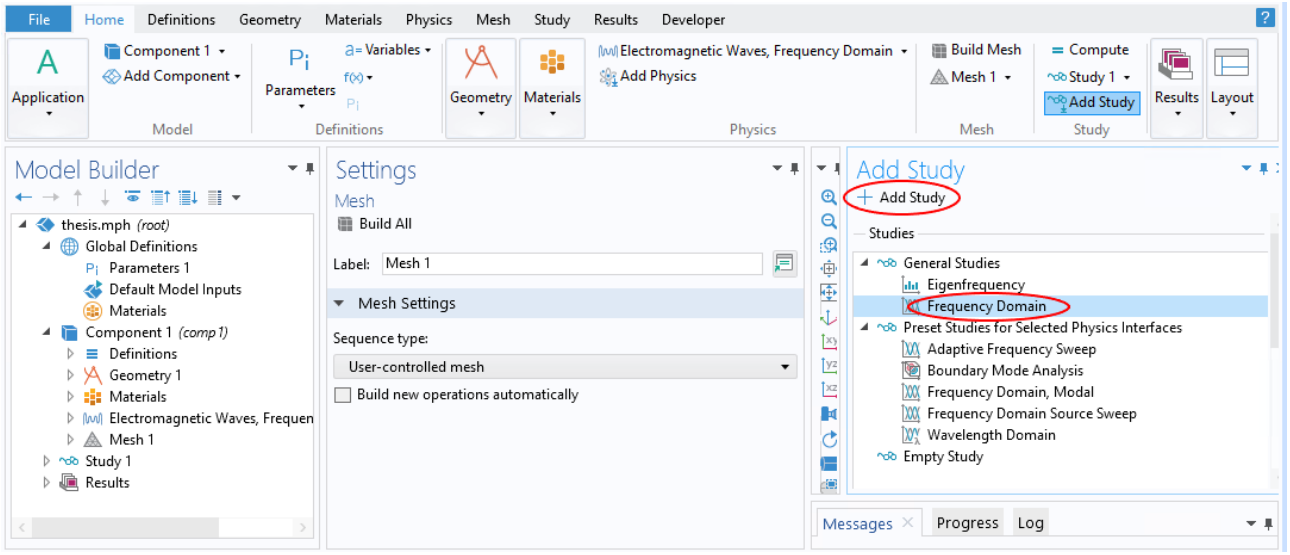

Under "Study 1" select "step 1: frequency domain" and in "Study Settings" set the frequency unit to Hz and as frequencies set $f0$, which we have previously defined in the "Global Parameters".

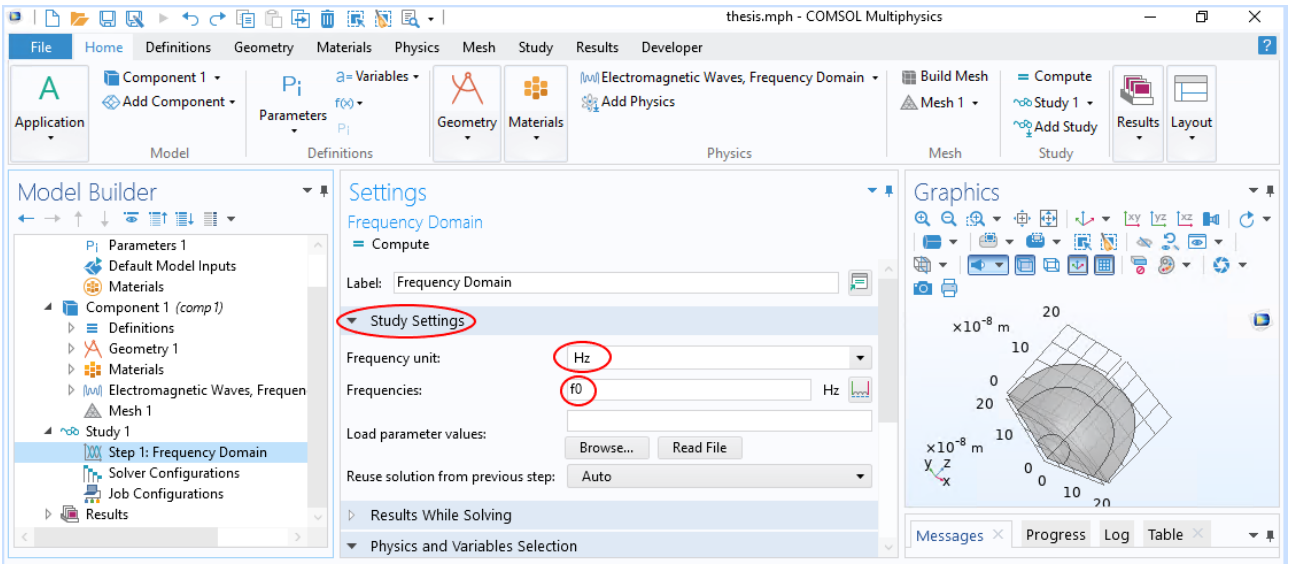

To set a range of frequency to run the simulation, right click on "Study 1" and select "Parametric Sweep".

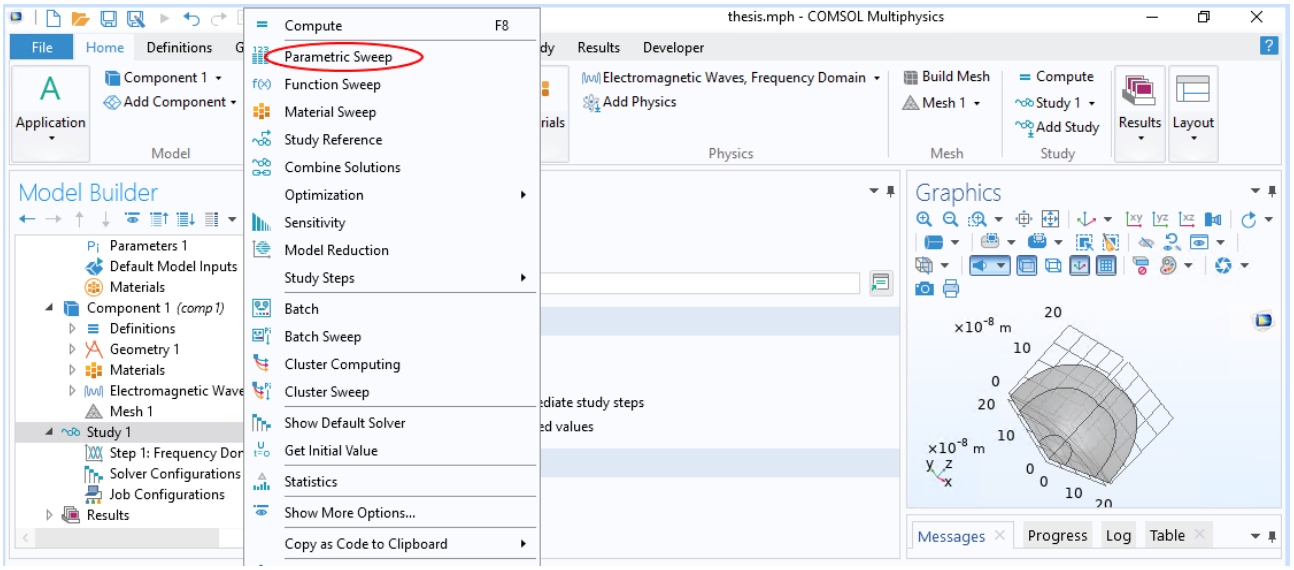

In the "Parametric Sweep" settings, under "Study settings" change the sweep from "Specified Combinations" to "All Combinations", then click on the "Add" button to add the parameter whose value we want to change.

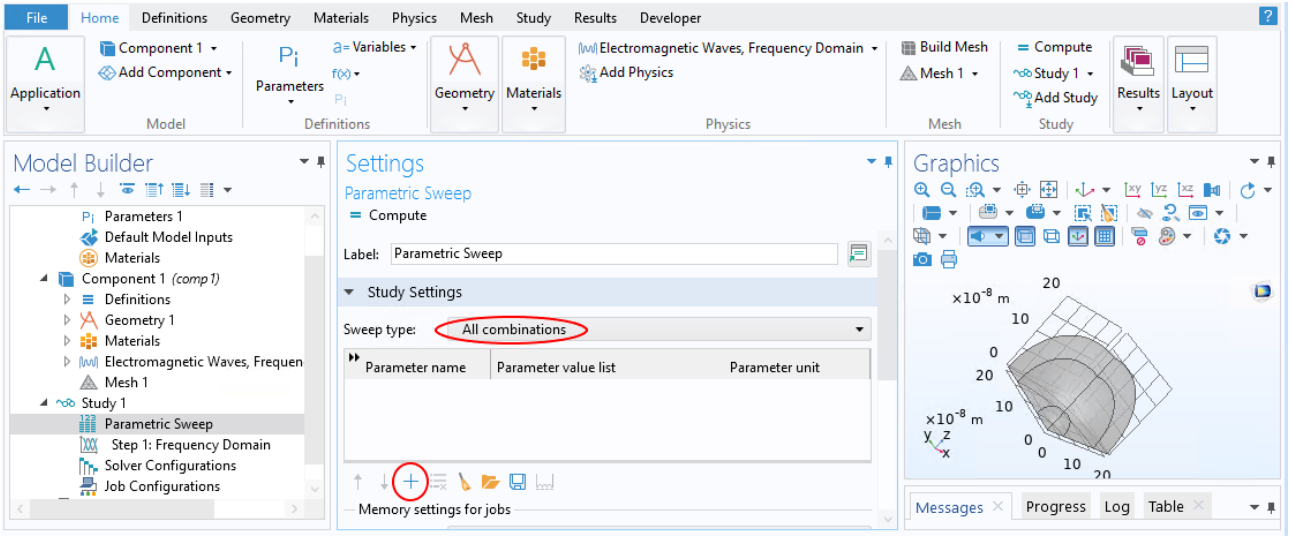

Under "Parameter Name" a list will appear, which contains the parameters that have been defined in the "Global Definitions".

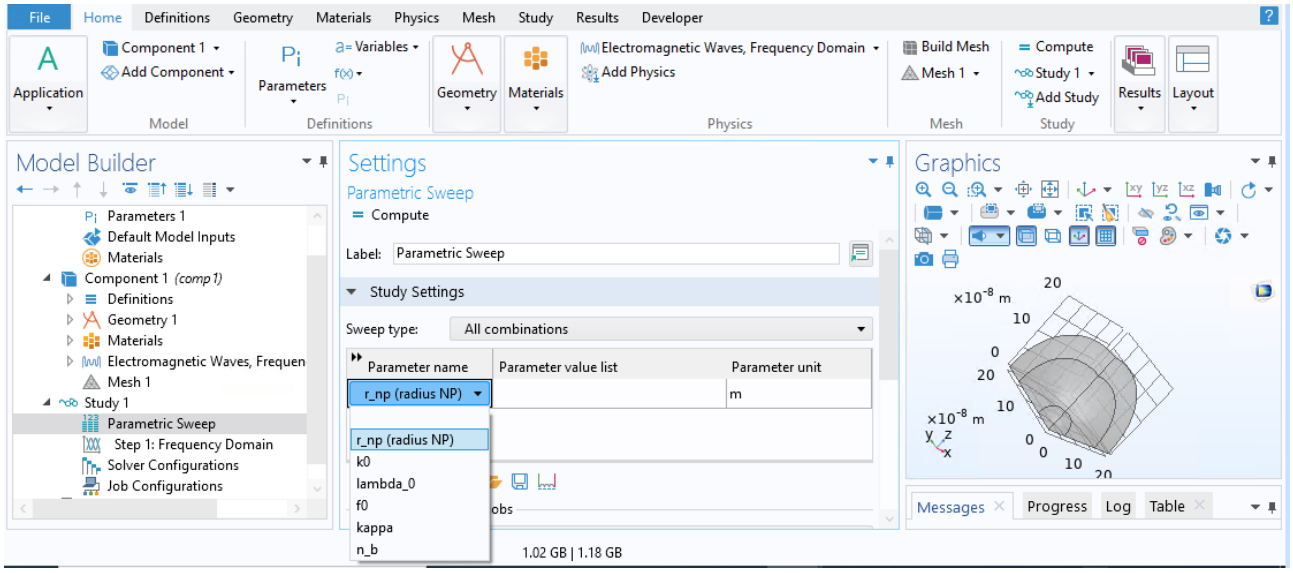

From the list select the frequency $f0$.

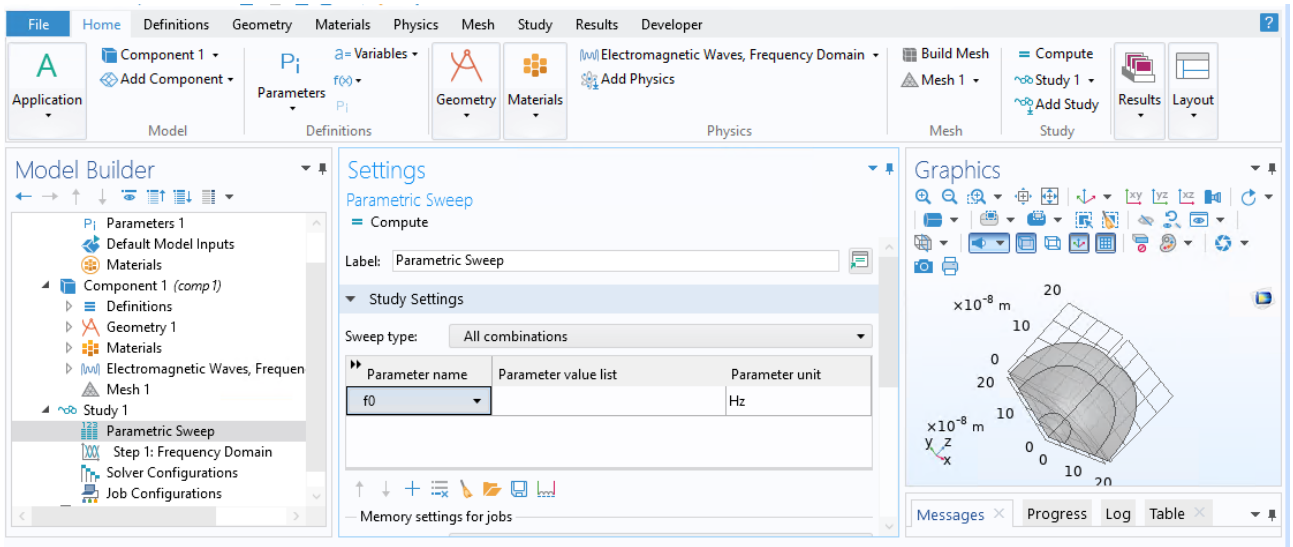

To select the range we want to consider click on the "Range" button below the table.

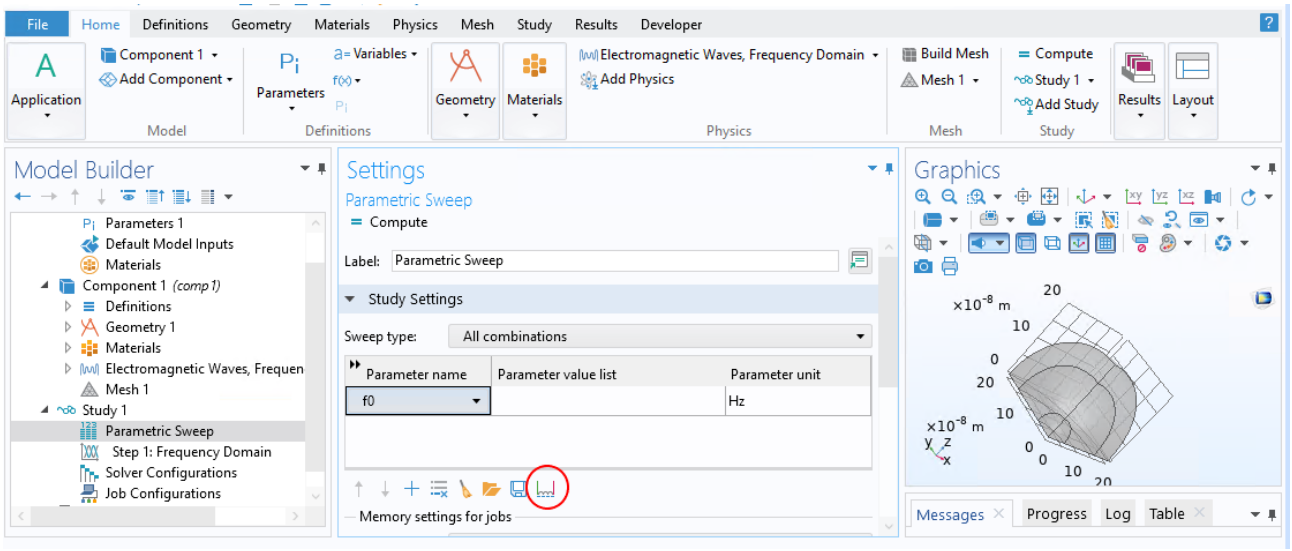

In the window that appears it is possible to set the values of the frequency interval in which we want to perform the simulations. Different entry methods can be chosen: we selected the number of values one.

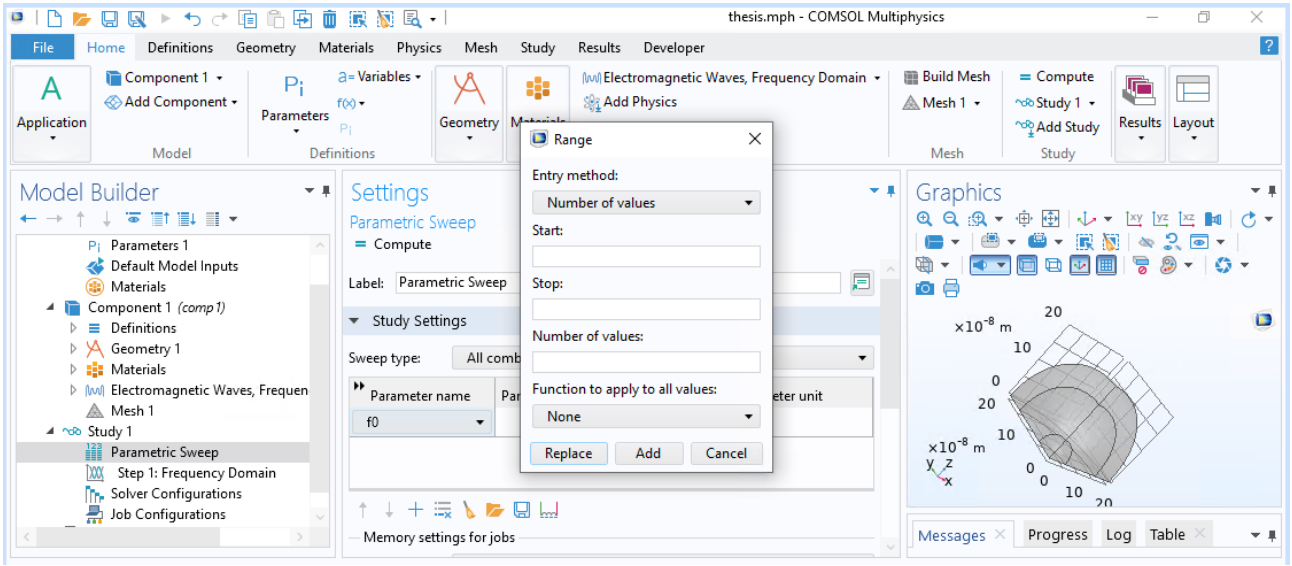

We set the number of values to 21. The number of frequencies at which we want to perform the study can be modified at will: by increasing it we get a more precise study, collecting results for many more frequency values, but we will also increase the simulation run time and the used memory, while decreasing the considered number of values we would gain in terms of simulation speed but we would get less precise results.

The frequency interval was chosen as 375 THz to 1000 THz, which corresponds to a wavelength interval 300 nm to 800 nm.

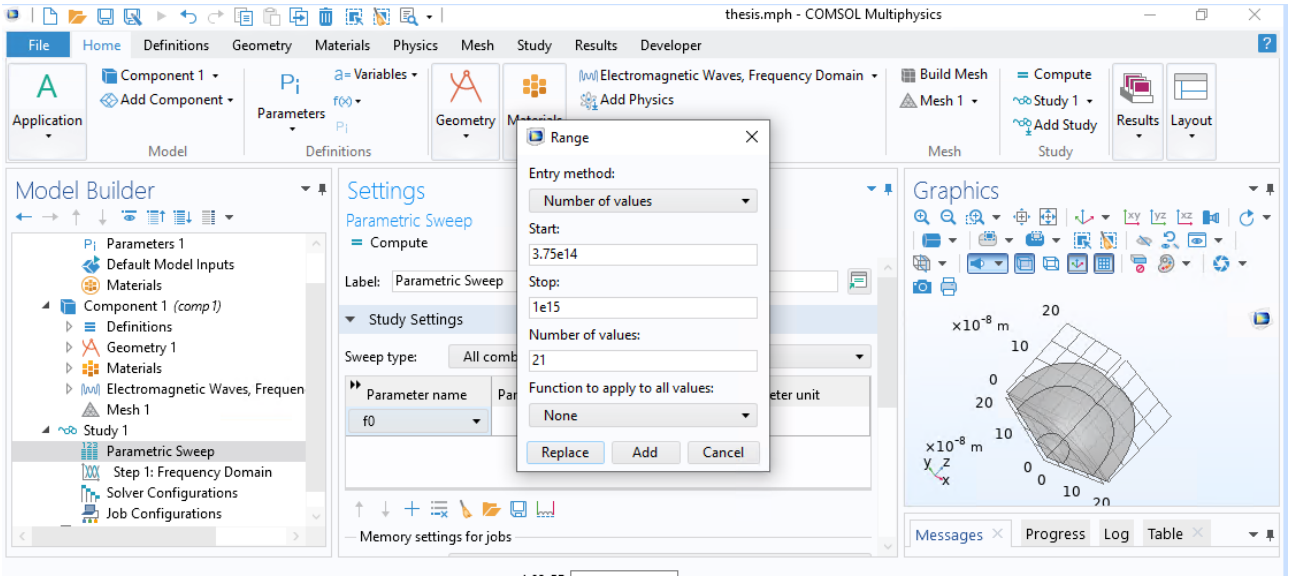

By clicking on the "Add" button the range will be added in the frequency domain settings.

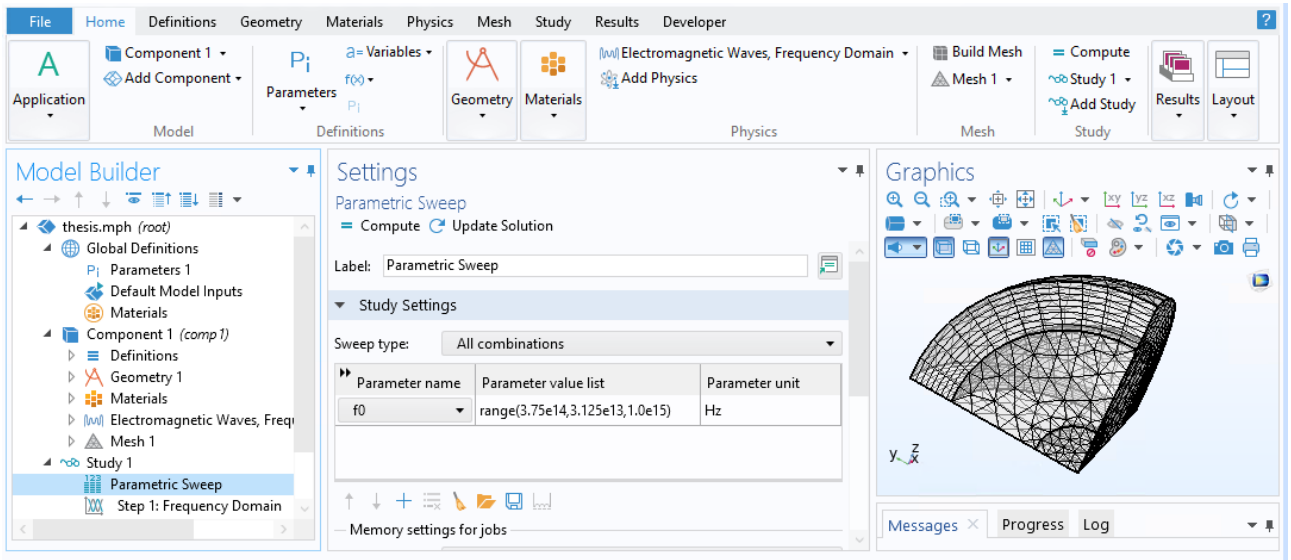

2.1.9 Running the simulation

Now the simulation can be run: click on "Study" and click on the "Compute" button.

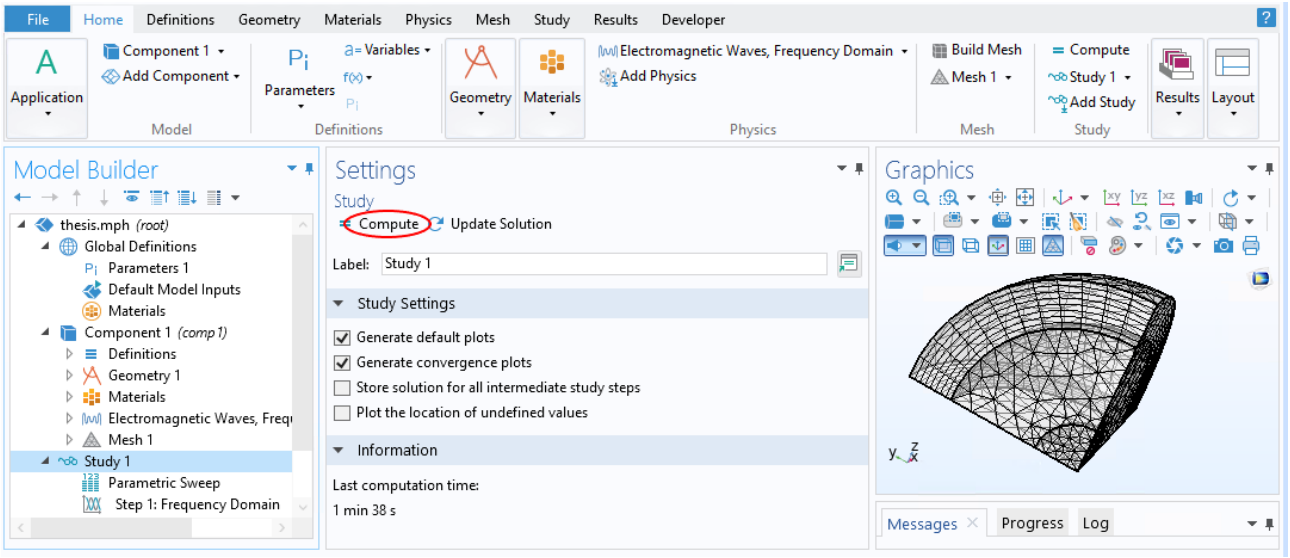

After the computation is completed, what appears is shown in the figure below. It is possible to see also the computation time that was needed to perform the simulation.

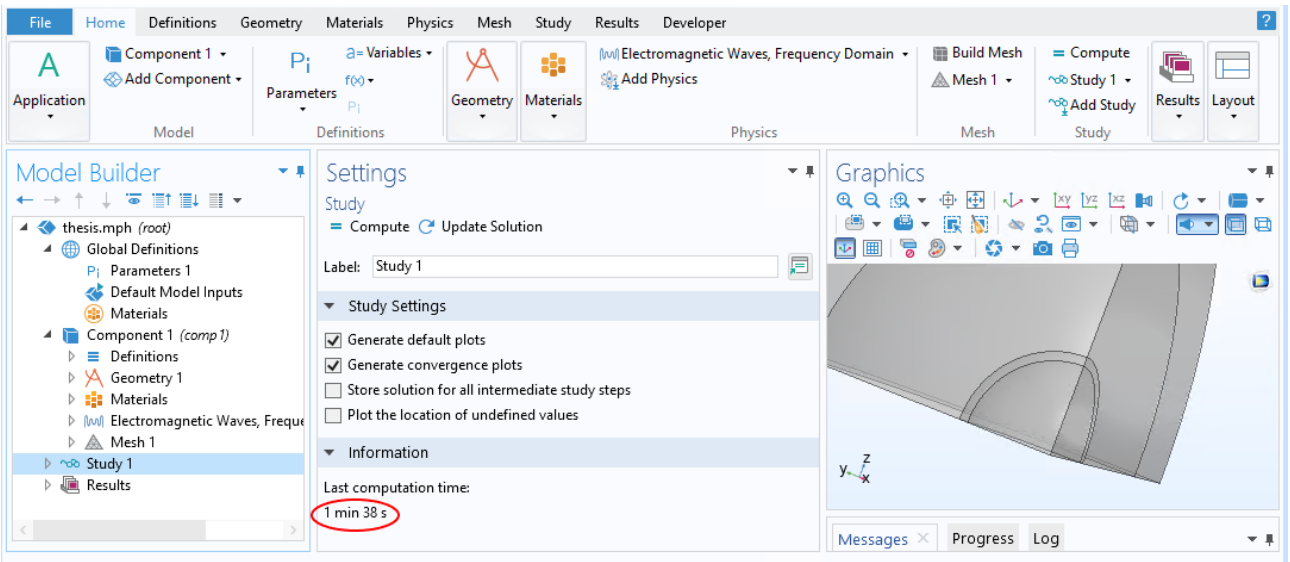

The solution for the scattered electric field will be under "Results". Under "Electric Field (ewfd)" the plot of the electric field amplitude for every frequency value of the chosen range can be found.

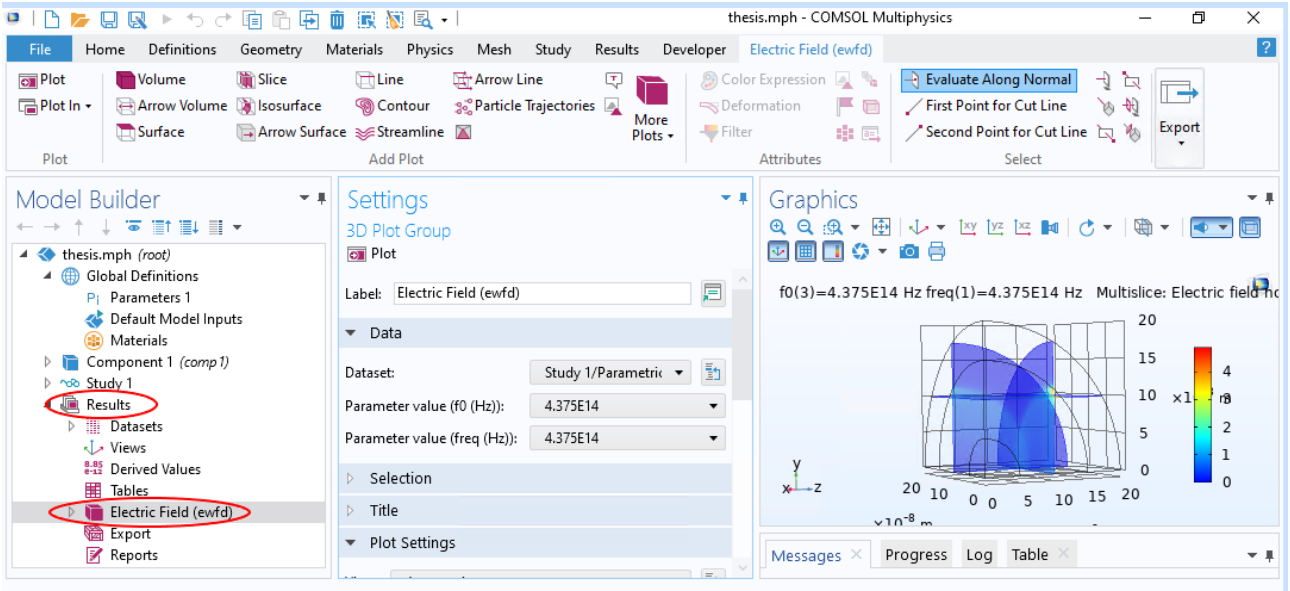

2.1.10 Computation of the cross sections and the maximum scattered electric field

Now we can compute the quantities of interest for the metallic nanoparticle, which are in our case its absorption and scattering cross sections and the maximum electric field on its surface. We are going to show the expressions for each of these quantities and how they can be calculated in COMSOL®.

2.1.11 Absorption cross section

The absorption cross section can be computed as the absorbed power, P_{abs} in W, divided by the intensity of input light, intended here as the flux of radiant intensity, with units W/m^2:

$$\sigma_{abs} = \frac{P_{abs}}{I_0} \tag{2.3}$$

The absorbed power P_{abs} can be obtained as the integral over the nanoparticle volume of the resistive losses, Q_{res}, whose units are W/m^3 and which is written as

$$Q_{res} = \frac{1}{2}\,\varepsilon_0\,\omega\,Im(\varepsilon)|\boldsymbol{E}|^2 \tag{2.4}$$

The intensity of the incoming light wave, I_0, can be computed as $I_0 = \frac{\langle S \rangle}{2\eta}$, where $\langle S \rangle$ is the intensity of the Poynting vector, whose time-average for a plane wave is $\langle S \rangle = |\boldsymbol{E_0}|^2$, while η is the impedance of the transmission medium with relative permittivity ε_r, which can be written as $\eta = \frac{\eta_0}{\sqrt{\varepsilon_r}} = \frac{1}{\varepsilon_0 \, c \sqrt{\varepsilon_r}}$. Hence the absorption cross section can be rewritten as

$$\sigma_{abs} = \frac{\int_{V_{np}} \frac{\omega}{2} \varepsilon_0 \, Im(\varepsilon) \, |\boldsymbol{E}| \, dV}{\frac{1}{2} \varepsilon_0 \, c \, \sqrt{\varepsilon_r} \, |\boldsymbol{E_0}|^2} = \frac{\omega}{c \, \sqrt{\varepsilon_r} \, |\boldsymbol{E_0}|^2} \int_{V_{np}} Im(\varepsilon) \, |\boldsymbol{E}|^2 \, dV \tag{2.5}$$

To make the computation in COMSOL® , right click on "Derived Values" and select "Integration" and "Volume Integration".

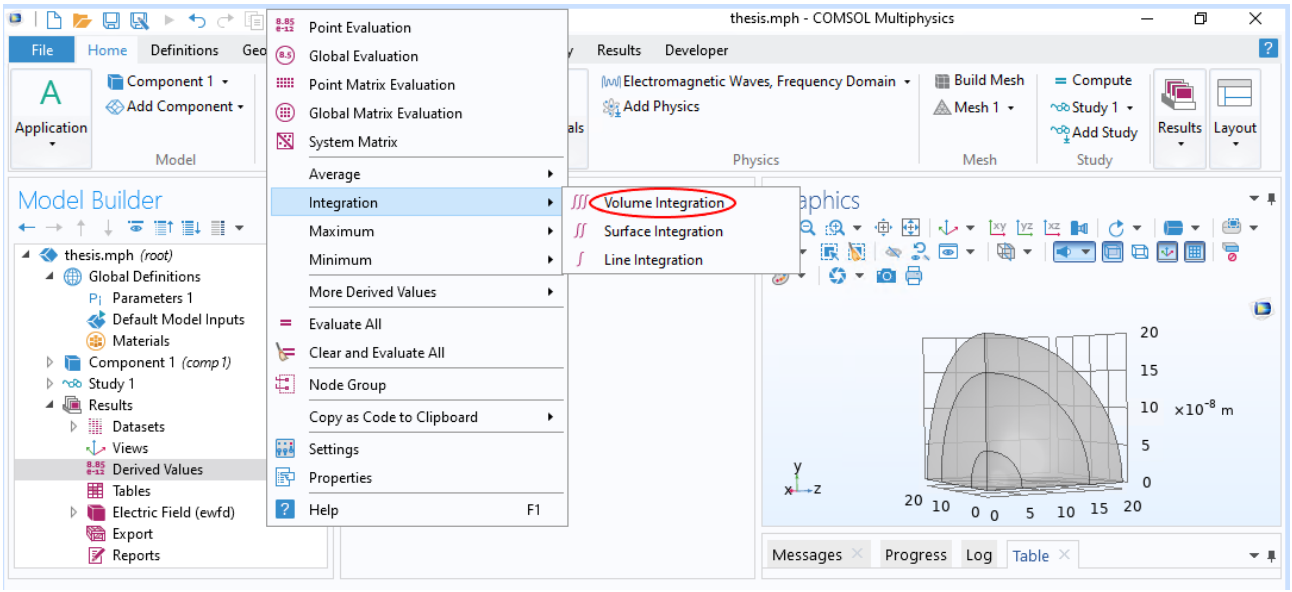

Then in the settings insert as domain the nanoparticle and in "Expressions" write the argument of the integral. To add the quantities to the integral argument click on the "Add Expression" button.

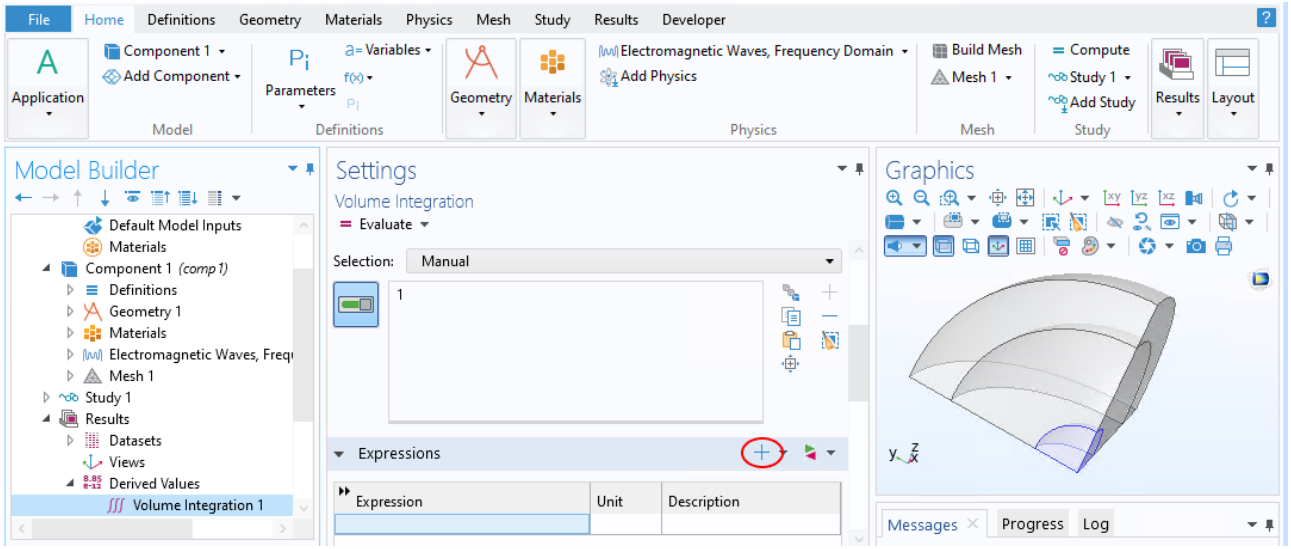

Select from the list the quantities to add. For example, the resistive losses can be found under "Component/Electromagnetic Waves, Frequency Domain/Heating and Losses" as "ewfd.Qrh".

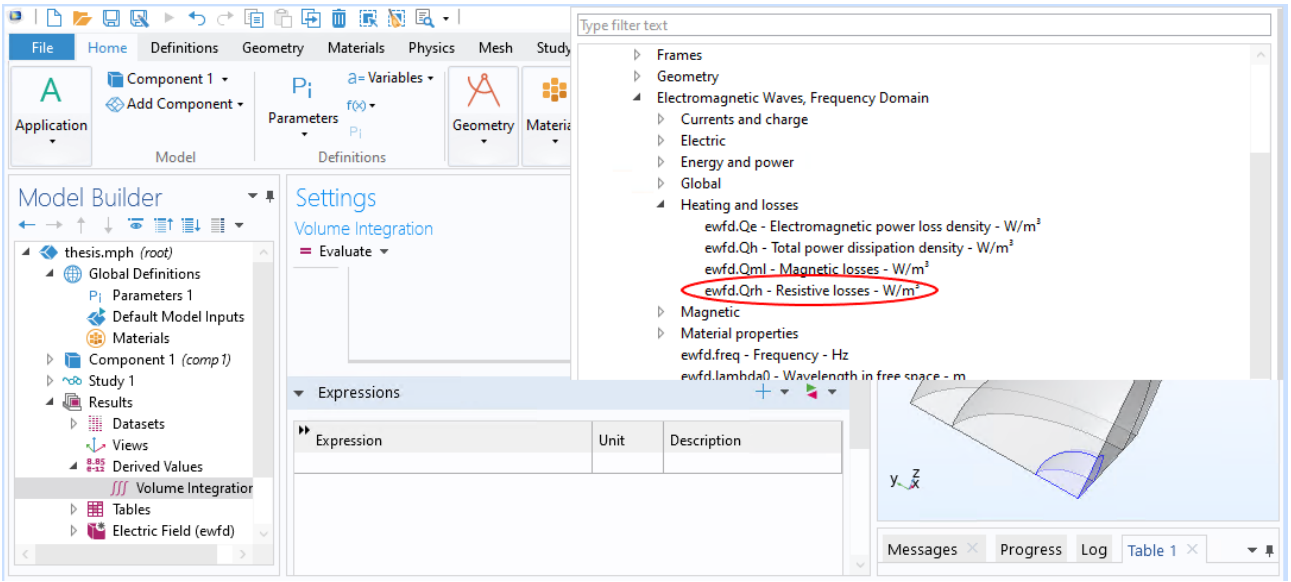

The expressions for the absorption cross section as it has to be written in COMSOL® results to be as reported below.

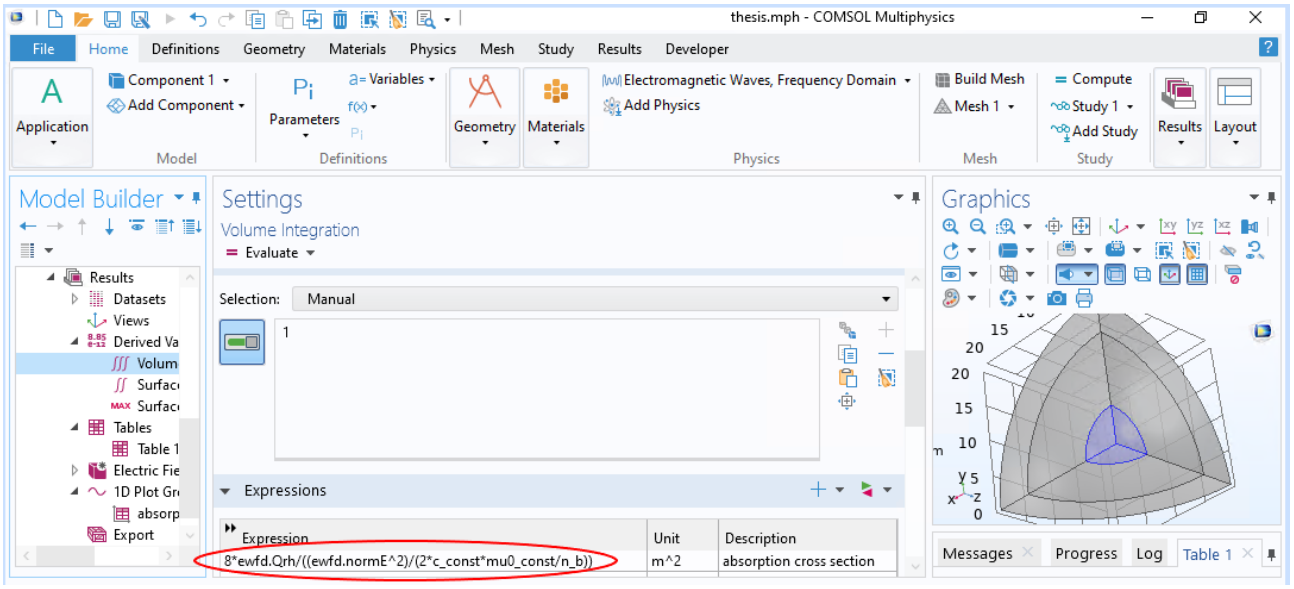

The integral value has to be multiplied by eight to obtain the result for the whole nanoparticle.

2.1.12 Scattering cross section

The scattering cross section can be computed as the scattered power, P_{sca} divided by the intensity of the impinging light, I_0

$$\sigma_{sca} = \frac{P_{sca}}{I_0}, \tag{2.6}$$

where P_{sca} can be computed as the integral over the background surface of the power outflow of the relative fields (time-averaged), S_{rel}, with units W/m^2.

Hence we can write the scattering cross section as

$$\sigma_{sca} = \int_S P_{rel} \frac{2\,\mu_0\,c}{|\boldsymbol{E}|^2\,\varepsilon_r} dS. \tag{2.7}$$

To add the expression for this quantity right click on "Derived Values" and under "Integration" select "Surface Integration".

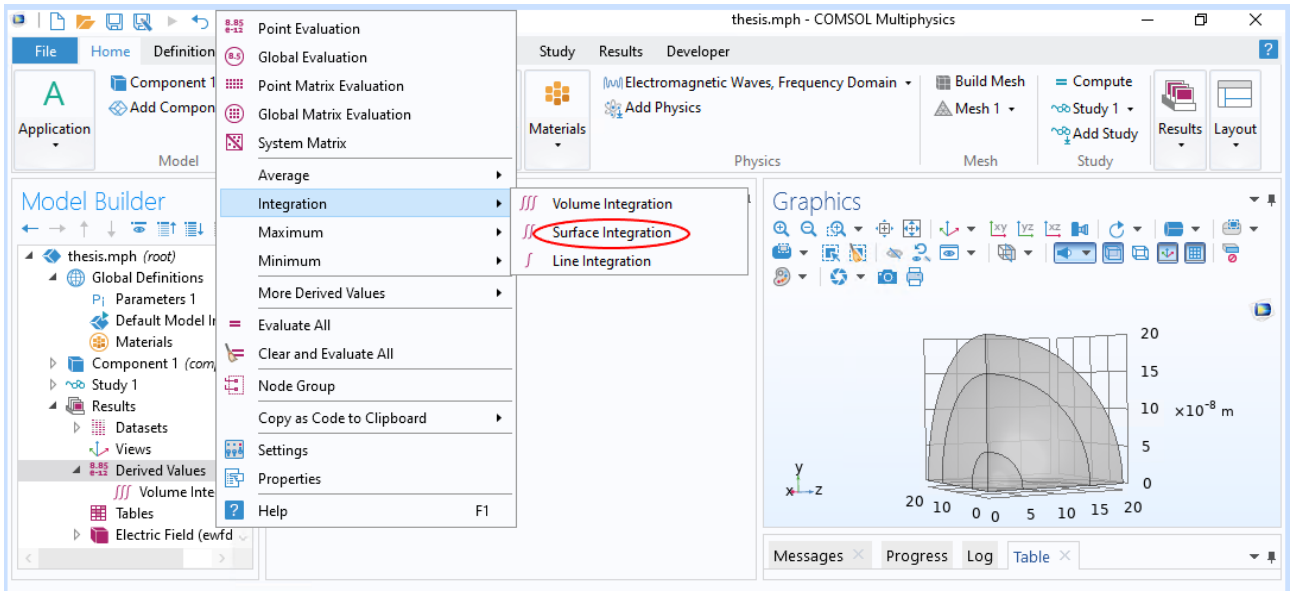

In the settings select as domains all the surfaces of the background, excluding the PML, and then insert in the expressions field the argument of the integral. The expression to be used in COMSOL® for the power outflow of the relative fields, P_{rel}, can be found in the list from "Add Expressions" under "Component/Electromagnetic Waves, Frequency Domain/Energy and Power". The integral argument has to be multiplied by eight to obtain the result for the whole structure.

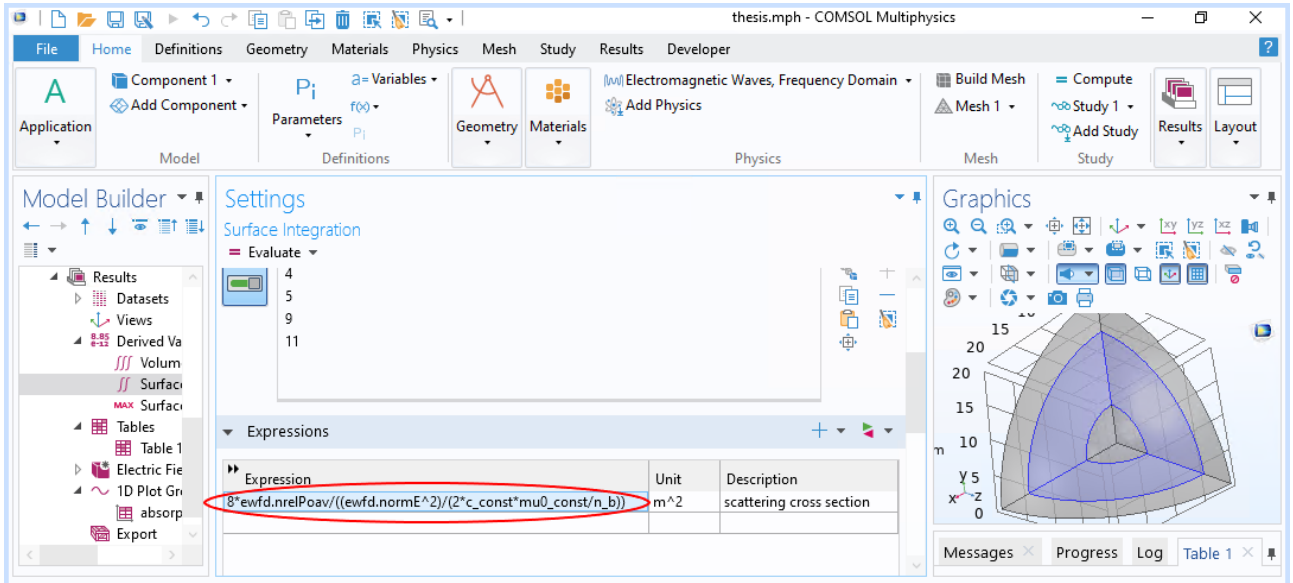

2.1.13 Maximum surface field

The maximum scattered electric field on the plasmonic nanostructure surface can be computed by right clicking on "Derived Values" and selecting under "Maximum" "Surface Maximum", as we are interested in the maximum scattered field by the nanoparticle on its surface.

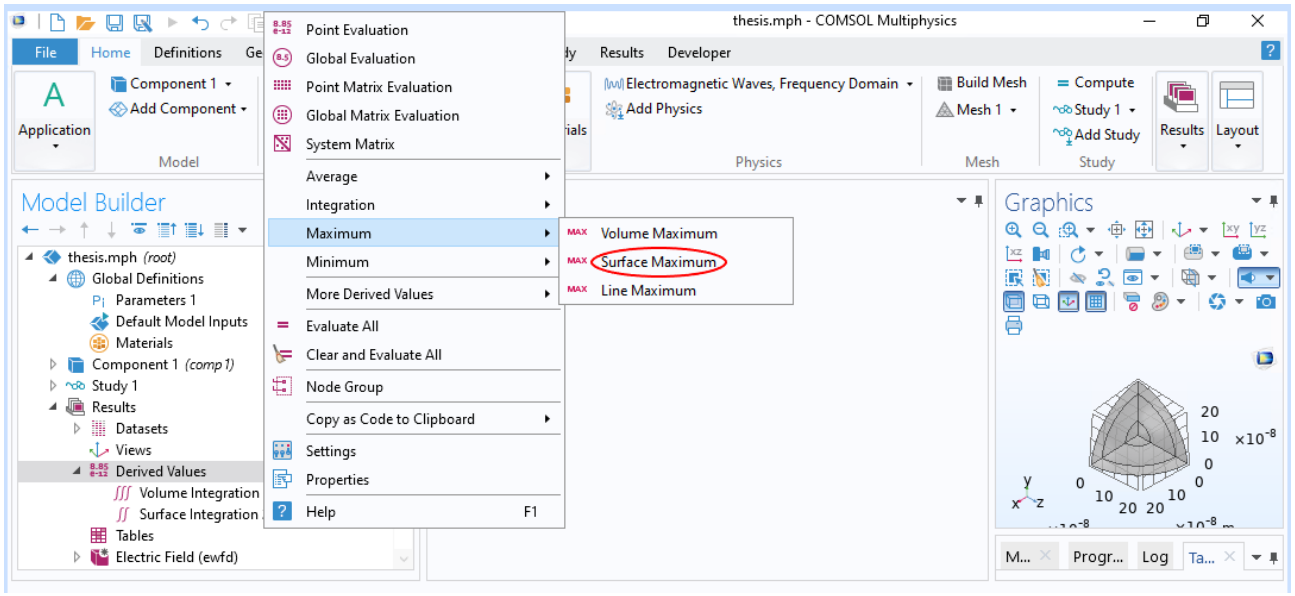

Select as domains all the surfaces of the nanoparticle, and add in the expressions field "ewfd.normE", which is the intensity of the scattered electric field.

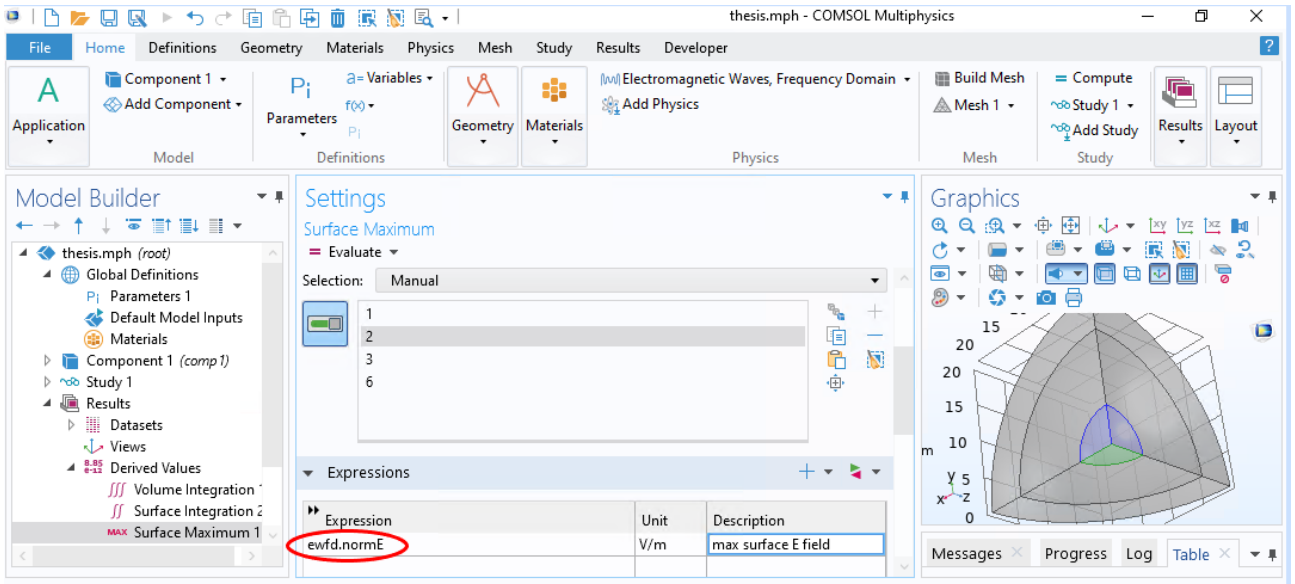

Now we can perform the evaluation of each of these quantities in the range of frequen-

cies we have chosen. In the settings of each derived value, under "Data", set "Parametric Solutions" as "Database" and press "Evaluate" to get the computation done. We will show the process to obtain the quantities of interest just for the absorption cross section, but the steps are the same for any other quantity.

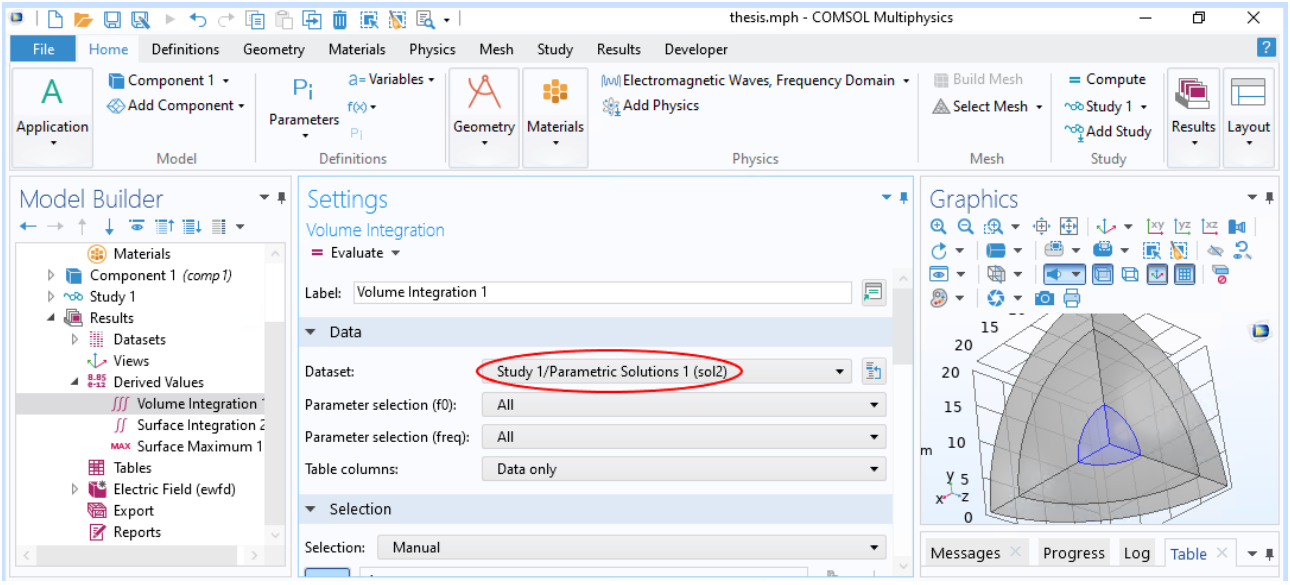

The result will appear as a table in the space below Graphics.

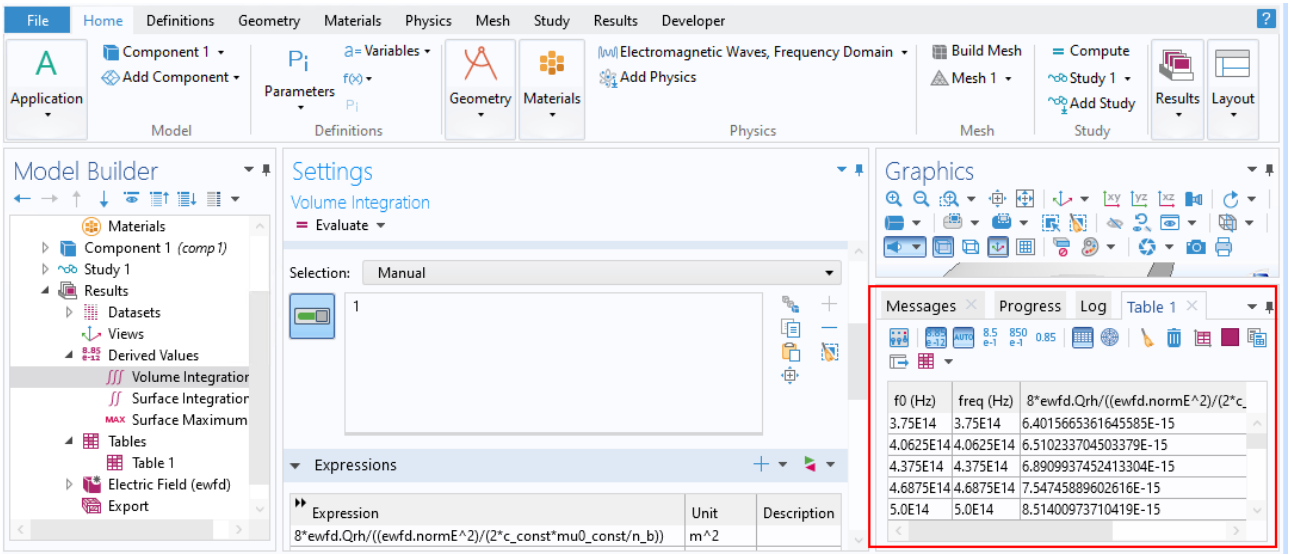

The table is saved under "Tables" in the "Model Builder" list, from which it is possible to modify the settings and the name of the table.

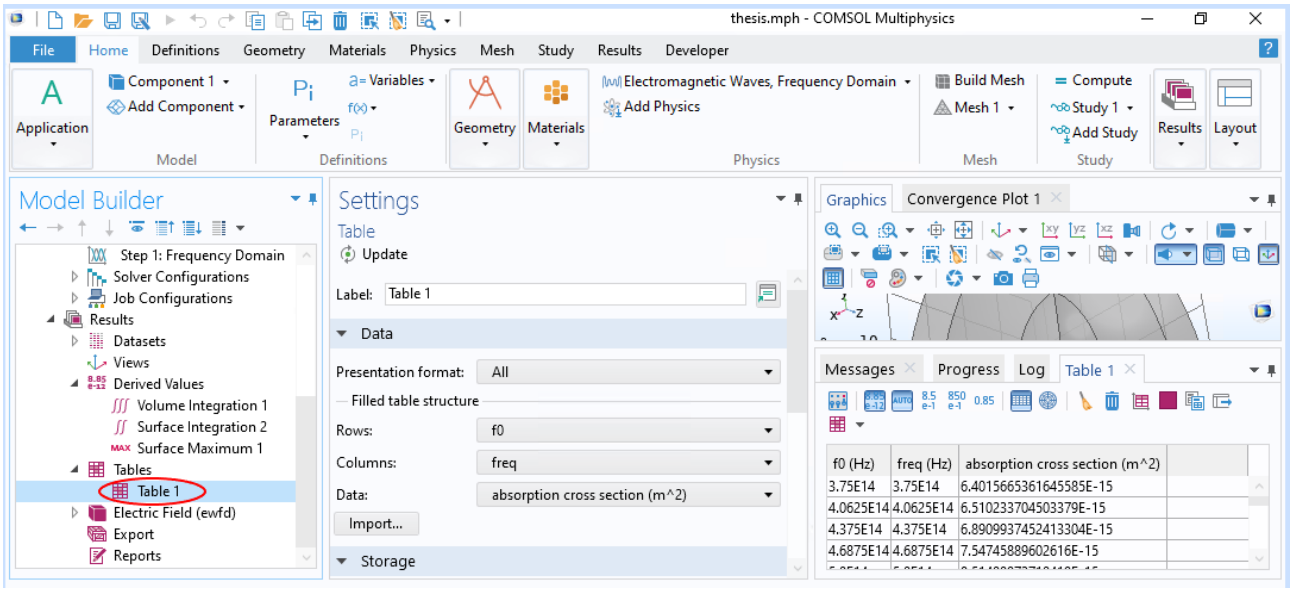

It is also possible to plot the data we have obtained by clicking on the button "Table Graph" in the toolbar above the data table.

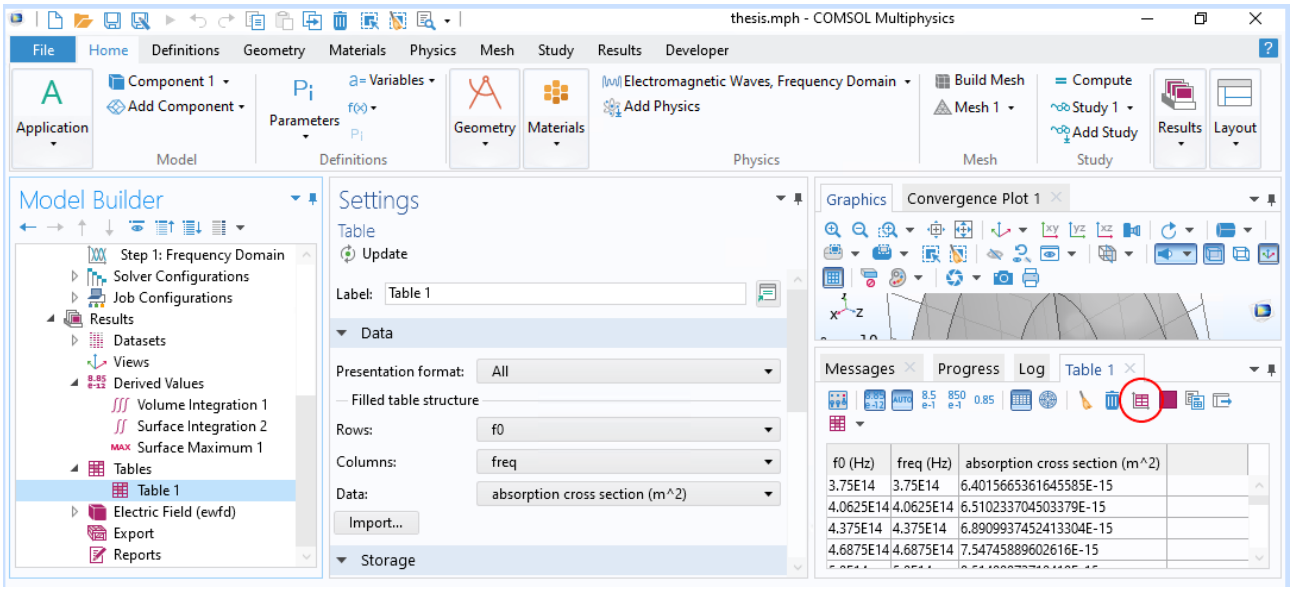

The plot will appear in the Graphics space and it will have by default as y axis the values of the computed quantity reported in the table and as x axis the corresponding position in the column they occupy. It will be saved under "Results/1D Plot Group".

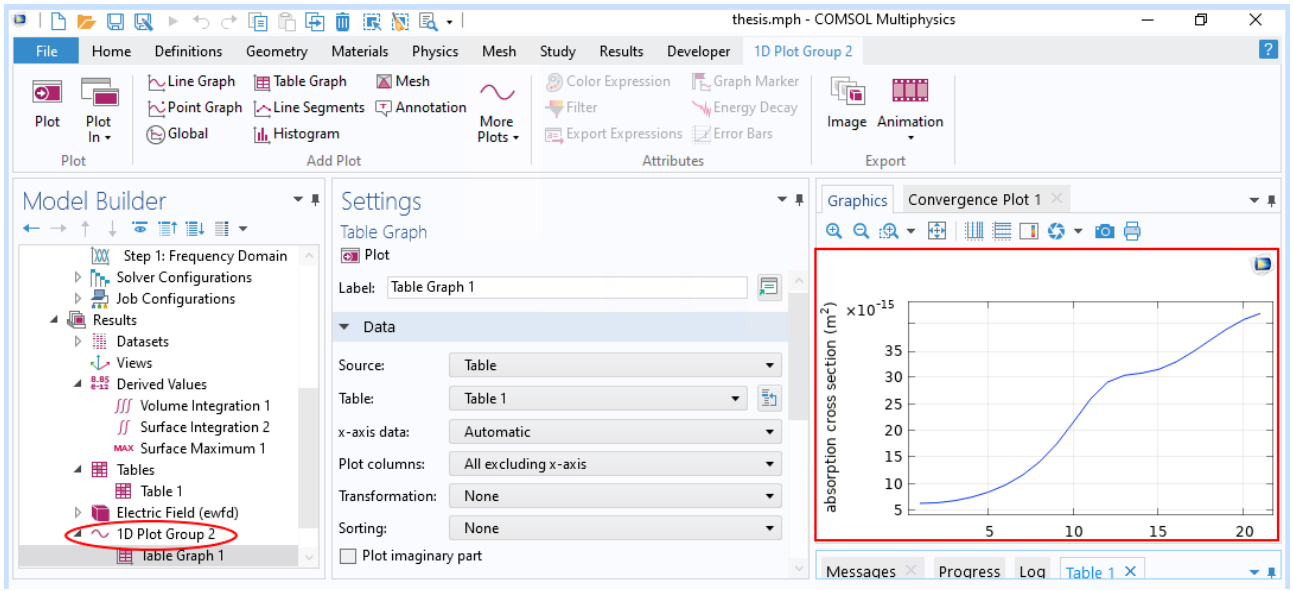

The axes can be modified by changing the settings of "Table Graph". To set the frequency as x axis select "freq (Hz)" under "x axis data" and under "Plot columns" set "Manual" and then select the computed quantity we want to represent, which is in our example "absorption cross section".

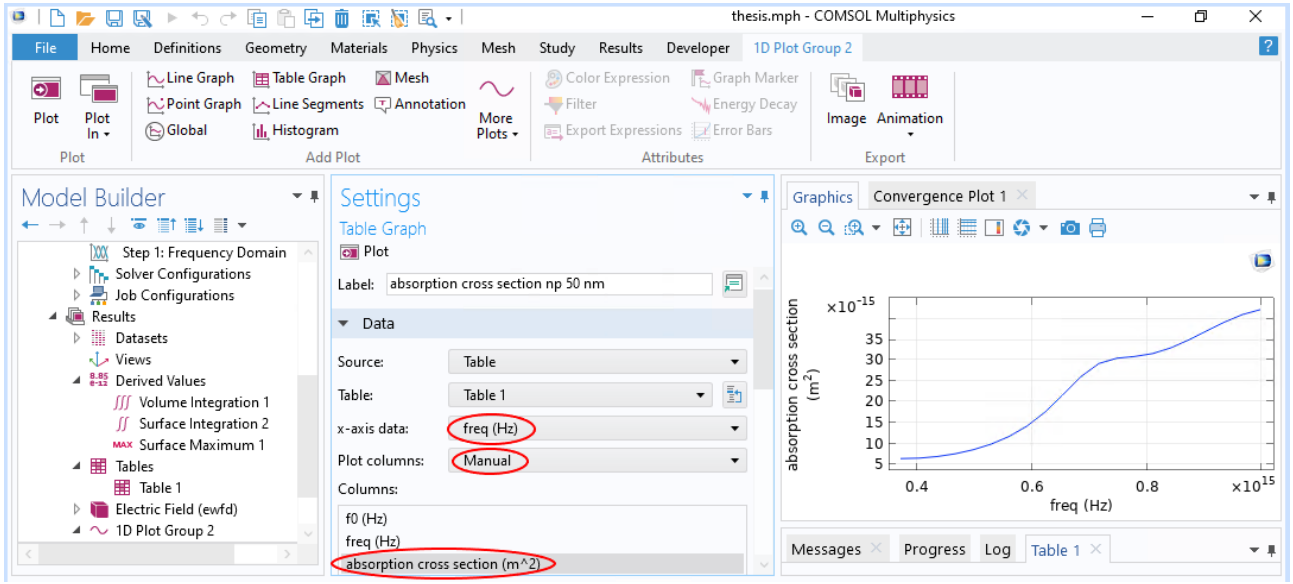

These steps conclude the part regarding the plasmonic nanoparticle, how to simulate it in a specific environment and how to get the quantities related to it to study its properties when an external electromagnetic field is applied.

2.1.14 Some results

As an example of the results obtained, we report in fig.2.1 and 2.2 the absorption and scattering cross sections, respectively, for one of the gold nanostructures analyzed, a gold nanorod of radius 20 nm and aspect ratio 1.5.

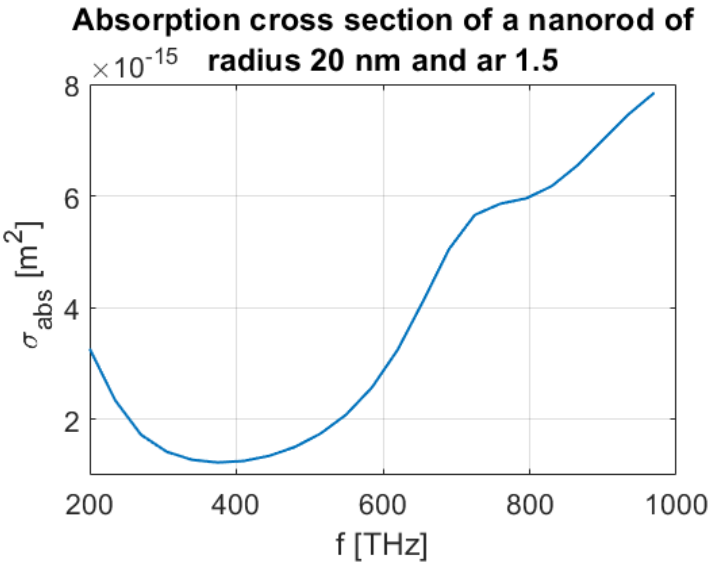

Figure 2.1

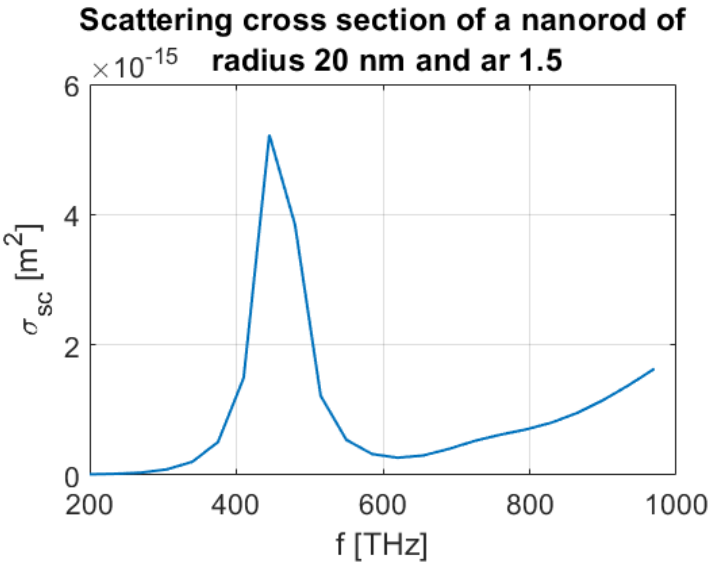

Figure 2.2

We also report in fig.2.3, 2.4 and 2.5 the maximum electric field distribution at the LSPR frequency for the different types of structures we studied, nanorods, nanospheres and nanocubes respectively.

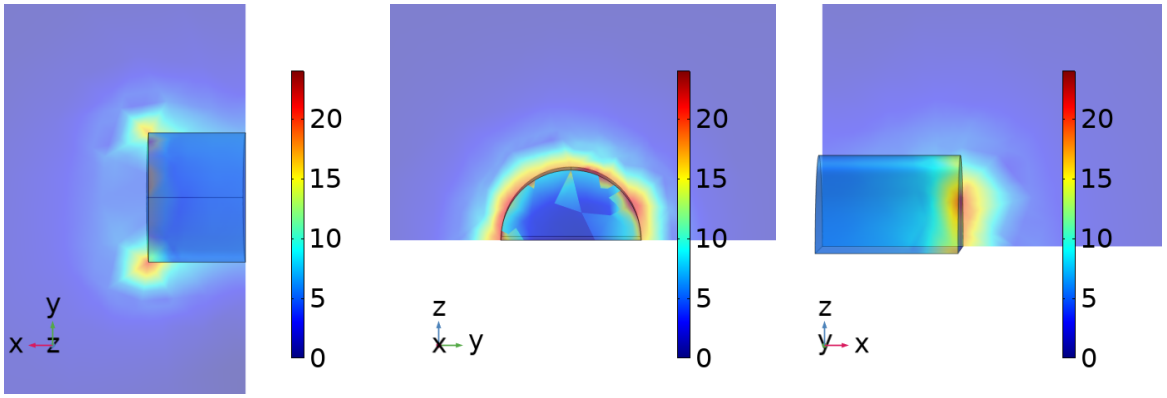

(a) (b) (c)

Figure 2.3: *Maximum surface field on the surface of a gold nanorod of radius 20 nm and AR 1.5.*

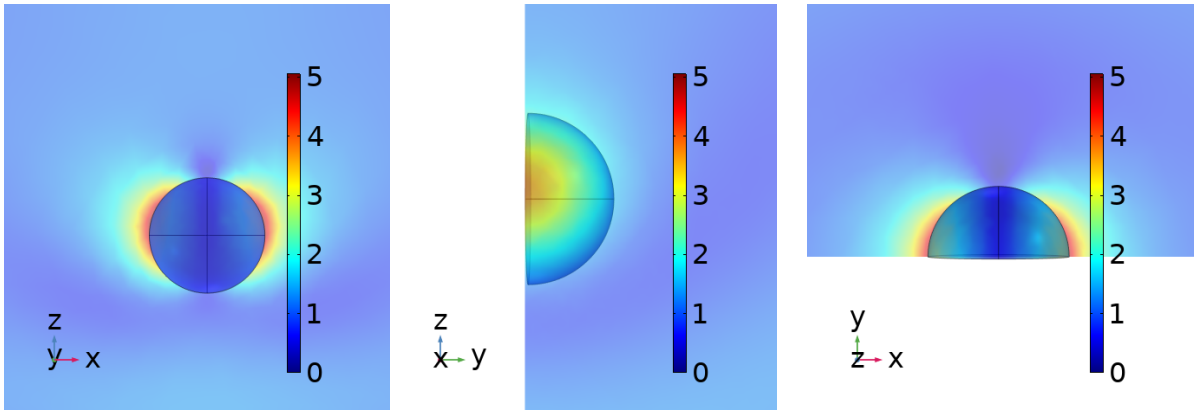

(a) (b) (c)

Figure 2.4: *Maximum surface field on the surface of a gold nanosphere of radius 90 nm.*

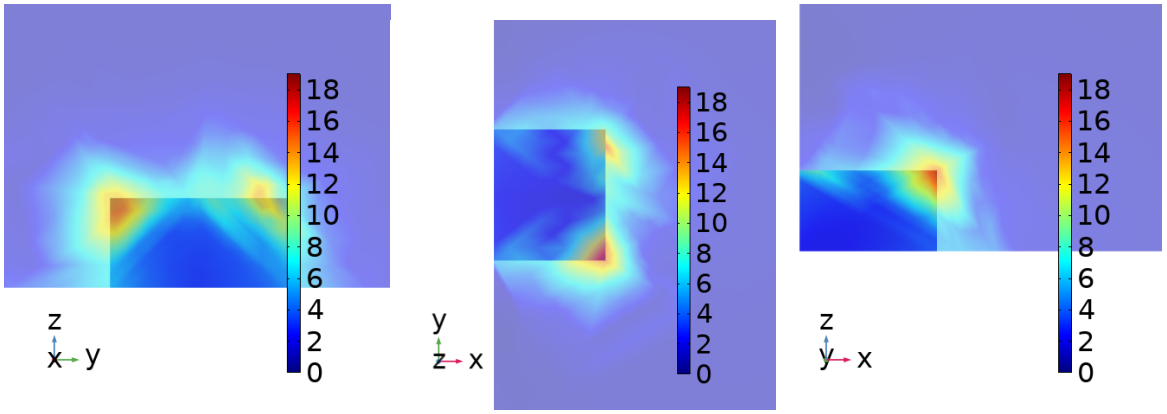

(a) (b) (c)

Figure 2.5: *Maximum surface field on the surface of a gold nanocube of side length 10 nm and AR 1.7.*

2.2 Photosensitizers

We simulated in COMSOL® also the PSs we considered in this work, in order to compare their absorption in the absence and in the presence of a gold nanostructure. To end this, for each PS, we first simulated a shell made of PS around the gold nanotructures. In particular, we associated each PS to the plasmonic structures whose LSPR overlapped with the absorption peak of the PS. In this way we were able to compute the absorption cross section of the PSs in the presence of plasmonic nanostructures. Then, we simulated for each PS a nanosphere made of it, with the same volume as the shells that were built around the plasmonic nanostructures of interest for that PS. Hence we were able to compare the absorption cross sections in the two cases for all the considered PSs.

Since the compounds we analyzed are not present as materials in the COMSOL® library, we added them manually as interpolation functions of their refractive index. First, we took from the literature the values for the extinction molar coefficient or the absorbance of the considered PSs as function of wavelength. From these data it is possible to obtain the imaginary part of the PSs refractive index $n - i\kappa$, since

$$\kappa = \frac{\mu_{abs}}{4\pi} \tag{2.8}$$

where μ_{abs} is the absorption coefficient and it is linked to the absorbance and the molar extinction coefficient by

$$\mu_{abs} = e\, c\, ln(10) = \frac{A}{d}\, ln(10) \tag{2.9}$$

being e the molar extinction coefficient, in liters/moles cm, c the concentration, in moles/liter, A the absorbance and d the optical path length, in cm.

Instead, the real part of the refractive index was assumed to be 1.33 for all the PSs, since to be delivered they are usually diluted in water with relatively small concentrations. Hence, the optical properties of the resulting solution are mainly due to those of the water solvent. Moreover, we are mainly interested in the imaginary part of the refractive index, since it is the one related to the absorption and we want to compute the PSs absorption cross sections.

Therefore, we created a table containing the values of the imaginary part of the refractive index for each PS with the corresponding wavelength. Then we imported all the tables in the COMSOL® software to be able to simulate the PSs.

We report in fig.2.6-2.11 the spectra of the extinction molar coefficient or absorbance found in the literature for each considered PSs, together with the corresponding imaginary part of the refractive index that was computed.

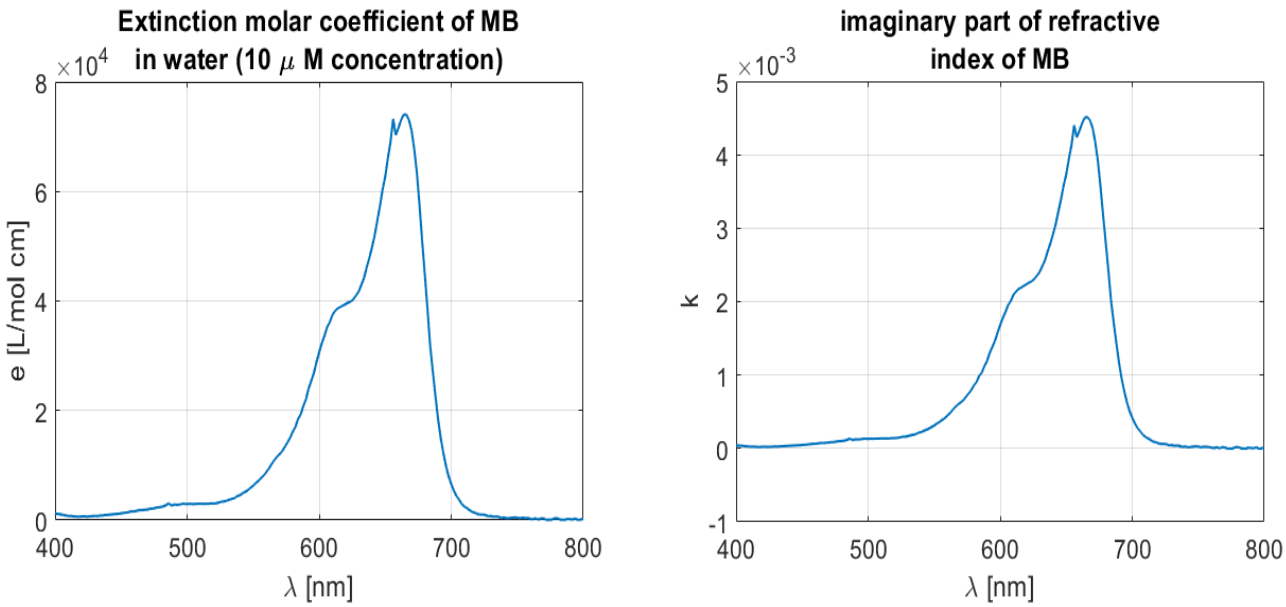

Figure 2.6: *(**a**) Extinction molar coefficient of methylene blue diluted in water with a concentration of 5 μM [26] and (**b**) imaginary part of the refractive index of MB.*

The objective of simulating the PSs in COMSOL® was to understand whether the absorption of each PS is actually enhanced by the presence of the gold nanostructure whose LSPR has been designed to overlap with the PS absorption peak.

In fig.2.12a it is reported the structure built in COMSOL® to compute the PSs absorption in the presence of a gold nanorod of radius 30 nm and AR 1.5, where the PS constitutes a 5 nm shell around it. Instead, in fig.2.12b it is shown the nanosphere, with the same volume as the shell, built to compute the PS absorption alone, in order to be able to compare the absorption cross sections of the PS in the two cases.

In fig.2.13 we report, as an example of the results obtained, the absorption spectra of methylene blue (MB) in the presence and in the absence of a gold nanostructure. The

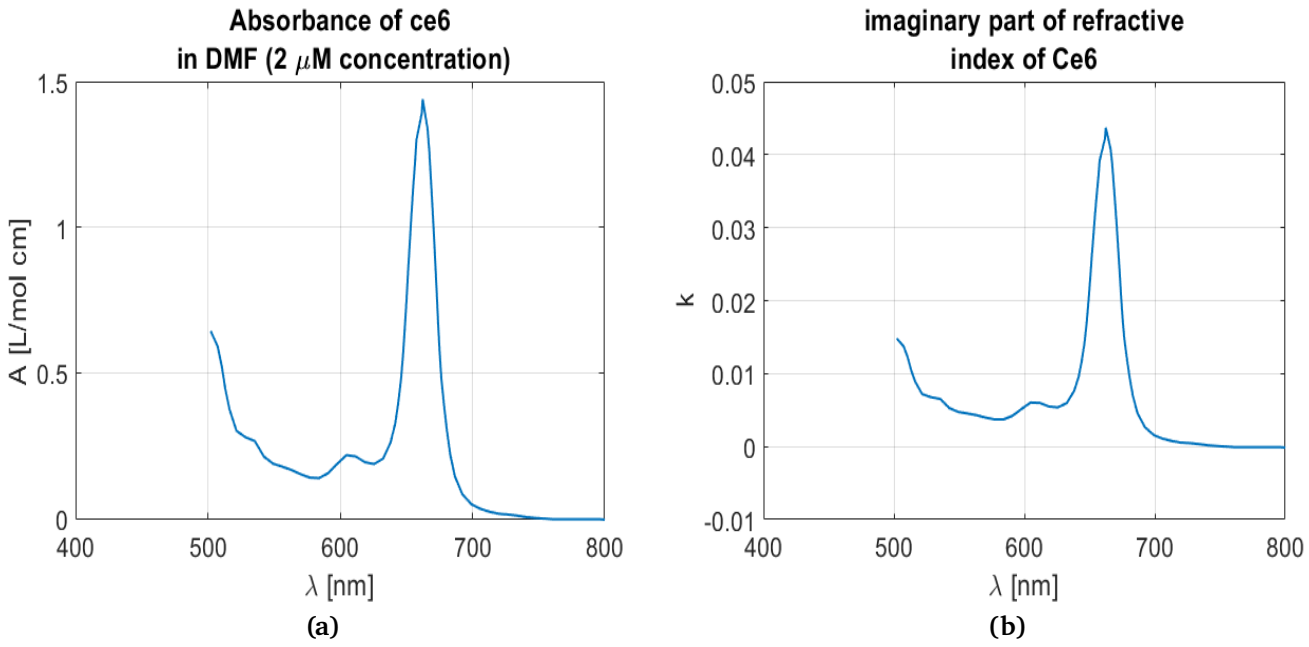

(a) **(b)**

Figure 2.7: *(**a**) Absorbance of chlorin e6 in DMF (dimethylformamide) with a concentration of 2 μM [27] and (**b**) imaginary part of the refractive index of ce6.*

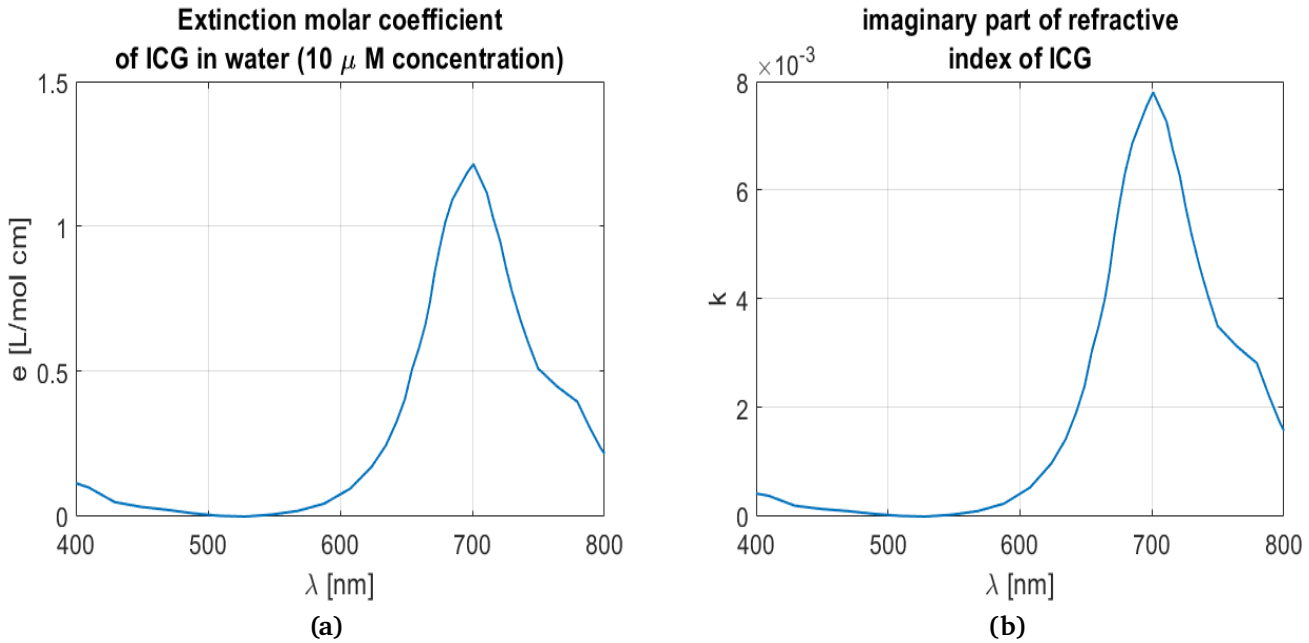

(a) **(b)**

Figure 2.8: *(**a**) Extinction molar coefficient of indocyanine green (ICG) in water with a concentration of 10 μM [28] and (**b**) imaginary part of the refractive index of ICG.*

absorption spectrum of MB in the presence of the gold nanostructure was obtained setting MB as a 5 nm shell around a nanorod of radius 30 nm and AR 1.5, while the spectrum of MB alone was computed for an MB nanoparticle with same volume as the shell and

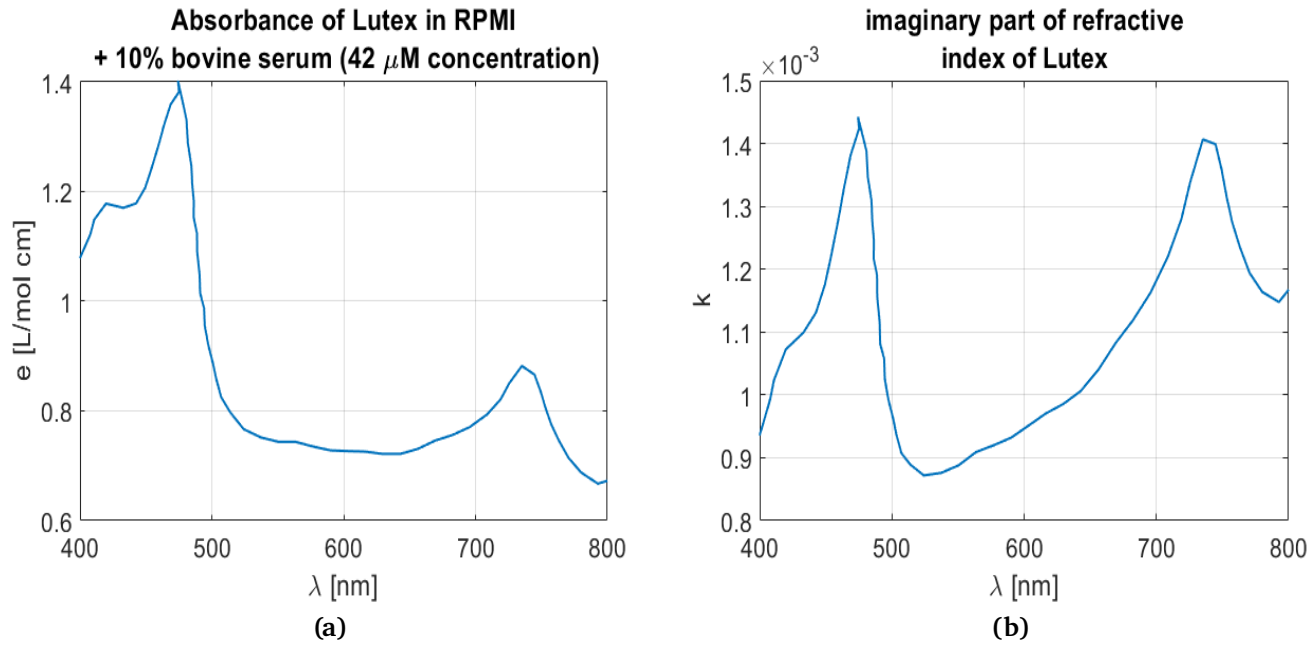

(a) **(b)**

Figure 2.9: *(**a**) Absorbance of Lu-Tex® in RPMI + 10% bovine serum with a concentration of 42 μM [29] and (**b**) imaginary part of the refractive index of Lu-Tex®.*

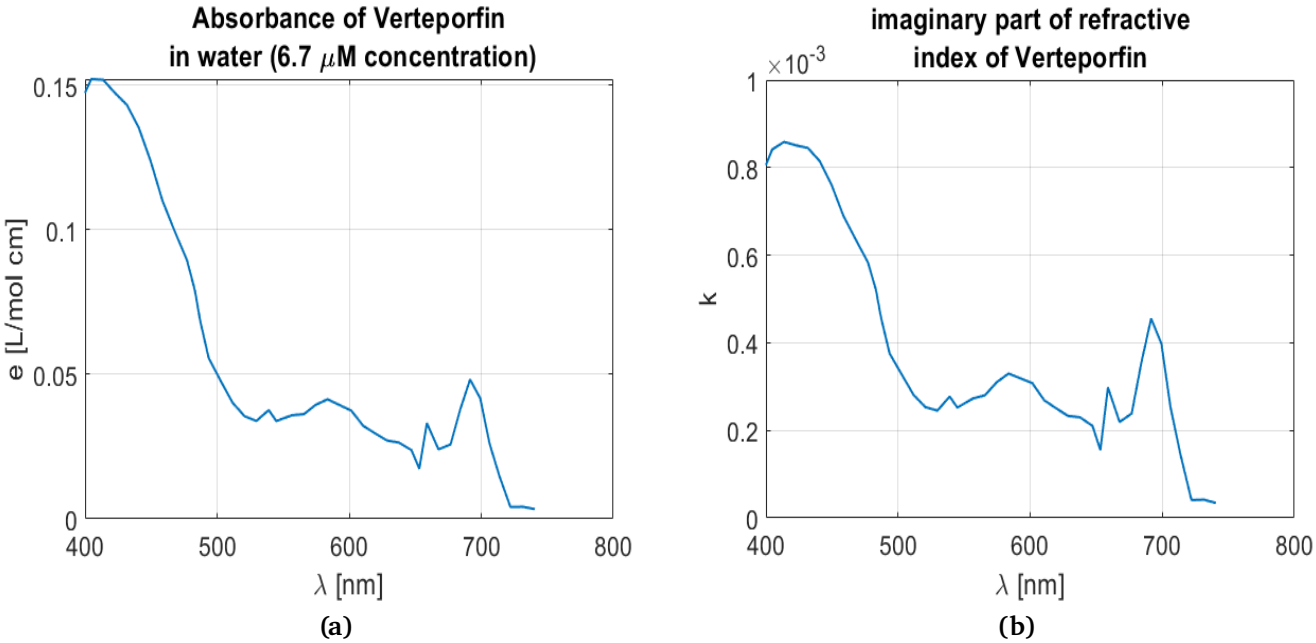

(a) **(b)**

Figure 2.10: *(**a**) Absorbance of verteporfin in anhydrous dichloromethane with a concentration of 6.7 μM [30] and (**b**) imaginary part of the refractive index of verteporfin.*

subject to the same external electric field. The volume of the MB shell results to be in this case $1.30 \cdot 10^{-22}\, m^3$, corresponding to a nanosphere radius equal to 31.4 nm.

The results obtained from the comparison between the absorption of all the PSs in

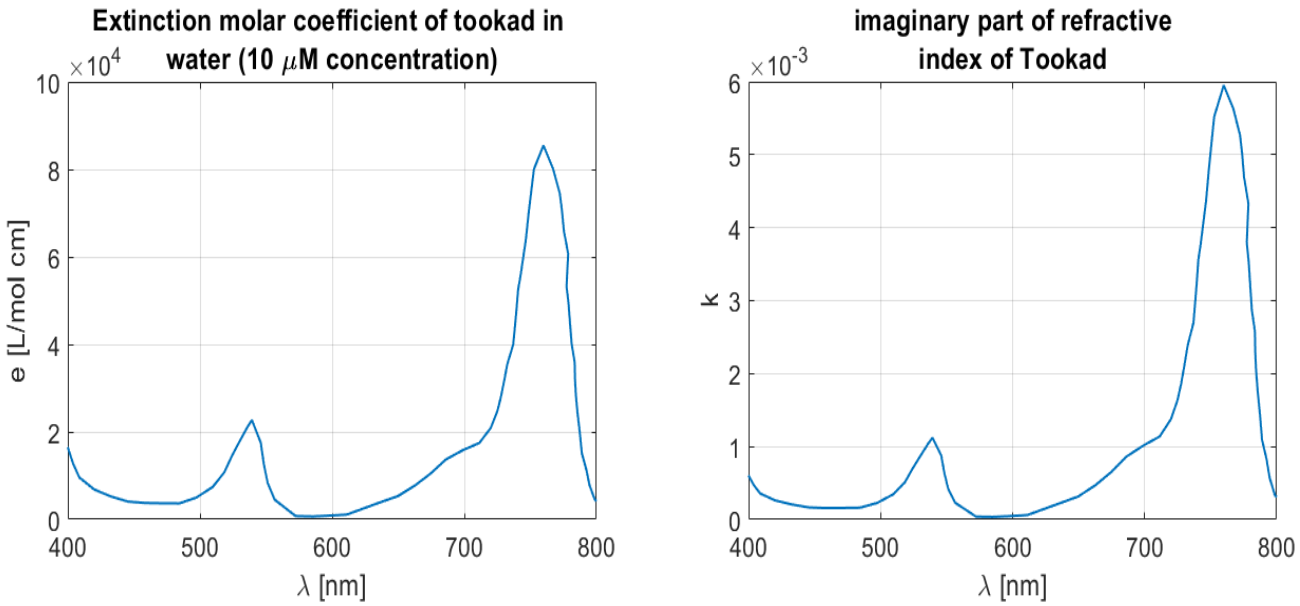

(a) **(b)**

Figure 2.11: *(**a**) Extinction molar coefficient of Tookad® in aqueous micellar solution with a concentration of 11 μM [31] and (**b**) imaginary part of the refractive index of Tookad®.*

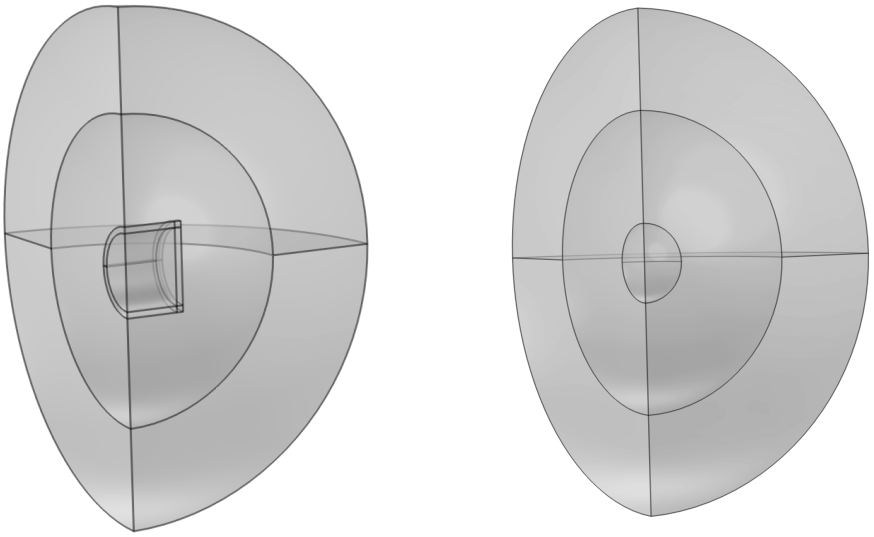

(a) **(b)**

Figure 2.12: *(**a**) Structure built in COMSOL® to compute the absorption of each PS in the presence of a gold nanosphere, where the shell around it is made of the considered PS, and (**b**) structure built to compute the absorption of the PS alone, without the plasmonic nanostructure, which is a PS nanosphere with the same volume as the shell.*

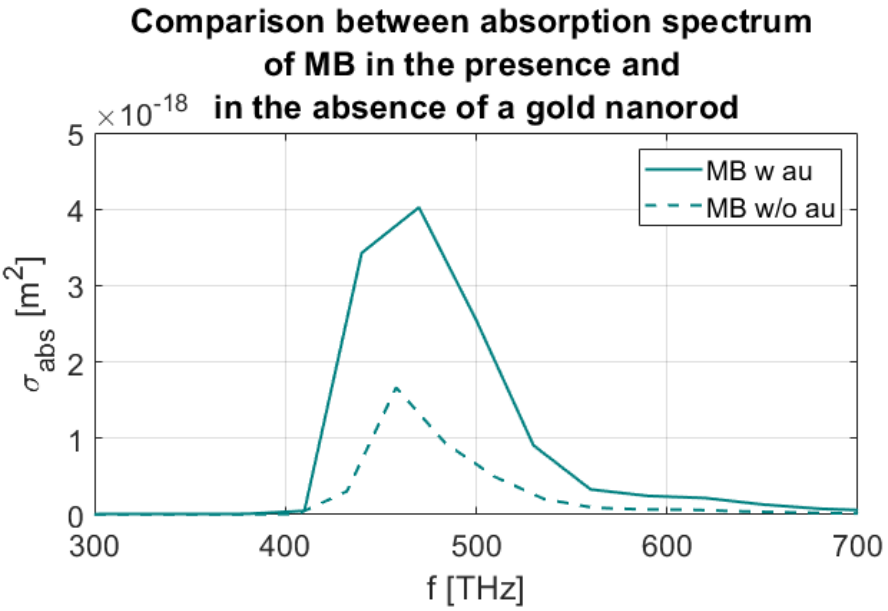

Figure 2.13: *Comparison between the absorption spectra of MB in the presence and in the absence of a gold nanostructure.*

the presence and in the absence of the relative overlapping gold nanostructures will be shown in the next chapter.

Chapter 3

Simulations results

In this chapter we will present the results obtained through the COMSOL® software. In particular we will show, for each considered PS, the overlap between its absorption peak and the maximum scattered electric field from different gold nanostructures, under plane wave illumination, without the PS shell being present. The nanostructures we considered were spheres (NP), rods (NR), which were shaped like cylinders, and parallelepipeds with square-shaped base, which we will simply call nanocubes (NC).

3.1 Methylene Blue

Methylene blue (MB) absorption peak is at 445 THz in water. In Fig.3.1 the normalized absorption spectrum of MB and the maximum scattered surface field of two gold nanoparticles are reported. The nanospheres for which the LSPR is at the same frequency of MB absorption peak have radii 90 nm and 100 nm, as shown in the figure. It is possible to obtain the overlap with nanospheres of two different sizes because of the fact that their LSPR peak is wide, covering a relatively large range of frequencies. It is also reported a scheme to show the shape of the considered nanostructure, the direction of propagation of the incident light, identified by the wavevector $\mathbf{k}$, and its polarization, identified by the electric field $\mathbf{E}$.

In the case of nanospheres the direction of polarization chosen has no relevance on the LSPR. However, for asymmetrical structures, polarization had to be set directed along the long axis of the structure, as the main resonance is due to the longitudinal LSPR, the

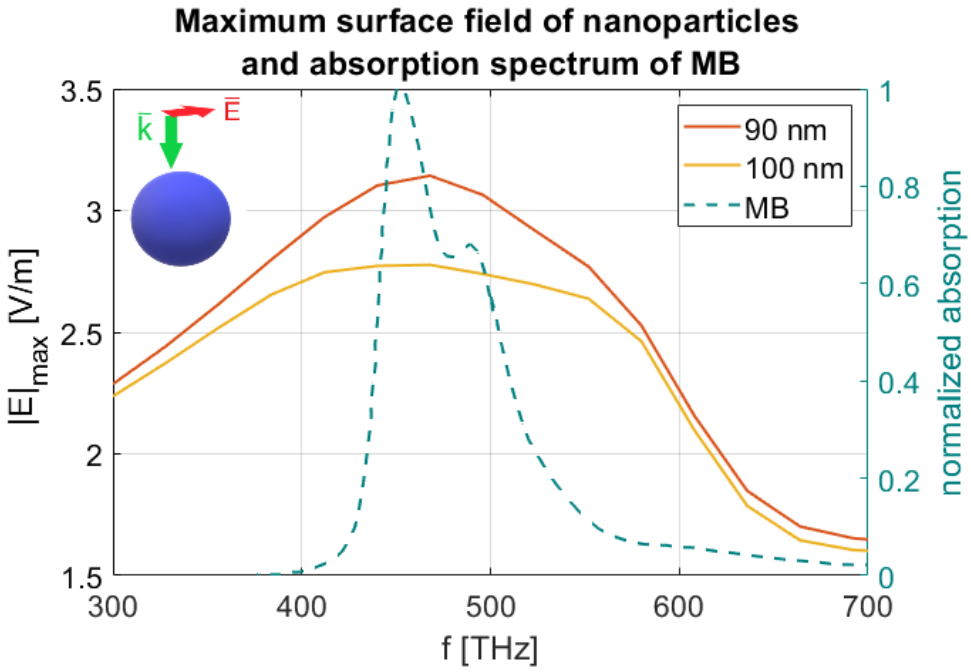

Figure 3.1: *Maximum surface electric field of nanoparticles, made only of gold, subject to plane wave illumination, and normalized absorption spectrum of methylene blue.*

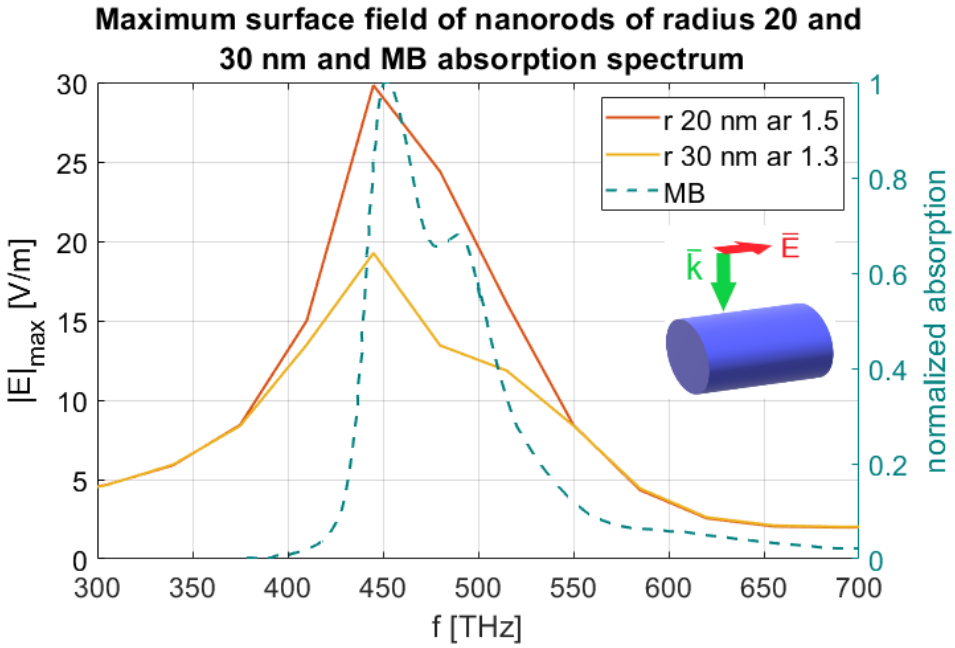

Figure 3.2: *Maximum surface electric field of gold nanorods, subject to plane wave illumination, and normalized absorption spectrum of methylene blue.*

one excited by light polarized parallel to the long axis of the structure. This was the case for nanorods and nanocubes, as can be seen in Fig.3.2 and 3.3. The sizes reported for the nanorods indicate the radius of the rod and its aspect ratio (AR), defined as the ratio

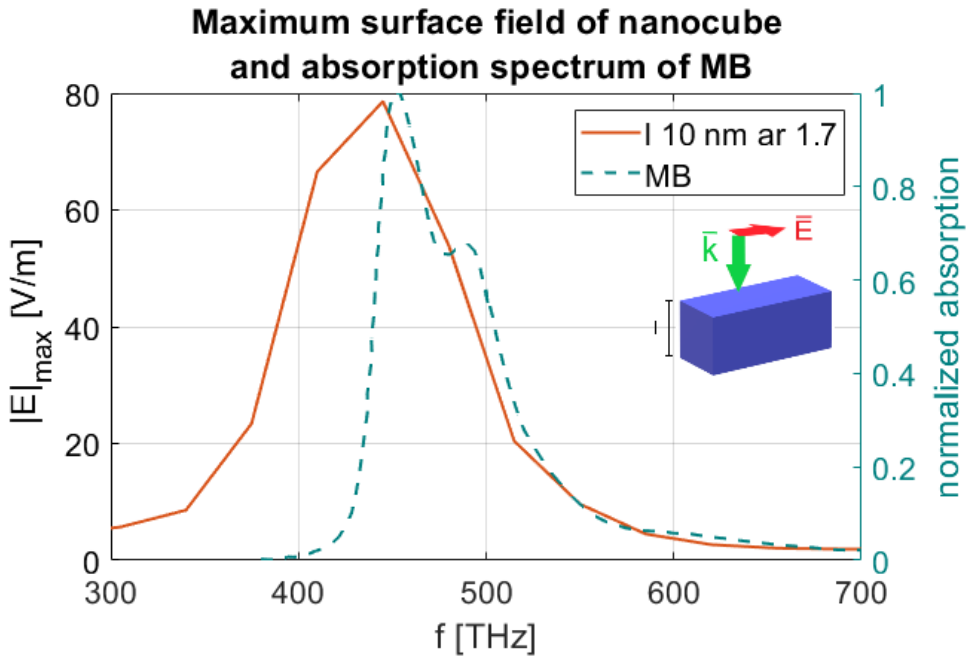

Figure 3.3: *Maximum surface electric field of gold nanocubes, subject to plane wave illumination, and normalized absorption spectrum of methylene blue.*

between its length and its diameter. Instead, for the nanocubes we have indicated the length of the smaller side and the AR between the long side and the small one.

All the spectra of the maximum surface field of the gold nanostructures were obtained without the presence of the PS around them.

We also computed the ratios between the absorption of the PS in the presence of the gold nanostructures and the absorption in absence of it, whose values are reported in table 3.1.

Table 3.1: *Absorption ratio of MB*

size	absorption ratio
NP 90 nm	2.8825
NP 100 nm	3.5384
NR 20 nm AR 1.5	2.4177
NR 30 nm AR 1.3	2.4929
NC 10 nm AR 1.7	2.4868

3.2 Chlorin e6

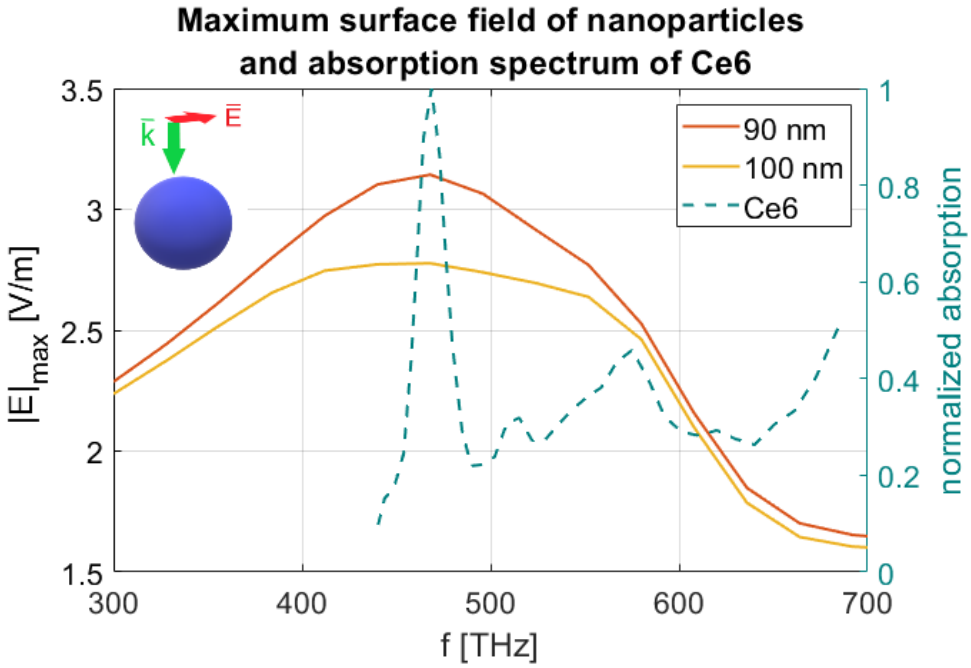

Figure 3.4: *Maximum surface electric field of nanoparticles, subject to plane wave illumination, and normalized absorption spectrum of chlorin e6.*

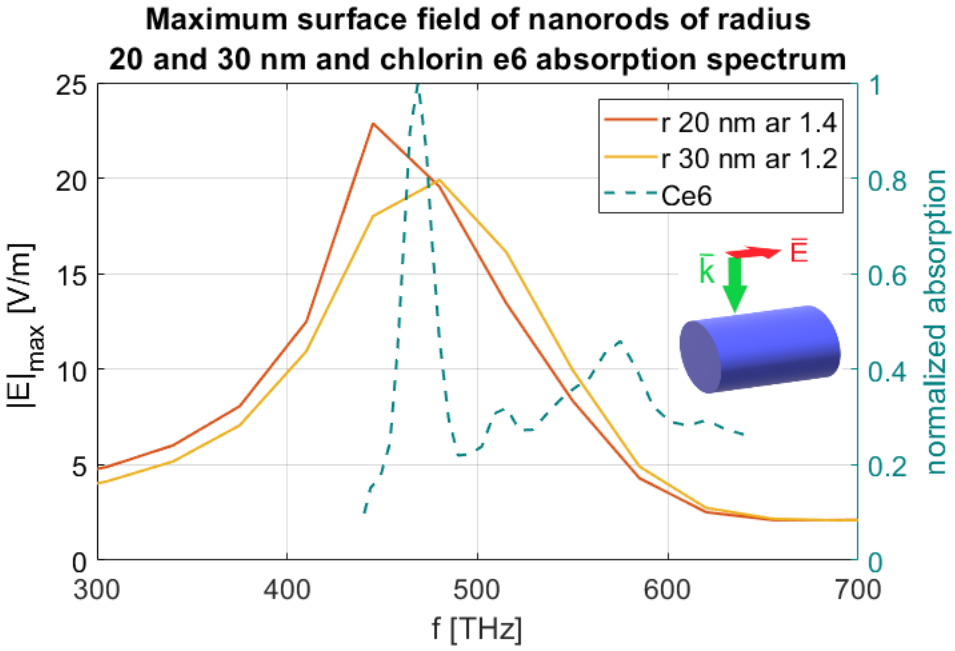

Figure 3.5: *Maximum surface electric field of nanorods, subject to plane wave illumination, and normalized absorption spectrum of chlorin e6.*

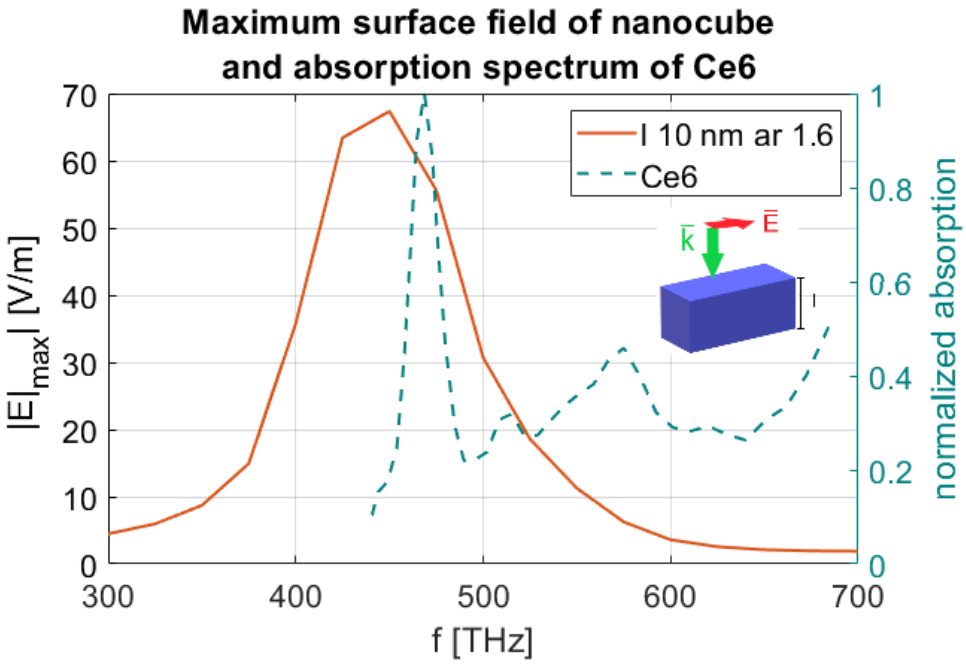

Figure 3.6: *Maximum surface electric field of nanocubes, subject to plane wave illumination, and normalized absorption spectrum of chlorin e6.*

The absorption peak of chlorin e6 (Ce6) is spectrally located at 463 THz in water. The structures for which we had an overlap between their LSPR and Ce6 absorption peak were nanospheres of radius 90 nm and 100 nm (speigare perché due???), nanorods with radius 20 nm and AR 1.4 and with radius 30 nm and AR 1.2, and nanocubes with side 10 nm and AR 1.6. The respective maximum surface electric fields are shown in Fig.3.4, 3.5 and 3.6, together with the normalized absorption spectrum of Ce6. In the table 3.2, the absorption ratios of Ce6 in the presence and in the absence of the overlapping plasmonic structures are reported.

All the spectra of the maximum surface field of the gold nanostructures were obtained without the presence of the PS around them.

Table 3.2: *Absorption ratio of Ce6*

size	absorption ratio
NP 90 nm	3.0942
NP 100 nm	3.7983
NR 20 nm AR 1.4	2.8095
NR 30 nm AR 1.2	2.8994
NC 10 nm AR 1.6	2.8231

3.3 Indocyanine Green

The superposition of indocyanine green (ICG) absorption peak, located at 384 THZ, and the maximum scattered electric field of gold nanostructures was obtained with nanorods of radius 20 nm and AR 2.2 and of radius 30 nm and AR 1.8, and with nanocubes of side length 20 nm and AR 3 and of side length 30 nm and AR 2.8, as can be seen in Fig.3.7 and 3.8. The overlap was not obtained for nanospheres, since to have the LSPR spectrally positioned in the IR region they would need to have a radius greater than 120 nm, which is too large for PDT applications. In table 3.3, we have written the values of the ratio between ICG absorption in the presence and the absorption in absence of the gold nanostructures.

All the spectra of the maximum surface field of the gold nanostructures were obtained without the presence of the PS around them.

Table 3.3: *Absorption ratio of ICG*

size	absorption ratio
NR 20 nm AR 2.2	3.2694
NR 30 nm AR 1.8	3.3321
NC 20 nm AR 3	3.3274
NC 30 nm AR 2.8	4.7017

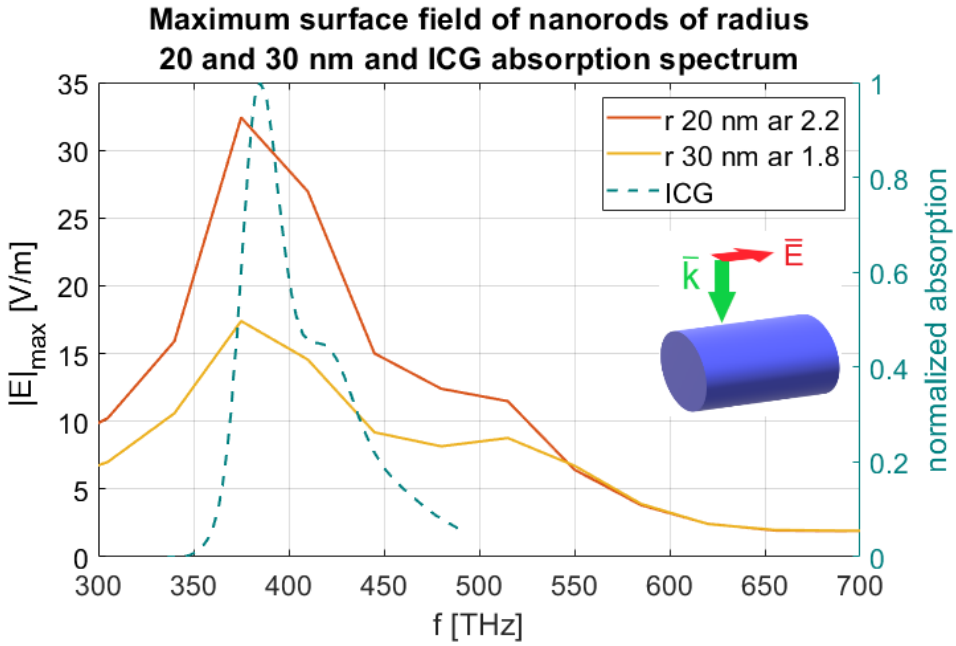

Figure 3.7: *Maximum surface electric field of nanorods, subject to plane wave illumination, and normalized absorption spectrum of indocyanine green.*

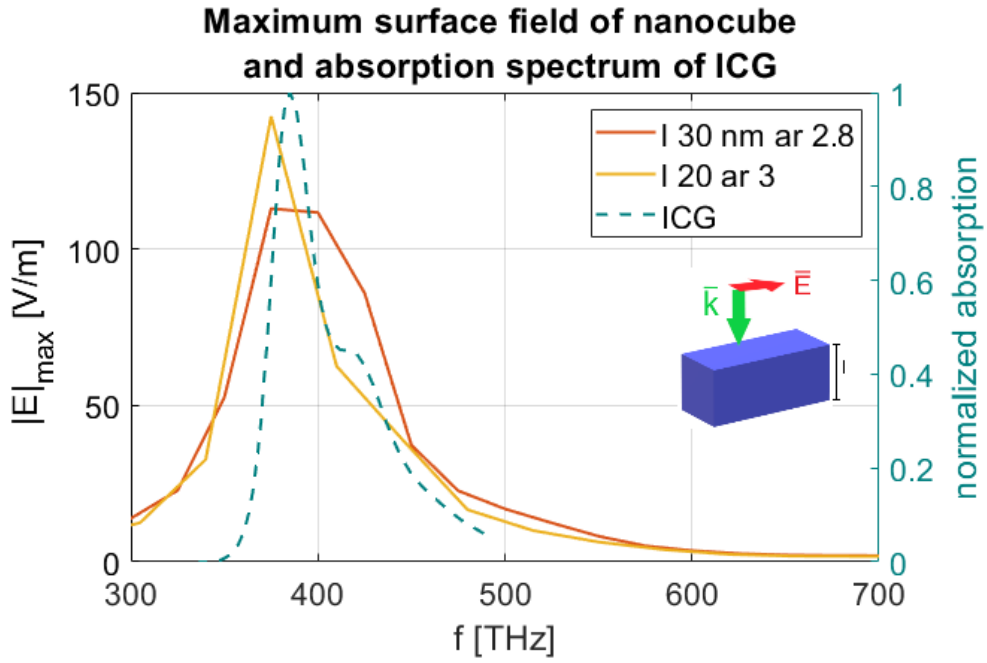

Figure 3.8: *Maximum surface electric field of nanocubes, subject to plane wave illumination, and normalized absorption spectrum of indocyanine green.*

3.4 Lutetium Texaphyrin (Lu-Tex®)

Lutetium Texaphyrin (Lu-Tex®) has the absorption peak at 403 THz. Also in this case, gold spherical nanoparticles are not suitable to be used with this PS, as they would need

to be relatively large and impractical. Instead, the overlap can be obtained with nanorods of radius 20 nm and AR 1.8 and of radius 30 nm and AR 1.6, and also with nanocubes of side 20 nm and AR 1. In Fig.3.9 and 3.10 the maximum surface field spectra of these structures are reported together with the normalized absorption of Lu-Tex®. The values of the absorption ratio of Lu-Tex® , in the case of presence and absence of a gold nanostructure, are shown in table 3.4.

All the spectra of the maximum surface field of the gold nanostructures were obtained without the presence of the PS around them.

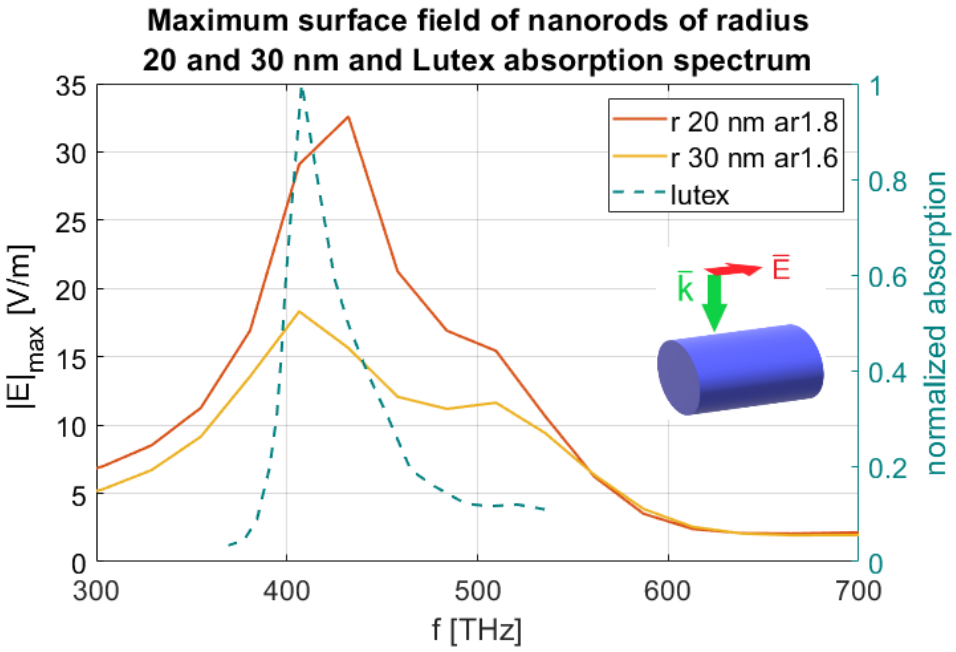

Figure 3.9: *Maximum surface electric field of nanorods, subject to plane wave illumination, and normalized absorption spectrum of Lu-Tex®.*

Table 3.4: *Absorption ratio of Lu-Tex®*

size	absorption ratio
NR 20 nm AR 1.8	3.4311
NR 30 nm AR 1.6	3.5275
NC 20 nm AR 1	2.5391

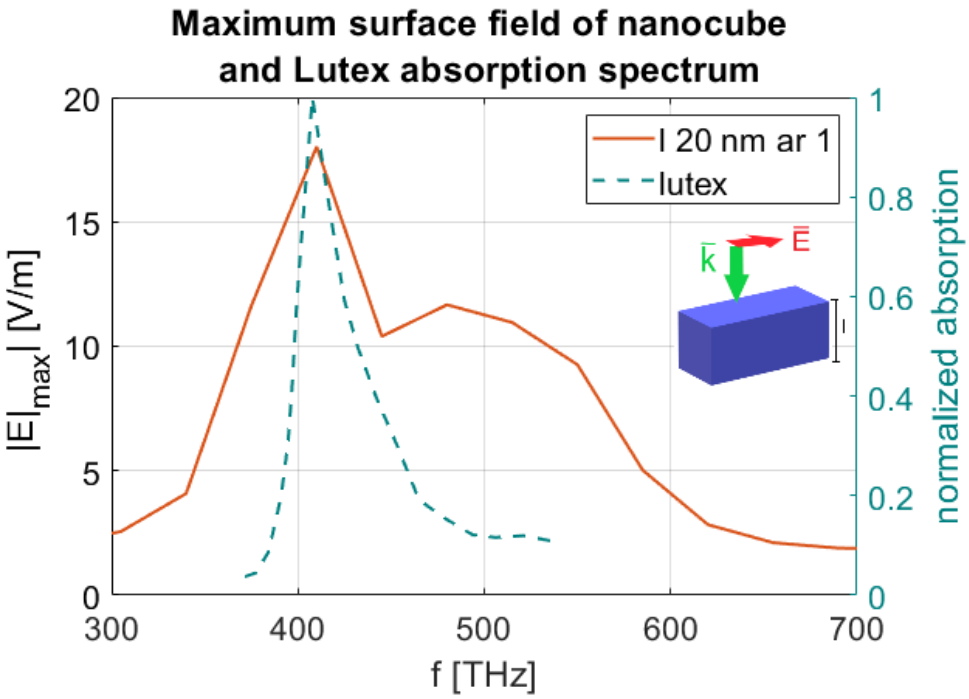

Figure 3.10: *Maximum surface electric field of nanocubes, subject to plane wave illumination, and normalized absorption spectrum of Lu-Tex®.*

3.5 Verteporfin (Visudyne®)

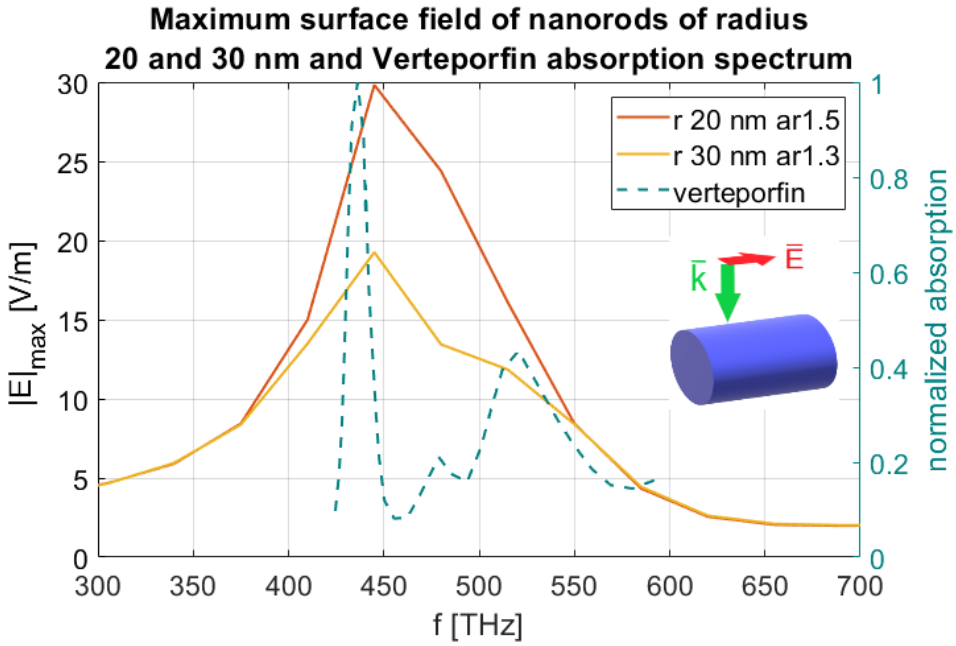

Figure 3.11: *Maximum surface electric field of nanorods, subject to plane wave illumination, and normalized absorption spectrum of verteporfin.*

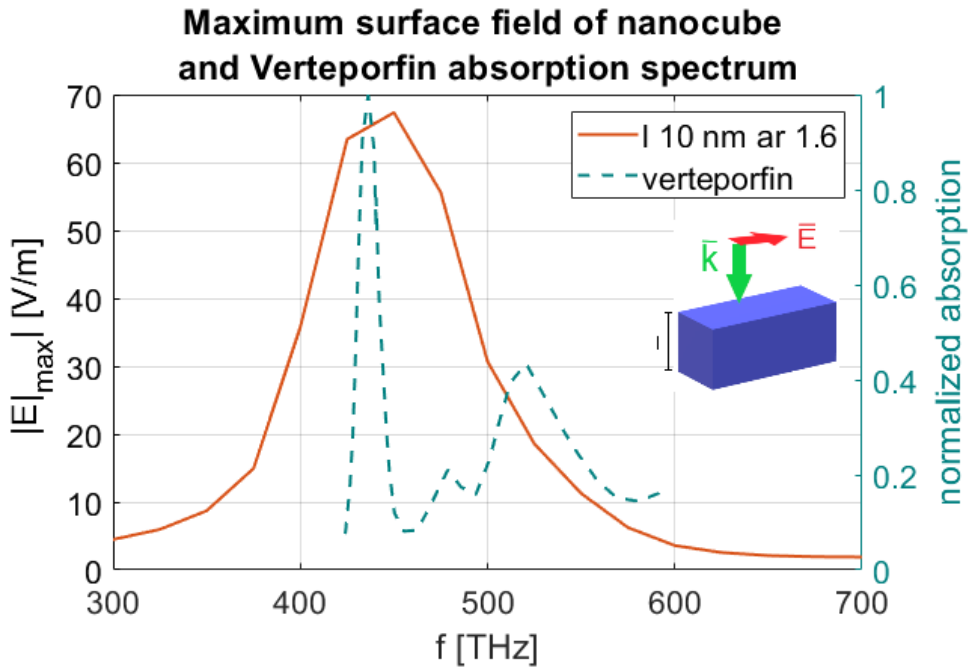

Figure 3.12: *Maximum surface electric field of nanocubes, subject to plane wave illumination, and normalized absorption spectrum of verteporfin.*

The absorption peak of verteporfin that is relevant for PDT is the one located at 428 THz. The nanostructures that have the LSPR overlapped with this frequency are nanorods with radius 20 nm and AR 1.5 and with radius 30 nm and AR 1.3, and also nanocubes with side length 10 nm and AR 1.6. The normalized absorption spectrum of the PS is shown together with the maximum scattered electric field spectrum of nanorods and nanocubes in Fig.3.11 and 3.12, respectively. Also with verteporfin the use of spherical nanoparticles is not suitable for PDT. The values obtained for verteporfin absorption ratio, intended as the ratio between its absorption in the presence and in the absence of a gold nanostructure, are reported in table 3.5.

All the spectra of the maximum surface field of the gold nanostructures were obtained without the presence of the PS around them.

Table 3.5: *Absorption ratio of verteporfin*

size	absorption ratio
NR 20 nm AR 1.5	3.5622
NR 30 nm AR 1.3	3.6729
NC 10 nm AR 1.6	1.8493

3.6 Tookad®

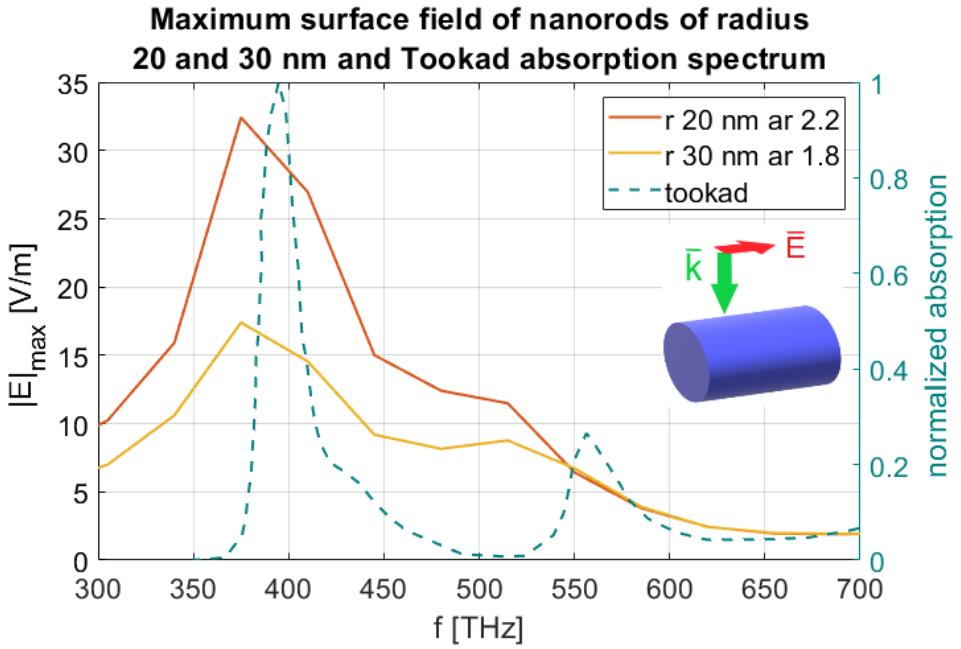

Figure 3.13: *Maximum surface electric field of nanorods, subject to plane wave illumination, and normalized absorption spectrum of Tookad®.*

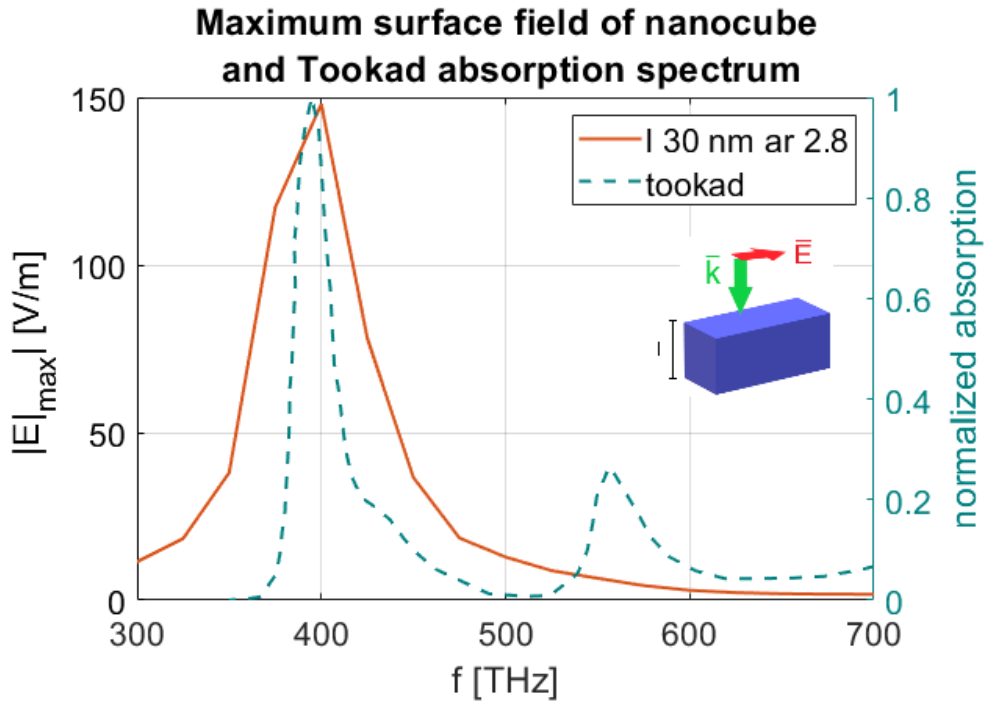

Figure 3.14: *Maximum surface electric field of nanocubes, subject to plane wave illumination, and normalized absorption spectrum of Tookad®.*

The absorption peak of interest for Tookad®, in its use in PDT, is the one at 389 THz, very close to the one of ICG. Hence, nanospheres are too large to be used also with this PS. Instead, the absorption peak superposition with the LSPR of gold nanostructures can be obtained with nanorods of radius 20 nm and AR 2.2 and of radius 30 nm and AR 1.8, and also with nanocubes with side length 30 nm and AR 2.8. The normalized absorption spectrum of Tookad® and the maximum surface electric field spectrum are reported in Fig.3.13 for nanorods and in Fig. 3.14 for nanocubes. In table 3.6 the absorption ratios of Tookad® in the presence and in the absence of a gold nanostructures, are shown.

All the spectra of the maximum surface field of the gold nanostructures were obtained without the presence of the PS around them.

Table 3.6: *Absorption ratio of Tookad®*

size	absorption ratio
NR 20 nm AR 2.2	3.2404
NR 30 nm AR 1.8	1.7824
NC 30 nm AR 2.8	5.9974

Conclusions

In this conclusion chapter we will first summarize the obtained results and their relevance in the PDT field. Then we will give an overview of the limitations of the work, together with recommendations for the future research.

This thesis work was intended to be a sistematic study of how geometric parameters of plasmonic nanostructures influence the enhancement of PSs absorption, to improve the efficiency of PDT. We first discussed how the LSPR spectral position of a plasmonic nanostructure varies with its shape and size, in order to highlight how to change the LSPR frequency by changing these parameters. The obtained results indicate that it is possible to get an overlap between the LSPR of plasmonic nanostructures and the peak of absorption of several PSs, hence maximizing the singlet oxygen generation of these latter. Moreover, computing the ratio between each PS absorption cross section in the presence and in the absence of the LSPR overlapping nanostructures, it was found that the plasmonic nanostructures provided an actual enhancement of the PSs absorption.

The obtained results are supposed to be a ground for a more sistematic study of PDT and, in particular, of the use of plasmonic nanostructures in this field. The research could make a use of this sistematicity to achieve a better a priori knowledge about the use of plasmonic nanoparticles, not only in the PDT field, but also in other ones, in which they find useful applications.

In this work we focused mainly on the design of gold nanostructures to enhance PDT efficiency, as gold has a good biocompatibility. The PSs we considered were methylene blue, chlorin e6, indocyanine green, lutetium texaphyrin (Lu-Tex®), verteporfin (Visudyne®) and Tookad® , which are among the most clinically successful or the most promising PSs in terms of efficiency of PDT. Hence, the gold nanostructures design could be done for many other PSs which we do not take into considerations. Moreover, since we exploited the

COMSOL Multiphysics® simulation software, the nanostructures design was simplified, as well as the environment around them, which was considered to be only made of water. Therefore, a confrontation with the obtained results and the ones that would be obtained in a laboratory would be necessary to understand whether this approximation of the problem is valid.

Another aspect that needs to be addressed is the fact that, in a realistic scenario, nanostructures would be randomly aligned. For asymmetric nanostructures, the main resonance is due to the longitudinal LSPR, the one excited by light polarized along their long axis, which is the case we considered in our work. In real applications it would not be possible to get this alignment, hence it would be worth to verify how much it affects the PSs absorption enhancement and singlet oxygen generation control.

Also, it would be interesting to have a better understanding on the physical processes that make the LSPR spectral position change with the size and the geometry on the nanostructure, as the models that scientists have proposed up to now are not fully satisfactory. Also PSs still need to be improved in their physical and chemical properties, as well as dosimetry needs to be better understood. Both of these problems could be solved again with the use of plasmonic nanostructures, as they can be used as nanocarriers for the PSs to reach the site to be treated, improving their stability with a silicon coating for example, and they can also be used as fluorescent agents for imaging the site and also for real time monitoring.

It is also worth to mention a result that was not expected and that would be worth further studies. We found that square-based parallelepipeds with a relatively high aspect ratio, intended as the ratio between the long and the short side, were able to enhance up to 5 times the absorption of the considered PSs, much more than the other nanostructures. Probably the linewidth of their resonances is narrower, so they have a larger quality factor, and hence a larger field enhancement. This was a result obtained from simulations, therefore it would be interesting to better understand the physical reasons why this happens and if also in laboratories experiments the same result is obtained.

Bibliography

[1] Spikes J. D. “The historical development of ideas on applications of photosensitised reactions in health sciences”. In: *Primary Photoprocesses in Biology and Medicine* (1985), pp. 209–227.

[2] Daniell M. D. and Hill J. S. “A history of photodynamic therapy”. In: *Aust. N.Z. J. Surg.* 61 (1991), pp. 340–348.

[3] Grzybowski A. and Pietrzak K. “From patient to discoverer-Niels Ryberg Finsen (1860-1904)-the founder of phototherapy in dermatology”. In: *Clinics in Dermatology* 30 (2012), pp. 451–455.

[4] Raab O. “Uber die Wirkung fluorescierenden Stoffe auf Infusorien”. In: *Z. Eiol.* 39 (1900), pp. 524–546.

[5] von Tappeiner H. and Jesionek A. “Therapeutische Versuche mit fluorescierenden Stoffen”. In: *Munch. Med. Wochenschr.* 47 (1903), pp. 2042–2044.

[6] von Tappeiner H. and Jodlbauer A. “Uber Wirkung der photodynamischen (fluorescierenden) Stoffe auf Protozoan und Enzyme”. In: *Drsch. Arch. Klin. Med.* 80 (1904), pp. 427–87.

[7] Baskaran R. et al. “Clinical development of photodynamic agents and therapeutic applications”. In: *Biomaterials Research* (2018), pp. 22–25.

[8] Ron R. Allison et al. “Oncologic photodynamic therapy photosensitizers: A clinical review”. In: *Photodiagnosis and Photodynamic Therapy* (2010), pp. 61–75.

[9] Patterson MS Wilson BC. “The physics, biophysics and technology of photodynamic therapy”. In: *Phys Med Biol.* 53(9) (2008), R61–109.

[10] Yamei Liu et al. “Water Insoluble Photosensitizer Nanocolloids Stabilized by Supramolecular Interfacial Assembly towards Photodynamic Therapy”. In: *Scientific Reports* 7, 42978 (2017).

[11] Chan Feng et al. “Targeted Delivery of Chlorin e6 via Redox Sensitive Diselenide-Containing Micelles for Improved Photodynamic Therapy in Cluster of Differentiation 44 Overexpressing Breast Cancer”. In: *Frontiers in Pharmacology* 10:390 (2019).

[12] Tardivo J.P. et al. “Methylene blue in photodynamic therapy: From basic mechanisms to clinical applications”. In: *Photodiagnosis and Photodynamic Therapy* 2 (2005), pp. 175–191.

[13] Kofler B. et al. “Photodynamic Effect of Methylene Blue and Low Level Laser Radiation in Head and Neck Squamous Cell Carcinoma Cell Lines”. In: *Internation Journal of Molecular Science* 19 (2018), p. 1107.

[14] Wilson B.C. Bisland S.K. Chien C. and Burch S. “Pre clinical in vitro and in vivo studies to examine the potential use of photodynamic therapy in the treatment of osteomyelitis”. In: *Photochem Photobiol Sc* 5 (2006), pp. 31–38.

[15] Suarez E.R. et al. Wagner M. “Methylene blue photodynamic therapy in malignant melanoma decreases expression of proliferating cell nuclear antigen and heparanases”. In: *Clin Exp Dermatol* 37 (2012), pp. 527–533.

[16] Engel E. et al. “Light induced decomposition of indocyanine green”. In: *Invest. Ophtalmol. Vis. Sci.* 49 (2008), pp. 1777–1783.

[17] Giraudeau C. et al. “Indocyanine green: Photosensitizer or Chromophore? Still a Debate”. In: *Current Medicinal Chemistry* 21 (2014), pp. 1871–1897.

[18] Lim Hyun-Ju et al. “Indocyanine green based photodynamic therapy with 785 nm light emitting diode for oral squamous cancer cells”. In: *Photodiagnosis and Photodynamic Therapy* 8 (2011), pp. 337–342.

[19] Yiye Li et al. “Localized Electric Field of Plasmonic Nanoplatform Enhanced Photodynamic Tumor Therapy”. In: *Acs Nano* 8 (2014), pp. 11529–11542.

[20] Willets K.A. et al. “Localized Surface Plasmon Resonance Spectroscopy and Sensing”. In: *Annu. Rev. Phys. Chem.* 58 (2007), pp. 267–97.

[21] Maier S. A. *Plasmonics: Fundamentals and Applications*. Springer, 2007.

[22] Huffman D. Bohren C. *Absorption and Scattering of Light by Small Particles*. Wiley-Interscience Publication, 1983.

[23] Juvé V. et al. “Size Dependent Surface Plasmon Resonance Broadening in Nonspherical Nanoparticles: Single Gold Nanorods”. In: *Nano Letters* 13 (2013), pp. 2234–2240.

[24] Wokaun A. et al. “Radiation Damping in Surface Enhanced Raman Scattering”. In: *Phys. Rev. Lett.* 48 (1982), p. 957.

[25] Novotny L. “Effective Wavelength Scaling for Optical Antennas”. In: *Phys. Rev. Lett.* 98 (2007), pp. 266802-1 –4.

[26] Scott Prahl. *Tabulated Molar Extinction Coefficient for Methylene Blue in Water*. 1998. URL: https://omlc.org/spectra/mb/mb-water.html.

[27] Losytskyy M. Yu. et al. “Uptake of Chlorin e6 Photosensitizer by Polystyrene-Diphenyloxazole-Poly(NIsopropylacrylamide) Hybrid Nanosystem Studied by Electronic Excitation Energy Transfer”. In: *Nanoscale Research Letters* 13 (2018), p. 116.

[28] Scott Prahl. *Optical Absorption of Indocyanine Green (ICG)*. 2018. URL: https://omlc.org/spectra/icg/l.

[29] Marie J. Hammer-Wilson. “Photodynamic Activity of Lutetium-Texaphyrin in a Mouse Tumor System”. In: *Lasers in Surgery and Medicine* 24 (1999), pp. 276–284.

[30] Pellosi D. et al. “Pluronic® P123/F127 mixed micelles delivering sorafenib and its combination with verteporfin in cancer cells”. In: *International Journal of Nanomedicine* 11 (2016), pp. 4479–4494.

[31] Borle F. et al. “Evaluation of the Photosensitizer Tookad® for Photodynamic Therapy on the Syrian Golden Hamster Cheek Pouch Model: Light Dose, Drug Dose and Drug–light Interval Effects”. In: *Photochemistry and Photobiology* 78 (2003), pp. 377–383.